

**Estimation of Evaporative Fraction and Evapotranspiration From
Remotely Sensed Data Using A Complementary Relationship**

by
Virginia Venturini

Thesis submitted to the postgraduate academic committee of the

FACULTAD DE INGENIERIA Y CIENCIA HÍDRICAS

As a part of the requirements to obtain the degree of

DOCTORA EN INGENIERIA

Of the

UNIVERSIDAD NACIONAL DEL LITORAL

2007

DECLARACIÓN DE LA AUTORA

Esta disertación ha sido remitida como parte de los requisitos para la obtención del grado académico de Doctora en Ingeniería – Mención Recursos Hídricos ante la Universidad Nacional del Litoral y ha sido depositada en la Biblioteca de la Facultad de Ingeniería y Ciencias Hídricas para que esté a disposición de sus lectores bajo las condiciones estipuladas por el Reglamento de la mencionada Biblioteca.

Citaciones breves de esta disertación son permitidas sin la necesidad de un permiso especial, en la suposición de que la fuente sea correctamente citada. Solicitudes de permiso para la citación extendida o para la reproducción parcial o total de este manuscrito serán concedidas por el portador legal del derecho de propiedad intelectual de la obra.

I would like to dedicate this work to little Carmen,
for all she has given me without even knowing
“why?... what for?”

Acknowledgments

Back in Cincinnati, OH-USA at the beginning of this process so-called doctoral dissertation, I remember many hours of work with Gautam Bisht and the shared concerns of coding those new and strange files (MODIS images). I believe that supportive teammates like Gautam and Dave Small made this beginning ...encouraging. Thank you Gautam for getting net radiation files for this thesis. I also want to thanks Dr. Le Jiang for sharing his expertise with me.

Dr. Leticia Rodriguez and Dr. Carlos Vionnet opened the door for me and provided a nice work environment, where this thesis smoothly finished. I particularly express my gratitude to Leticia, who trusted on my work and gave me her precious time.

I will always be grateful to Dr Shafiqul Islam. I can fill a page thanking him for his guidance and teaching. Nonetheless, I want to specially thank him for tolerating my health whims and my own whims, encouraging me to be a researcher in spite of the odds.

My parents do not understand hydrology or remote sensing physics but they do understand the meaning of effort and satisfaction. I thank my parents, one more time, for all they put on my person.

Table of Content

Table of Figures	vi
Table of Tables.....	ix
Resumen Extendido en Español.....	xii
Abstract	xvii
Chapter 1 : Evapotranspiration Estimation by Remote Sensing: An	
Overview.....	1
1.1 Introduction.	1
1.2 Bouchet and Granger's Models.....	7
1.3 Objectives of this Thesis	10
1.4 Thesis Outline.....	10
Chapter 2 : Methodology.....	12
2.1 ET Model.....	12
2.2 Proposed Method to Estimate T_u	20
2.3 Bouchet or Granger's Complementary Models?.....	25
Chapter 3 : Model Application.	27
3.1 Study Area.....	27
3.2 Ground Data Availability	29
3.3 MODIS Products	33
3.3 Validation with Ground Measurements.....	43
3.4 Contrast Between Equation 12 and 24	52
Chapter 4 : Uncertainty Analysis.	55

4.1 First Order Analysis of Uncertainty	55
4.2 One-channel Brightness Temperature Vs. MODIS Ts Product.	58
4.3 The Wind Speed effect.	65
Chapter 5 : Comparison with Different Modified Priestley and	
Taylor’s Equation for Unsaturated Surfaces.....	70
5.1 Introduction	70
5.2 Overview of Different Approaches to Estimate ET	72
5.2.1 Surface and Atmospheric Parameterization	72
5.2.2 Surface Parameterization.....	73
5.2.3 Atmospheric Parameterization	75
5.3 Compare and Contrast Different ET Estimation Approaches	76
5.3.1 Surface Vs Atmospheric-Surface Parameterizations.....	77
5.3.2 Atmospheric Vs Atmospheric-Surface Parameterizations	83
Chapter 6 : Conclusions and Future Work	87
6.1 Conclusions	87
6.2 Future Work.....	92
References.....	94
Appendix I: Abstract of Published Paper.	106
Appendix II: IDL Code to Calculate ET	107
Appendix III: An Introduction to an Alternative Tu Calculation.....	118
Introduction	118
Method to Estimate Tu from Night-Day Ts Maps	120
F and ET Estimation with Night-Day Ts Maps.....	121

Table of Figures

Figure 2.1: Sketch of the saturation vapor pressure curve and the relationship among T_u , T_s , e_s and e_u^* in the context of surface at temperature T_s . The overlying air is characterized by T_a and T_d and vapor pressure e_a 13

Figure 2.2: Schematic of the linearized saturation vapor pressure curve and the relationship between $(e_s - e_a)$ and $\Delta_1(T_u - T_d)$, and $(e_s^* - e_a)$ and $\Delta_2(T_s - T_d)$ 14

Figure 2.3: T_s -NDVI Triangle space with upper and lower bounds, where T_{min} is the in-land water temperature and T_{max} is the temperature of a dry bare surface. 21

Figure 2.4: Sketch with T_u derivation from the saturation vapor pressure curve. 22

Figure 2.5: Buck's saturation vapor pressure curve. e_a was obtained with T_d , e_s with T_u , e_a^* with T_a and e_s^* with T_s . T_a vs. e_a are shown with violet diamonds and T_s vs. e_s with black dots. 24

Figure 3.1: The southern Great Plains location and extension. 28

Figure 3.2: Picture of an Energy Balance Bowen Ratio system installed in the study area. 33

Figure 3.3: Overview of the Southern Great Plain area and EBBR stations, where the Central facility is at the center of the SGP. The Boundary facilities are at the four boundaries of the SGP-rectangle. The extended facilities are distributed evenly over the area and the three intermediate facilities complete the Central facility. 35

Figure 3.4: (a) Comparison between observed and retrieved air temperature from MODIS data product (MOD07) at 1000 hPa level. (b) Comparison between observed and modeled Instantaneous Net Radiation (INR) estimates for all study days. 45

Figure 3.5: Observed and modeled mean ET (Wm^{-2}).	47
Figure 3.6: Point-to pixel contrast between calculated and observed ET (Wm^{-2}) for seven clear sky days.	49
Figure 3.7: Maps of (a) T_s , (b) T_d , (c) T_u and (d) ET for September 6th, 2003.	51
Figure 3.8: Comparison between Bouchet and Granger's complementary models against ground measurements.	53
Figure 4.1: Comparison between T_s y T_{31} for (a) March 23 rd , (b) March 31 st and (c) April 1 st of 2003.	60
Figure 4.2: Comparison between F-31 and F-s for (a) March 23 rd , (b) March 31 st and (c) April 1 st of 2003.	62
Figure 4.3: Comparison between ET with F-31 and ET with F-s for (a) March 23 rd , (b) March 31 st and (c) April 1 st of 2003.	63
Figure 4.4: Contrast between ground observations and ET estimates with T_s and T_{31} .	65
Figure 4.5: Examples of observed daily cycle of ET (Wm^{-2}), wind speed (ms^{-1}) variation and modeled instantaneous ET(Wm^{-2}).	69
Figure 5.1: Mean ET (Wm^{-2}) observed and calculated with the proposed equation, Barton's equation, Jiang and Islam methodology and Granger and Gray approach.	78
Figure 5.2: Comparison between Barton and proposed method against ground measurements.	80
Figure 5.3: Comparison between Jiang and Islam (J-I) and proposed method against ground measurements.	82
Figure 5.4: Comparison between ET estimates from Jiang and Islam (J-I) and Barton methods for two days.	83

Figure 5.5: Buck's saturation vapor pressure curve. e_a was obtained with Td, e_s with Tw, e_a^* with Ta and e_s^* with Ts. Ta vs. e_a are shown with violet diamonds and Ts vs. e_s with black dots. (a) corresponds to March 31st, 2003 and (b) corresponds September 19th, 2006. 85

Figure 5.6: Comparison between Granger and Gray (G-G) and proposed method against ground measurements. Results with Priestley-Taylor's equation (P-T) are also over plotted as a reference. 86

Table of Tables

Table 2.1: Table of symbols and units.	18
Table 3.1: Site name and station name, elevation, latitude, longitude and surface type. Source: http://www.arm.gov/sites/sgp/geoinfo.stm	34
Table 3.2: Date, Day of the Year, overpass time and image quality of the seven study days.....	36
Table 3.3: Summary of the MODIS products used and ground observations data	43
Table 3.4: Observed, modeled regional and modeled ET (Wm^{-2}) means and standard deviations (S).....	46
Table 3.5: ET (Wm^{-2}) Comparison between observations and proposed method estimates at the pixel scale. Calculated refers to estimated value at the pixel where the ground station is located.	48
Table 3.6: ET (Wm^{-2}) comparison between Bouchet and Granger complementary relationships.....	52
Table 4.1: Mean and standard deviation (S) values for F first order analysis.....	57
Table 4.2: Ts y T31 mean, Maximum, Minimum and Standard deviations.....	61
Table 4.3: Contrast of ET calculated with F-s and F-31 (Wm^{-2}) measured in terms of RMSE, bias and correlation coefficient (R^2).....	64
Table 5.1: Summary of different methods to modify Priestley and Taylor's equation.	71
Table 5.2: Observed and modeled ET (Wm^{-2}) means and standard deviations (S).	78
Table 5.3: ET (Wm^{-2}) comparison between Barton's and proposed method estimates.	79

Table 5.4: ET (Wm^{-2}) comparison between Jiang and Islam's method (J-I) and new proposed method estimates.....	81
Table 5.5: ET (Wm^{-2}) comparison between Granger and Gray's assumption (G-G) and the proposed method estimates.....	84

Resumen Extendido en Español

Estimación de la fracción evaporable y evapotranspiración mediante una nueva relación complementaria e imágenes satelitales.

**Tesis Doctoral
Virginia Venturini**

Introducción

Muchos modelos hidrológicos, los modelos de circulación global y el manejo agrícola requieren estimaciones de la evapotranspiración (ET) y de la fracción evaporable (FE). La comunidad científica ha desarrollado una variedad de métodos para estimar estas variables hidrológicas. Las metodologías disponibles se extienden desde modelos complejos que simulan el proceso de transferencia de energía (Deardorff, 1970; Brutsaert & Sugita, 1990; Sugita et al., 2001; Parlange & Katul, 1995) hasta métodos simples que requieren pocas variables y parámetros (Priestley & Taylor, 1972; Jiang & Islam, 1999; Barton, 1979).

Pocas metodologías para estimar ET se han desarrollado basándose en una relación complementaria. Bouchet (1963) postuló que la ET regional puede ser estimada como una función complementaria de la evapotranspiración potencial (Epot) y de la evapotranspiración de ambientes húmedos (Ew), para una amplia gama de valores de la energía disponible. Luego de un análisis minucioso de los conceptos potenciales de la evaporación, Granger (1989) desarrolló una relación complementaria basada en la física de los procesos. Además, el concepto de evaporación relativa introducido por Granger y Gray (1989) realza la relación complementaria con un coeficiente adimensional, resultando en un modelo complementario más simple.

El advenimiento de la tecnología satelital proporcionó observaciones de la temperatura superficial (Ts) en forma rutinaria y distribuida en el espacio. En la actualidad, los sensores remotos representan una fuente de información importante, no sólo por su eficiencia en monitorear los ecosistemas sino también por el tipo y calidad de los datos registrados. En particular, el producto atmosférico derivado del sensor MODIS proporciona perfiles diarios de temperatura de aire y de punto rocío para 20 niveles verticales de presión atmosférica. La combinación de este producto atmosférico con mapas de Ts provee una oportunidad única para revisar las relaciones complementarias que relacionan Epot y Ew con ET (Crago & Crowley, 2005; Ramírez et al., 2005).

En esta tesis se propone un modelo para calcular ET y FE basado en la relación complementaria propuesta por Granger (1989) y la ecuación de Priestley y Taylor (1972), de ahora en adelante referida como P-T.

Metodología

El método propuesto toma como base el modelo complementario formulado por Granger (1989), en particular la expresión propuesta para calcular la evaporación relativa publicada por Granger & Gray (1989).

La relación complementaria propuesta por Granger es:

$$ET + E_{pot} \frac{\gamma}{\Delta} = E_w \left(\frac{\Delta + \gamma}{\Delta} \right) \quad (1)$$

donde E_w es la evapotranspiración real de una superficie húmeda que se corresponde con el concepto propuesto por Penman (1948) y E_{pot} es la evapotranspiración potencial.

En 1989 Granger y Gray formularon una expresión para cuantificar la evaporación relativa, definida como el cociente entre ET y E_{pot} , que tiene la siguiente forma:

$$\frac{ET}{E_{pot}} = \frac{f_u (e_s - e_a)}{f_u (e_s^* - e_a)} \quad (2)$$

donde f_u es función de la velocidad del viento y de la altura de la vegetación, e_s es la presión de vapor de agua real de la superficie, e_a es la presión de vapor de agua real del aire y e_s^* es la presión de vapor de agua de saturación de la superficie.

Las ecuaciones (1) y (2) permiten obtener un modelo para calcular ET que depende sólo de E_w y es independiente de los términos de resistencia a la acción del viento.

Desde el punto de vista de la teleobservación, el efecto de enfriamiento causado por ET es observable en T_s . Por lo tanto, e_s debería ser relacionado a la temperatura del sistema suelo-vegetación. Por otra parte, la relación entre la presión de vapor de agua y la temperatura no es lineal aunque la misma es comúnmente rectificada para pequeñas diferencias de temperaturas.

En la Figura 1 se puede observar la relación entre las diferentes variables en juego, e_u^* representa la presión de vapor de saturación de la superficie correspondiente a una temperatura de superficie T_u desconocida hasta el momento.

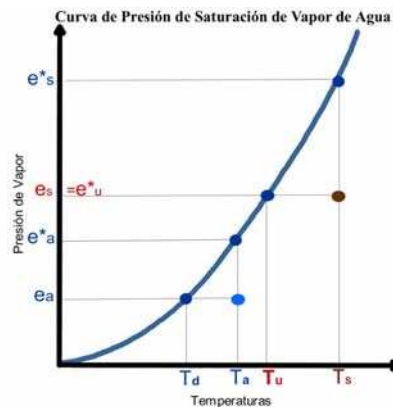


Figura 1: Esquema de la curva de presión de vapor de saturación y la relación entre las variables involucradas en el método.

Una analogía con el concepto de temperatura punto rocío (T_d) sugiere que T_u sería la temperatura de la superficie si ésta es saturada sin cambiar la presión de vapor de agua real de la misma. Por lo tanto e_s podría ser derivada a partir de T_u , aunque esta temperatura no sería observada de la misma manera que T_d .

De esta forma, la evaporación relativa, ET/E_{pot} , puede escribirse como sigue:

$$F = \frac{(T_u - T_d)}{(T_s - T_d)} \quad (3)$$

F es un coeficiente adimensional, por lo tanto varía entre 0 y 1. El valor F=0 corresponde a ET=0 y F=1 a ET=Epot.

Para estimar ET con la ecuación (1) se necesita una expresión para modelar Ew. En este método se utilizó la ecuación de P-T para reemplazar Ew. Combinando las ecuaciones (1), (3) y Ew se obtiene:

$$ET = \alpha \left(\frac{F\Delta}{F\Delta + \gamma} \right) (R_n - G) \quad (4)$$

donde α es el parámetro de P-T, el que puede ser calculado con la expresión analítica propuesta por Eichinger et al. (1996) o reemplazado por el valor 1.26, valor empírico propuesto por Priestley & Taylor (1972).

La ecuación (4) podría ser aplicada a un amplio rango de escalas espaciales. Extensas regiones pueden ser estudiadas con datos teledetectados si se tiene en cuenta que los sensores MODIS-Terra y MODIS-Aqua proveen datos diarios y espacialmente distribuidos de Ts, Ta y Td (<http://modis-atmos.gsfc.nasa.gov>).

Para calcular el valor de Tu en cada píxel, se propuso una metodología basada en la ecuación que describe la curva de SVP, la que comúnmente se modela con una función exponencial. La pendiente de la curva de SVP puede calcularse como la derivada primera en Ts y Td y también linealizando la curva en el intervalo [Tu, Ts] y [Td, Tu], cuyas pendientes se denotan Δ_1 y Δ_2 , respectivamente. Esto permite plantear un sistema de dos ecuaciones con dos incógnitas y derivar la siguiente expresión para Tu:

$$T_u = \frac{(e_s^* - e_a) - \Delta_1 T_s + \Delta_2 T_d}{\Delta_2 - \Delta_1} \quad (5)$$

La ecuación de Buck (1981) fue utilizada para modelar la curva de SVP dada su simplicidad. Los detalles del método pueden encontrarse publicados en Venturini et al. (2007)

Área de estudio y datos

Dada la falta de datos de ET observados a nivel nacional, el método fue aplicado en la región denominada Southern Great Plains (SGP) en los Estados Unidos de América, ubicada entre las latitudes 34,5° N y 38,5° N y las longitudes -95,3° y -99,5. Esta región ha sido continuamente instrumentada a partir de 1992 y hoy en día se dispone de una base de datos completa que permite la validación de muchos modelos hidrológicos y atmosféricos.

Esta región se caracteriza por un terreno plano y una importante variedad de coberturas vegetales. El programa Atmospheric Radiation Measurement (ARM) opera y mantiene varias estaciones de tipo Razón de Bowen para medir el balance de energía a nivel de la superficie en toda la región. Las estaciones de medición están distribuidas en todo el área, como se observa en la Figura 2. EF8 y EF22 están ubicadas en zonas ganadera. EF9 y EF4 en zonas de pasturas naturales. EF13 y EF24 en áreas de cultivos de trigo. EF15, EF7, EF27 y EF20 están ubicadas en pasturas. EF19 y EF18 en zona de pasturas no explotadas. EF12 está localizada en praderas naturales, EF2 está en zona de hierbas.

Se procesaron imágenes de los productos derivados del sensor MODIS. Los mismos corresponden a siete días en el año 2003 con aproximadamente un 80% del área en estudio libre de nubes.

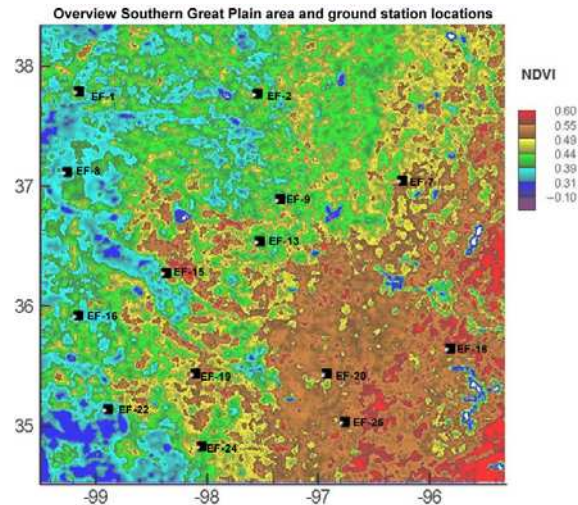


Figure2: El área en estudio (Southern Great Plains) y la ubicación de las estaciones de tipo Razón de Bowen.

Resultados

Para obtener valores instantáneos de ET con la ecuación (4) es necesario calcular la radiación neta (R_n). Para este estudio, R_n se estimó con la metodología propuesta por Bisht et al. (2005). El flujo de calor del suelo se calculó con el método de Moran et al. (1989). La pendiente de la curva SVP, Δ , se obtuvo con la ecuación propuesta por Buck (1981) y datos de T_a suministrados por los productos MODIS. Con todos los componentes estimados y con los mapas de T_s , se calcularon los coeficientes F y ET para cada día en estudio.

La validación de los resultados en la escala del píxel presume que las observaciones de ET son representativas de un área de 1 km^2 alrededor de la estación.. Las coordenadas geográficas de cada estación se utilizaron para localizar el píxel correspondiente para los propósitos de una comparación local. La comparación entre las observaciones de ET y las estimaciones en el píxel correspondiente se muestran en la la Figura 3. El RMSE y la tendencia general, con todas las observaciones disponibles, fueron de 33.89 (15% del valor de ET medio) y -10.96 Wm^{-2} respectivamente, con un R^2 de 0.79.

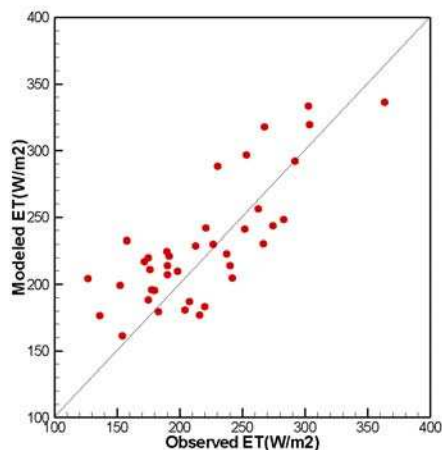


Figura 3: Validación de los resultados de ET (Wm^{-2}) para los siete días propuestos

Conclusiones

El método propuesto presenta una de las más simples modificaciones de la ecuación de P-T que incorpora las condiciones climáticas mediante el concepto de evaporación relativa y el coeficiente F, sin necesidad de calibración local.

En general, se observa una buena concordancia entre los valores observados y los modelados. Resultados similares han sido publicados por otros autores con metodologías más complejas. Aunque los resultados presentados no son exhaustivos, el método propuesto consideraría un conjunto de variables que resultan en estimaciones de ET con errores inferiores al 20% del valor de ET medio sin sacrificar la simplicidad de la ecuación de P-T y los beneficios de datos teledetectados.

Referencias Bibliográficas

- Atmospheric Radiation Measurements (ARM) Program, (1989). <http://www.arm.gov>.
- Barton, I. J. (1979). A parameterization of the evaporation from nonsaturated surfaces. *Journal of Applied Meteorology*, 18, 43-47.
- Bisht, G., Venturini, V., Jiang, L. & Islam, S. (2005). Estimation of Net Radiation using MODIS (Moderate Resolution Imaging Spectroradiometer) Terra Data for clear sky days. *Remote Sensing of Environment*, 97, 52-67.
- Bouchet, R.J. (1963). Evapotranspiration réelle et potentielle, signification climatique. International Association of Scientific Hydrology. *General Assembly of Berkeley, Transactions*, 2, Evaporation, Berkeley, Calif.
- Brutsaert, W. & Sugita, M. (1990). The extent of the unstable Monin-Obukhov layer for temperature and humidity above complex hilly grassland. *Boundary Layer Meteorology*, 51, 383-400.
- Buck, A. L. (1981). New equations for computing vapor pressure and enhancement factor. *Journal of Applied Meteorology*, 20, 1527-1532.
- Crago, R. & Crowley, R. (2005). Complementary relationship for near-instantaneous evaporation. *Journal of Hydrology*, 300, 199-211.
- Deardorff, J. W. (1970). Preliminary results from numerical integrations of the unstable planetary boundary layer. *Journal of Atmospheric Sciences*, 27, 1209-1211.

- Eichinger, W. E., Parlange, M. B. and Stricker, H. (1996). On the concept of equilibrium evaporation and the value of the Priestley-Taylor coefficient. *Water Resources Research*, 32 (1), 161-164.
- Granger, R.J. (1989). A complementary relationship approach for evaporation from nonsaturated surfaces. *Journal of Hydrology*, 111, 31-38.
- Granger, R.J. & Gray, D.M. (1989). Evaporation from natural nonsaturated surfaces. *Journal Hydrology*, 111, 21-29.
- Jiang, L., & Islam, S. (1999). A methodology for estimation of surface evapotranspiration over large areas using remote sensing observations. *Geophysical Research Letters*, 26(17), 2773-2776.
- Moran, M. S., Jackson, R.D., Raymond, L.H, Gay, L. W. & Slater, P.N. (1989). Mapping surface energy balance components by combining LandSat thematic mapper and ground-based meteorological data, *Remote Sensing of Environment*, 30, 77-87.
- Parlange, M. B. & Katul, G. G. (1995). Watershed scale shear stress from tethered wind profile measurements under near neutral and unstable atmospheric stability. *Water Resources Research*, 31(4), 961–968.
- Penman, H. L. (1948). Natural evaporation from open water, bare soil and grass. *Proceedings of the Royal Society of London, Series A*, (193), 120-145.
- Priestley, C. H. B. & Taylor, R. J. (1972). On the Assessment of Surface Heat Flux and Evaporation Using Large-Scale Parameters. *Monthly Weather Review*. 100, 81–92.
- Ramírez, J. A., Hobbins, M.T. & Brown, T.C. (2005). Observational evidence of the complementary relationship in regional evaporation lends strong support for Bouchet's hypothesis. *Geophysical Research Letters*, 32, L15401, doi:10.1029/2005GL023549.
- Sugita, M., Usui, J., Tamagawa, I. & Kaihotsu, I. (2001). Complementary relationship with a convective boundary layer to estimate regional evaporation. *Water Resources Research*, 37(2), 353-365.
- Venturini, V., Islam, S. y Rodríguez, L., (2007). Estimation of evaporative fraction and evapotranspiration from MODIS products using a complementary based model. *Remote Sensing of Environment*. doi:10.1016/j.rse.2007.04.014.

Abstract

A new formulation to derive evaporative fraction (EF) and evapotranspiration (ET) maps from remotely sensed data without auxiliary relationships or site-specific relationships is presented. This formulation is based on Granger's complementary relationship and Priestley-Taylor's equation. The proposed model eliminates the wind function and resistance parameters commonly applied to some calculations by including a relative evaporation parameter (ET/Epot). By combining this relative evaporation parameter, Granger's complementary relationship and Priestley and Taylor equation, a simple equation to estimate ET is obtained. The proposed formulation was tested and validated over the Southern Great Plains (SGP) region of the United States for seven clear sky days during March-October 2003. MODIS Atmospheric and Land products were the only source of data used in this study. Estimates of ET show an overall root mean square error and bias of 33.89 and -10.96 Wm^{-2} , respectively. These results suggest that the proposed approach is robust and valid for a wide range of atmospheric and surface conditions, during clear days. An uncertainty analysis was performed to quantify model errors and uncertainties due to measurement errors in the involved variables. These results showed that common errors in temperature estimates would result in an error of about 10% in ET. A contrast and comparison between modified Priestley and Taylor's equations shows that the proposed method seems to consider a set of atmospheric and surface variables that leads to ET estimates with errors lower than 20% of the mean ET, without forfeiting the simple form of Priestley and Taylor's equation.

Chapter 1 : Evapotranspiration Estimation by Remote Sensing:

An Overview.

1.1 Introduction.

Many hydrologic modeling and agricultural management applications require accurate estimates of the evapotranspiration (ET) and the evaporative fraction (EF). Over the last two decades, several models have been developed to estimate ET for a wide range of spatial and temporal scales provided by remote sensing data. The methods could be categorized as proposed by *Courault et al. (2005)*:

Empirical and semi-empirical methods: These methods use site specific or semi-empirical relationships between two or more variables. Models proposed by *Priestley and Taylor (1972)*, hereafter referred to as P-T, *Jackson et al. (1977)*; *Seguin et al. (1989)*; *Granger and Gray (1989)*; *Holwill and Stewart (1992)*; *Carlson et al. (1995)*; *Jiang and Islam (2001)* and *Rivas and Caselles (2004)*, lie within this category.

This type of methods is characterized by the use of parameters that inherit the complexity of linking two or more processes. For instance, Priestley and Taylor defined a parameter α that was the subject of many studies (*Zhang et al., 2004*; *Pereira, 2004*). Another example of a complex parameter is that proposed by Granger and Gray (1989). Their GG parameter comprises atmospheric and radiation variables in an exponential function.

One of the most used semiempirical models is that derived by Penman and Monteith (*Monteith and Unsworth, 1990*). In their model, two complex resistance

factor that attempt to represent the aerodynamic resistance of the plant and the stomatal resistance to environmental conditions are defined.

Residual methods: These types of models commonly calculate the energy budget and ET as the residual of the energy balance. The following models are examples of residual methods: SEBAL (*Bastiaanssen et al. 1998*), SEBS (*Su, 2002*) and the two-source model proposed by *Norman et al. (1995)*, among others.

In the energy balance, the net energy is divided between the soil heat fluxes (G) and the convective fluxes such as the sensible (H) and latent (LE) heat fluxes. Thus, the latent heat flux (easily converted to ET) is expressed in term of the other fluxes, which involve many variables. Thus, errors in every term of the energy balance will contribute to ET errors. However, the energy balance is widely used in agriculture applications, where the resistant factor of a homogenous field is less uncertain than in large heterogenous areas, basically because the stomatal resistant factor and the structure of the canopy can be better represented by a single parameterization.

In particular, the model SEBAL calculates the energy partition at regional scales using empirical and physically based parameters.

Indirect methods: These physically based methods involve Soil-Vegetation-Atmosphere Transfer (SVAT) models, presenting different levels of complexity. The complexity of the model depends on the process description, i.e. whether evaporation and transpiration are individually simulated. There are basically two schemes to represent vegetation in this type of models: the “one big leaf” and the “multiple layers of leaves”. The simulation of resistant factors associated to multiple layer schemes adds complexity to the model. The model ISBA (Interactions between Soil, Biosphere, and Atmosphere) (*Noilhan and Planton, 1989*) parameterizes land surface processes; it was developed to be

included within large scale meteorological models. The ISBA Ags model (*Calvet et al., 1998*) improved the canopy stomatal conductance and the CO₂ concentration with respect to the ISBA original model.

Among the first category, few methodologies to calculate ET have taken advantage of the complementary relationship. This relationship establishes a balance among ET, the potential evaporation (E_{pot}) and the wet environment evapotranspiration (E_w). Hence, understanding this type of balance requires the revision of the concepts and variables involved. For instance, ET can be driven by three sets of variables, i.e. the surface variables, the atmospheric variables and the available energy variables. In other words, ET is limited by a combination of all these variables. The concept of E_w suggests that the surface temperature and wetness are unlimited while the energy available for evaporation is limited. The concept of E_{pot} represents an extreme situation, where the surface is considered saturated, the net radiation is at its maximum and the air is dry, i.e there is no limitation for the evapotranspiration.

Bouchet (1963) proposed the first complementary model based on an experimental design. He postulated that regional ET could be estimated as a complementary function of the E_{pot} and E_w, for a wide range of available energy. The first complementary derivation has been the subject of many studies and discussions, mainly due to its empirical background. Examples of successful models based on Bouchet's heuristic relationship include those developed by *Brutsaert and Stricker (1979)*; *Morton (1983)* and *Hobbins et al. (2001)*. These models have been extensively applied to a wide range of surface and atmospheric conditions (*Brutsaert and Parlange, 1998*; *Kahler and Brutsaert, 2006*).

The foundations of the complementary relationship are the basis for operational estimates of ET by *Morton (1983)* to formulate the complementary relationship areal evapotranspiration (CRAE) models. The reliability of the CRAE model was tested with comparable long-term water budget estimates for 143 river basins in North America, Africa, Ireland, Australia and New Zealand.

A procedure to calculate ET requiring only common meteorological data was presented by *Brutsaert and Stricker (1979)*. Their Advection-Aridity approach (AA) is based on a conceptual model involving the effect of the regional advection on potential evaporation and Bouchet's complementary model. Thus, the aridity of a region is deduced from the regional advection of the drying power of air. The authors validated their model in a rural watershed finding good agreements with daily ET estimated with the energy budget method.

The CRAE model (*Morton, 1983*) and the Advection-Aridity (AA) model (*Brutsaert and Stricker, 1979*), were evaluated against independent estimates of regional evapotranspiration derived from long-term, large-scale water balances (1962–1988) for 120 minimally impacted basins in the conterminous United States. The results suggested that the CRAE model overestimates annual evapotranspiration by 2.5% of mean annual precipitation, and the AA model underestimates annual evapotranspiration by 10.6% of precipitation. Generally, higher humidity leads to decreasing absolute errors for both models, and higher aridity leads to increasing overestimation by the CRAE model and underestimation by the AA model, with the exception of high, arid basins, where the AA model overestimates evapotranspiration (*Hobbins et al., 2001*).

Morton's CRAE model was tested by *Granger and Gray (1990)* for field-sized land units under a specific land use, for shorter time intervals. They examined the CRAE

model with respect to the algorithms used to describe different terms and its applicability to reduced spatial and temporal scales. The assumption in CRAE that the vapor transfer coefficient is independent of the wind speed may lead to appreciable errors in computing evapotranspiration. Comparisons between ET estimates and ET measurements obtained from soil moisture and precipitation observations in the semi-arid, cold-climate Prairie region of western Canada demonstrate that the assumptions that the soil heat flux and storage terms are negligible, lead to large overestimation by the model during periods of soil thaw (*Granger and Gray, 1990*).

Three evapotranspiration models based upon the complementary relationship approach for estimating areal ET were evaluated by *Xu and Singh (2004)*. The tested models were the CRAE model of Morton, the advection– aridity (AA) model of Brutsaert and Stricker, and the Granger and Gray model (GG) that introduced the concept of relative evaporation. ET estimates were compared in three study regions representing a large geographic and climatic diversity: the NOPEX region in Central Sweden (cool temperate, humid), the Baixi catchment in Eastern China (subtropical, humid), and the Potamos tou Pyrgou River catchment in Northwestern Cyprus (semiarid to arid). The calculation was made on a daily basis and comparisons were made on monthly and annual bases. The results showed that when using original parameter values all three complementary relationship models worked reasonably well for the temperate humid region, while the predictive power decreased for regions of increasing soil moisture control, i.e. increasing aridity. In such regions, the parameters needed to be calibrated.

Granger (1989) developed a physically based complementary relationship after a meticulous analysis of potential evaporation concepts. The author used the term “potential evaporation” for the E_{pot} and E_w concepts, and clearly presented the

complementary behavior of common potential evaporation theories. The use of two potential evaporations, i.e. E_{pot} and E_w , seemed to generate a universal relationship, and therefore universal ET models. Conversely, attempting to estimate ET from only one potential formulation may need site-specific calibration or auxiliary relationships. In addition, the relative evaporation coefficient introduced by *Granger and Gray (1989)* enhances the complementary relationship with a dimensionless coefficient that yields a simpler complementary model.

The common thread among available complementary ET models is the use of Penman or Penman-Monteith equation (*Monteith and Unsworth, 1990*) to estimate E_{pot} . Specifically, Morton's CRAE model (*Morton, 1983*) uses Penman equation to calculate E_{pot} , and a modified P-T equation to approximate the wet environment evapotranspiration (E_w). *Brutsaert and Stricker (1979)* developed their AA model using Penman for E_{pot} and the P-T equilibrium evaporation to model E_w .

At the time those models were developed, networks of meteorological stations constituted the main source of atmospheric data, while the surface temperature or the soil temperature were available only at some locations around the World. The advent of satellite technology provided routinely observations of the surface temperature (T_s), but the source of atmospheric data was still ancillary. Thus, many of the current remote sensing approaches were developed to estimate ET with little amount of atmospheric data (*Price, 1990; Gillies et al., 1997; Jiang and Islam, 1999; Nishida et al., 2003*).

The recent introduction of the Atmospheric Profiles Product derived from MODIS sensors onboard of EOS-Terra and EOS-Aqua satellites is a significant advance for the scientific community. The MODIS Atmospheric profile product (MOD07 and MYD07) provides atmospheric and dew point temperature profiles on a daily basis at 20 vertical

atmospheric pressure levels and at 5x5km spatial resolution (*Menzel et al., 2002*). When combined with readily available land surface temperature (Ts) maps obtained from different sensors, this new remote source of atmospheric data provides a new opportunity to revise the complementary relationship concepts that relate ET and E_{pot}.

In addition, *Crago and Crowley (2005)* validated the complementary relationships at very short time scales (10-30 min). They published promising results that encourage the exploration of nearly instantaneous remotely sensed data and complementary models.

1.2 Bouchet and Granger's Models

Before describing the proposed method (next Chapter), a review of complementary relationships is provided here.

Bouchet (1963) conducted an experiment over a large homogeneous surface without advective effects. The surface was initially saturated and evaporated at potential rate. With time, the region dried but a small parcel was kept saturated, evaporating at the potential rate. The region and the parcel scales were such that the atmosphere could be considered stable. Thus, the author postulated that, as a well-watered surface dries, the decrease in ET is equal to the increase in E_{pot}. *Morton (1969)* utilized Bouchet's experiment to formally derive the following complementary relationship,

$$ET + E_{pot} = 2 E_w \quad (1)$$

where E_w is referred to as the wet-environment evapotranspiration, the evaporation that occurs when $ET = E_{pot}$. This relationship assumes that as ET increases, E_{pot} decreases by the same amount, i.e. $\delta ET = -\delta E_{pot}$, where the symbol δ means small variations. Bouchet's equation has been widely used in conjunction with Penman's

equation and Priestley-Taylor's equation (*Brutsaert and Stricker, 1979; Morton, 1983; Hobbins et al., 2001*).

After revising the diversity of potential evaporation concepts, *Granger (1989)* argued that the above relationship lacked a theoretical background, mainly due to Bouchet's assumption that $\delta ET = -\delta E_{pot}$. In order to derive a physically based complementary relationship between ET, E_w and E_{pot} , *Granger (1989)* proposed the inequality $E_{pot} \geq E_w \geq ET$ and demonstrated the following relationship:

$$ET + E_{pot} \frac{\gamma}{\Delta} = E_w \left(\frac{\Delta + \gamma}{\Delta} \right) \quad (2)$$

where γ is the psychrometric constant and Δ is the slope of the saturation vapor pressure (SVP) curve.

In equation (2), E_w is not the average of E_{pot} and ET. It can be easily verified that equation (2) is equivalent to equation (1) when $\gamma = \Delta$. The condition that the slope of the SVP curve equals the psychrometric constant is only true when the temperature is near 6 °C (*Granger, 1989*).

Granger and Gray (1989) proposed their ET model for unsaturated surfaces following the combination approach and the relative evaporation (the ratio of ET to E_{pot}) concept. The relative evaporation expression proposed by the authors is,

$$GG = \frac{ET}{E_{pot}} = \frac{f_u (e_s - e_a)}{f_u (e_s^* - e_a)} \quad (3)$$

where f_u is a function of the wind speed and the vegetation height, e_s is the surface actual vapor pressure, e_a is the air actual vapor pressure and e_s^* is the surface saturation vapor pressure.

Equation (3) was proposed based on Dalton's equations (*Granger, 1989*), simulating ET as the actual surface-air vapor pressure deficit and E_{pot} as the potential surface-air vapor pressure deficit if the surface is saturated. Both, actual and potential vapor pressure deficits are corrected by the same wind speed function, suggesting that its effect on E_{pot} and ET cancels out.

In order to estimate GG from readily available meteorological data, Granger and Gray pointed out that, as ET increases, the vapor pressure of the air also increases. Then, they assumed that the drying power of air, $E_a = f_u (e_a^* - e_a)$, reflects the drying process of the surface, suggesting that ET from a nonsaturated surface is a function of E_a.

The ratio ET/E_{pot} was empirically related to the relative drying power, $D = E_a / (E_a + Q)$, where $Q = R_n - G$ is the energy available from the net radiation (R_n) and the soil heat flux (G). The estimation of GG is complex and may require site-specific calibration because it was postulated based on relatively few measurements (*Granger and Gray, 1989*). In addition, the surface water condition is not represented in this parameterization of GG, although a vegetation cover index was included later on.

The relative evaporation coefficient was used in combination with equation (2) to obtain Granger's ET model (*Granger, 1989*). Even though the Granger and Gray's expression for GG is not physically based, the application of the relative evaporation to abridge equation (2) is very useful. For instance, *Crago and Crowley (2005)* recently provided an empirical validation of equation (2) and found promising results. These authors published a comparison of Bouchet and Granger's complementary approaches at small time scales (10–30 min) with point measurements, using data from four field experiments. A combination of Granger's complementary model with Penman and P-T equations performed very well. A combination of Bouchet and Granger's complementary

model, where E_{pot} was modeled with the mass transfer equation and E_w with P-T equation illustrates that Granger's complementary relationship provides more accurate ET estimates, being significantly different from the original relationship of Bouchet. The conclusion of their work is that the complementary approach appears to remain viable, especially in remote sensing applications with distributed data.

1.3 Objectives of this Thesis

The objective of this thesis was to derive a new method to estimate spatially distributed EF and ET maps from remotely sensed data without using auxiliary relationships such as those relating a vegetation index (VI) with the land surface temperature (Ts) or site-specific relationships. A premise was to obtain a model with a minimum number of parameters and they are universally related to the variables involved.

This new method for computing ET is based on Granger's complementary relationship and the P-T equation. The proposed approach could be applicable to different surface wetness conditions and scales. As previously mentioned, the recent availability of new remote sensing products allowed to resort to the complementary relationship concept that was not being extensively considered in the literature recently. The method and its application were already submitted and accepted for publication (*Venturini et al., 2007*). See Appendix I.

1.4 Thesis Outline

This thesis is organized as follows:

Chapter 1 provides an overview of the current state of knowledge for evapotranspiration estimation. Complementary models are reviewed in detail, as they are a key to the new calculation methodology described in Chapter 2. Chapter 3 presents the

model application, including the model validation. An uncertainty analysis was performed to quantify model errors and uncertainties due to most common errors in measurements of the involved variables. These results are described in Chapter 4. A comparison between modified P-T equations is discussed in Chapter 5. Conclusions and future work are outlined in Chapter 6.

Chapter 2 : Methodology.

2.1 ET Model

As discussed in Chapter 1, complementary models balance three evapotranspiration concepts in a single equation. There are well known ET methodologies that were derived from the modeling of each term of a complementary relationship (*Brutsaert and Stricker 1979; Morton 1983; Hobbins et al. 2001*), however the complementary equation can be simplified to establish a relationship between only ET and E_w . The proposed method uses Granger's methodology, particularly the relative evaporation expression, to abridge equation (2). Simplifying equation (2) by introducing the relative evaporation concept would render an expression for ET as a function only of one potential evaporation concept, E_w . Furthermore, the advantage of using the ratio ET/E_{pot} (see equation 3), is that eliminating the wind speed function and resistance factors reduces the uncertainty and complexity of the ET calculation. Thus, ET is expressed as a function the relative evaporation and E_w , which is simulated with P-T model, as it will be shown in this Chapter.

A key difficulty in applying equation (3) lies with the estimation of $(e_s - e_a)$, since there is no simple way to relate e_s to any readily available surface temperature. Thus, a new temperature should be defined.

From the remote sensing standpoint, the surface is a mixture of soil and vegetation. There are two common models to represent a heterogeneous pixel, i.e. one-source and two-source surfaces. The first type represents the surface as homogenous where soil and vegetation processes taking place are not considered separately. In the two-source model, soil and vegetation processes are distinguished and split. In this work, the pixel is

simulated as homogeneous, i.e. the first case is applied. Thus, soil evaporation is not separated from the vegetation transpiration, even though both processes are very different. The factors controlling the soil evaporation and plant transpiration are certainly not the same, however both combined as ET affects the surface temperature (T_s). The cooling effect of ET is observable in T_s , which generates an aggregated surface thermal signal (Sandholt *et al.*, 2002; Sun and Pinker, 2004).

Many studies have used temperature as a surrogate for vapor pressure (Monteith and Unsworth, 1990; Nishida *et al.*, 2003). Although the relationship between vapor pressure and temperatures is not linear, it is commonly linearized for small temperature differences. Hence, e_s and e_s^* could be related to soil+vegetation temperature that would account for water vapor pressure. Figure 2.1 shows the relationship between e_s , e_s^* and e_a and their corresponding temperatures; where e_u^* is the surface saturation vapor pressure at an unknown surface temperature T_u .

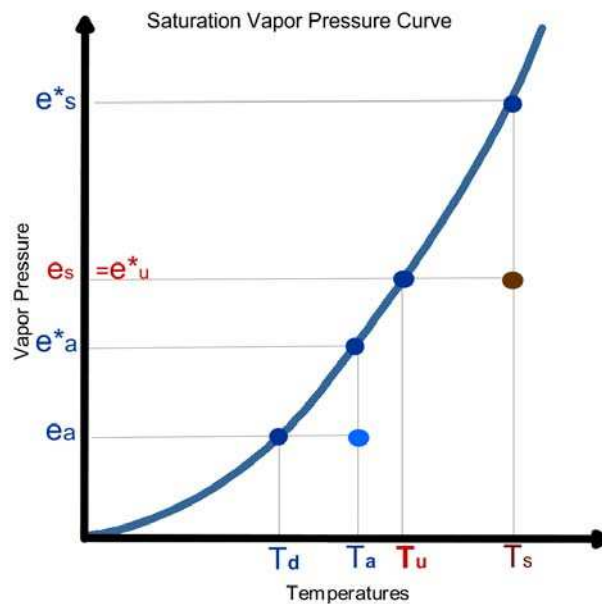


Figure 2.1: Sketch of the saturation vapor pressure curve and the relationship among T_u , T_s , e_s and e_u^* in the context of surface at temperature T_s . The overlying air is characterized by T_a and T_d and vapor pressure e_a .

An analogy to the dew point temperature concept (T_d) suggests that T_u would be the temperature of the surface if it is brought to saturation without changing the actual surface vapor pressure. Thus, T_u must be lower than T_s if the surface is not saturated and close to T_s if the surface is saturated. Consequently, e_s could be derived from the temperature T_u . Although T_u may not possibly be observed in the same way as T_d , it can be derived, for instance, from the slope of the exponential SVP curve as a function of T_s and T_d . This calculation is further discussed later in this chapter.

Assuming that the surface saturation vapor pressure at T_u would be the actual soil vapor pressure and that the SVP can be linearized, $(e_s - e_a)$ can be approximated by $\Delta_1(T_u - T_d)$ where Δ_1 is the slope of the linearized SVP curve between T_d and T_u , and $(e_s^* - e_a)$ by $\Delta_2(T_s - T_d)$, where Δ_2 is the slope of the linearized SVP curve between T_d and T_s . Figure 2.2 shows a schematic of these concepts.

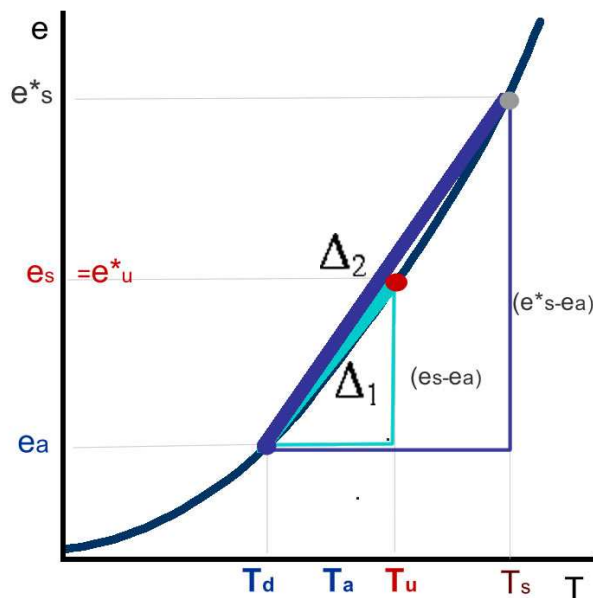


Figure 2.2: Schematic of the linearized saturation vapor pressure curve and the relationship between $(e_s - e_a)$ and $\Delta_1(T_u - T_d)$, and $(e_s^* - e_a)$ and $\Delta_2(T_s - T_d)$.

Therefore ET/Epot (see equation 3) can be rewritten as follows:

$$F \cong \left(\frac{f_u}{f_u} \right) \frac{(T_u - T_d)}{(T_s - T_d)} \left(\frac{\Delta_1}{\Delta_2} \right) \quad (4)$$

The new coefficient, F, is the fraction of the actual water vapor deficit over the potential water vapor deficit.

As previously mentioned, the wind function, f_u , depends on the vegetation height and the wind speed and it is independent of surface moisture. In other words, it is reasonable to expect that the wind function will affect ET and Epot in a similar fashion (*Granger, 1989*). The slopes of the SVP curve, Δ_1 and Δ_2 , can be computed from the SVP first derivative at Td and Ts without adding further complexity to this method. However, Δ_1 and Δ_2 will be assumed approximately equal from now on, as they will be estimated as the first derivative of the SVP at Ta. Thus, equation (4) may be approximated as:

$$F \cong \frac{ET}{Epot} \cong \frac{(T_u - T_d)}{(T_s - T_d)} \quad (5)$$

The relationship between Ts and Tu can be examined from the definition of Tu, that represents the surface saturation at e_s . For a saturated surface, Tu is expected to be very close or equal to Ts, in contrast, for a dry surface Ts would be much larger than Tu.

Since Epot is larger than or equal to ET, F ranges from 0 to 1. For a dry surface with $T_s \gg T_u$, $T_s - T_d$ would be larger than $T_u - T_d$ and $ET/Epot$ would tend to 0. In the case of a saturated surface with e_s close to e_s^* and Ts close to Tu, the difference $T_s - T_d$ would be similar to $T_u - T_d$ and $ET/Epot$ would tend to 1.

In order to estimate ET with equation (2), one needs to compute Ew. Granger's complementary model was derived using Penman's concept of potential evaporation, which was interpreted as Ew. In the proposed method, the P-T equation is used to

approximate E_w , while E_{pot} is estimated from the bulk water vapor mass transfer equations, hence the inequality $E_{pot} > E_w > E_T$ holds true (*Granger, 1989*).

The actual E_T for any surface condition is obtained combining equations (2), (5) and the P-T equation (equation 6)

$$E_w = \alpha (R_n - G) \frac{\Delta}{\Delta + \gamma} \quad (6)$$

$$E_{pot} = E_T/F \quad (7)$$

By introducing equation (7) in equation (2) one obtains:

$$E_T \left(1 + \frac{\gamma}{F\Delta} \right) = E_w \left(1 + \frac{\gamma}{\Delta} \right) \quad (8)$$

By substituting E_w by equation (6)

$$E_T \left(1 + \frac{\gamma}{F\Delta} \right) = \alpha \left(\frac{\Delta}{\Delta + \gamma} \right) (R_n - G) \left(1 + \frac{\gamma}{\Delta} \right) \quad (9)$$

$$E_T \left(\frac{F\Delta + \gamma}{F\Delta} \right) = \alpha (R_n - G) \quad (10)$$

$$E_T = \alpha \left(\frac{F\Delta}{F\Delta + \gamma} \right) (R_n - G) \quad (11)$$

where α is the P-T parameter for saturated surfaces. Table 2.1 summarizes symbols, definitions and units of the variables used in this derivation.

Equation (11) invokes the P-T assumption that the main driving force for E_T is the available radiant energy, $(R_n - G)$.

It is worth noting that *Eichinger et al. (1996)* analytically derived an expression for the parameter α . These authors distinguished expressions for α for saturated and unsaturated surfaces. For the last type of surfaces, they stated that α is a function of the same variables involved in F , i.e. e_s , e_s^* and e_a . Although α can be calculated analytically,

the empirical value of $\alpha=1.26$ proposed by *Priestley and Taylor (1972)* for saturated surfaces is used in the proposed method. Therefore, the form of equation (11) used from now on is,

$$ET = 1.26 \left(\frac{F\Delta}{F\Delta + \gamma} \right) (R_n - G) \quad (12)$$

Equation (11) was also derived by *Barton (1979)*, who extended the Priestley-Taylor's approach for unsaturated surfaces. Barton extended the P-T equation by introducing an additional parameter that was empirically related to the soil moisture content derived from satellite microwave sensors. At that time, limited amount of microwave data were available and the methodology was presented and validated with few measurements. Barton followed Penman's combination formula and defined the relative humidity right at the evaporating surface as $\sigma = e_s/e_s^*$. Then, a combination of the surface energy balance, the Bowen ratio (H/ET) and σ yields the same modified P-T equation as equation (11) if F is replaced by σ . Thus, Barton's equation and the proposed model not only differ on the theory behind them, but also on F and σ concepts and parameterization.

Table 2.1: Table of symbols and units.

Symbol	Definition
α	Priestley and Taylor's coefficient. $\alpha = 1.26$
Δ hPa/°C	Slope of the saturation water vapor pressure curve
γ hPa/°C	Psychometric constant
λE [W m ⁻²]	Latent heat flux
σ	Relative humidity as defined by Barton
$B = H/\lambda E$	Bowen Ratio
e_a [hPa]	Air actual water vapor pressure, function of Td
e_a^* [hPa]	Air saturation water vapor pressure, function of Ta
e_s [hPa]	Surface actual water vapor pressure, function of Tu
e_s^* [hPa]	Surface saturation water vapor pressure, function of Tu
e_u^* [hPa]	Surface saturation water vapor pressure, function of Tu. Equal to e_s
E_a [W m ⁻²]	Drying power of the air
ET [W m ⁻²]	Actual evapotranspiration
E_w [W m ⁻²]	Evapotranspiration of wet environment
E_{pot} [W m ⁻²]	Potential evapotranspiration
F	Proposed relative evaporation coefficient
GG	Grager and Gray's relative evaporation coefficient
G [W m ⁻²]	Soil heat flux
H [W m ⁻²]	Sensible heat flux
Q [W m ⁻²]	Available energy, ($R_n - G$)
R_n [W m ⁻²]	Net radiation at the surface
T_a [°K] or [°C]	Air temperature
T_d [°K] or [°C]	Dew temperature
T_s [°K] or [°C]	Surface temperature
T_u [°K] or [°C]	Surface temperature if it is brought to saturation without changing the surface actual vapor pressure

A key advantage of this simple formulation is that it is physically based and is expected to hold true for a range of atmospheric and surface conditions. This new model considers the air and the surface actual vapor pressure, making it applicable to a wide

range of vegetation coverages and surface wetnesses under varying air conditions (as shown in Chapter 3). The advection factor, imbedded in the wind function f_u , is considered in F as it would affect ET as well as E_{pot} . Hence, it is not explicitly included in this present derivation.

The spatial scales involved in this method must be analyzed in the context of the background concepts. In his complementary method, *Granger (1989)* defined the surface as “*a surface of sufficient size such that there are no significant inputs of energy by local advection*”. The same definition is applied in the P-T theory (*Priestley and Taylor, 1972*). So the main hypothesis is that of a homogenous-advection-free surface. The assumptions made in these theories imply that ET is a convective-diffusive process. The exchange of water vapor between the surface and the atmosphere is driven by the available energy, as suggested by P-T.

On the other hand, the relative evaporation calculation is based on the bulk water vapor mass transfer theory. It was shown that it is applicable to parcel-size scales, where the local surface and atmospheric conditions are driving factors (*Granger, 1989*). In practice, the estimation of ET is the result of the available radiant energy and the local atmospheric-surface conditions. ET estimates are the result of correcting the main regional ET by the local conditions found at the pixel scale.

The method proposed in this thesis is also expected to be applicable for a wide range of spatial scales. Large scales can be studied from spatially distributed remotely sensed data in the same manner that small scales can be investigated from ancillary sources of data.

2.2 Proposed Method to Estimate T_u

In order to fully determine F , and later on ET , a methodology to estimate T_u must be developed. Before deriving a methodology to estimate T_u , antecedent studies and methods are revised.

A similar T_u concept was proposed by *Jackson et al. (1988)*, *Moran and Jackson (1991)* and *Carlson et al. (1995)* to estimate the water deficit index or ET from the so-called Trapezoidal Space defined by T_s and vegetation indexes (VI). For instance, the minimum temperature observed in each VI class represents the maximum soil moisture or evapotranspiration in the study region. Based on the triangle T_s - VI space, *Jiang and Islam (1999)* adopted the mean in-land water temperature to represent the regional equilibrium evaporation. The minimum temperatures in the T_s - VI space assume that each pixel within a VI class can reach the saturation point at the same T_s . In the T_s - VI space, the geographic location of the pixel is lost and different vegetation and land cover types could be hidden in the VI class. The normalized difference vegetation index ($NDVI$) is probably the most widely VI used to generate the T_s - VI space. Figure 2.3 shows an example of the T_s - $NDVI$ space and the triangle bounds, where the upper and lower limits enclose all the pixels of an image. The minimum temperature (T_{min}), associated to the lower bound, is the same along the $NDVI$ axis, as proposed by *Jiang and Islam (2001)*. On the other hand, the maximum temperature (T_{max}) for each $NDVI$ is not constant. Although T_{min} is not necessarily constant, i.e. it can vary for every $NDVI$ class, it is commonly assumed constant for ET calculation.

By definition, different types of soils and water content would render different T_u values. Hence, from the above discussion it seems reasonable to estimate T_u from the

pixel-local variables or from the atmospheric and surface vapor pressure deficits. In this thesis, it is proposed to estimate the key variable T_u from the SVP curve.

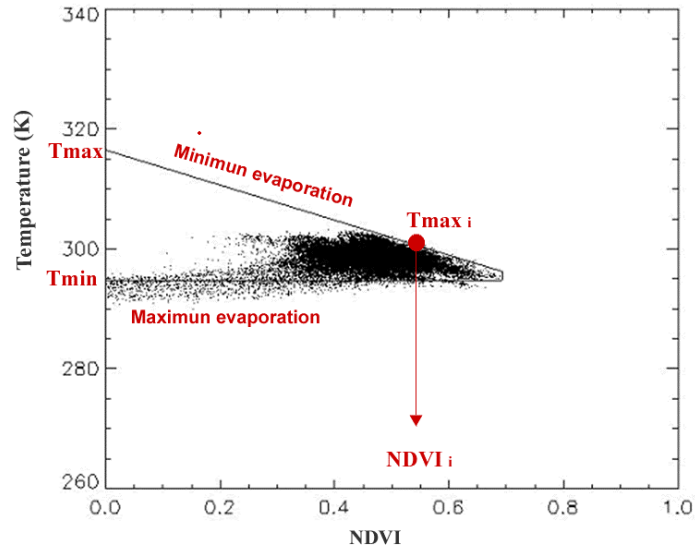


Figure 2.3: Ts-NDVI Triangle space with upper and lower bounds, where T_{min} is the in-land water temperature and T_{max} is the temperature of a dry bare surface.

The concept of T_d assumes an adiabatic process where the temperature exchange is fast enough to preserve the energy. A similar adiabatic process is implicit in the T_u concept, since its definition is analogous to that of T_d . Consequently, it can be assumed that e_s is larger or equal to e_a and lower or equal to e_s^* , thus T_u must lie between T_s and T_d . Even for the case of highly vegetated areas, the soil+vegetation surface tends to be at higher temperature than the air. In addition, the water vapor in the air is subject to fewer forces than in the surface.

The first derivative of the SVP curve at T_d , [equation (13)] and at T_s , [equation (14)] represents the SVP slope at those points. It can also be computed approximately from the linearized SVP curve between the intervals $[T_u, T_s]$ and $[T_d, T_u]$, which are

symbolized as Δ_1 and Δ_2 , respectively (see Figure 2.4) . Thus, an expression for T_u is derived from a simple system of two equations with two unknowns, as follows,

$$\Delta_1 = \frac{e_s - e_a}{T_u - T_d} = \left. \frac{d(\text{SVP})}{dT} \right|_{T_d} \quad (13)$$

$$\Delta_2 = \frac{e_s^* - e_s}{T_s - T_u} = \left. \frac{d(\text{SVP})}{dT} \right|_{T_s} \quad (14)$$

Equations (13) and (14) form a system where T_u and e_s are the unknowns. An equation to estimate T_u is obtained by solving the system, thus

$$T_u = \frac{(e_s^* - e_a) - \Delta_1 T_s + \Delta_2 T_d}{\Delta_2 - \Delta_1} \quad (15)$$

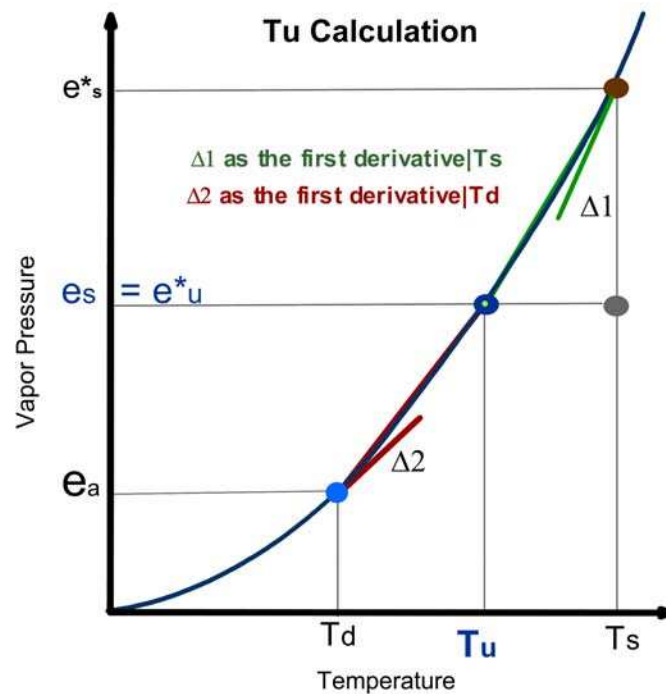


Figure 2.4: Sketch with T_u derivation from the saturation vapor pressure curve.

Several exponential functions that relate SVP and temperature have been compared, i.e. *Murray (1967)*; *Bolton (1980)*; and *Buck (1981)*. Any of these parameterizations

would be applicable for this study. Equation (16), corresponding to Buck's formulation, was chosen because of its simple form,

$$e = 6.1121 \exp\left(\frac{17.502 T}{240.97 + T}\right) \quad (16)$$

where e is water vapor pressure [hPa] and T is temperature [°C].

In order to apply equation (15), the first derivative of Buck' function is obtained,

$$\frac{de}{dT} = \left[\frac{421.45694}{(240.97 + T)^2} \right] * 6.1121 \exp\left(\frac{17.502 T}{240.97 + T}\right) \quad (17)$$

Then, the slope Δ_1 is estimated solving equation (17) at T_d and the slope Δ_2 is estimated at T_s . With these two values, a first estimate of T_u is calculated. In this first calculation, a large segment of the SVP curve is linearized; so the process is iterated by re-calculating Δ_2 with this first value of T_u and computing a new T_u (wich is presented in Figure 2.4). As an example, in Figure 2.5 it can be seen how the air and surface actual vapor pressures relate to the corresponding temperatures for a given day. The e_a and e_s curves present little superposition, suggesting large $e_s - e_a$ differences. It should be noted that the air SVP curves are at 2°K off set. The air, violet diamonds, seems to be dry (separated from the SVP curve), while the surface, plotted with black dots, seems to have few wet pixels which are close to the SVP curve.

Although the T_u calculation from the SVP curve may not be physically based, it depicts a natural surface situation (as shown in Figure 2.5). In nature, the air and the surface may have different vapor pressure conditions and a mixture of wet-dry pixels of air and/or surface defines the region.

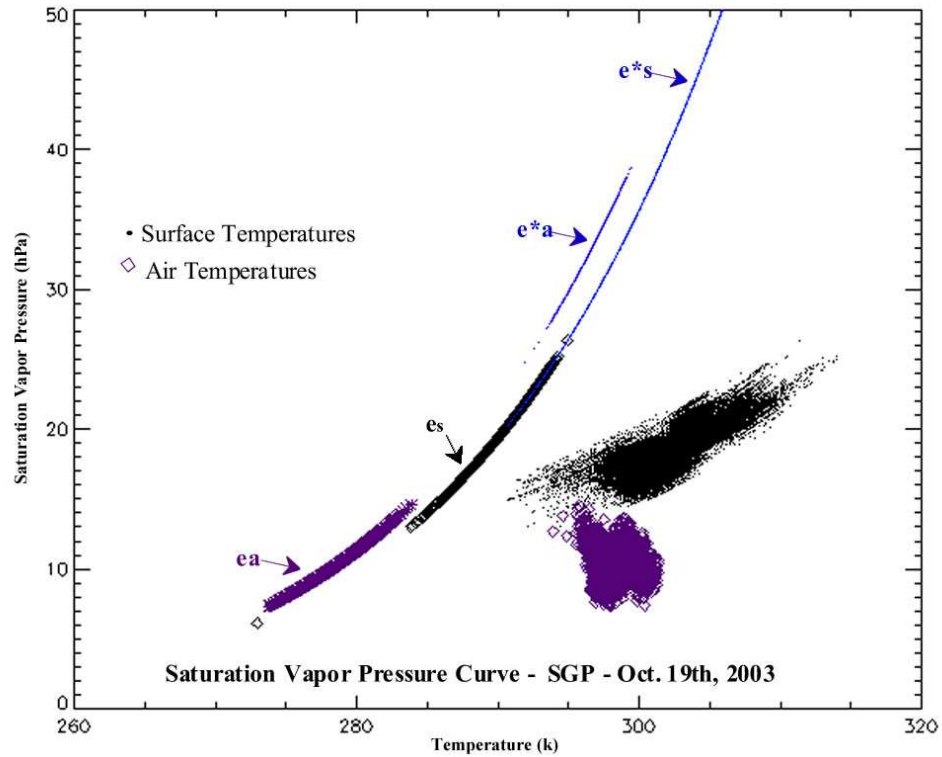


Figure 2.5: Buck's saturation vapor pressure curve. e_a was obtained with T_d , e_s with T_u , e_a^* with T_a and e_s^* with T_s . T_a vs. e_a are shown with violet diamonds and T_s vs. e_s with black dots.

The estimation of T_u could be improved by introducing another surface variable, such as soil moisture. However, in order to demonstrate the strength of this methodology, the T_u calculation is kept simple, with minimum data requirements. However, it is recognized that this calculation simplifies the physical process. The saturation vapor pressure concept assumes a free-water surface, where the forces holding the water molecules to the surface are the bonds among the nearest molecules. These connections are broken by the thermal energy to produce evaporation (*Monteith and Unsworth, 1990*). Therefore, one can infer that, for an unsaturated surface, where multiple forces hold the water to the soil+vegetation surface and where the water is not pure, more thermal energy would be required to vaporize the soil+vegetation water molecules (*Monteith and Unsworth, 1990*). In terms of vapor pressure, e_s for an unsaturated surface would be

smaller than that derived from a SVP curve. It is worthy to note that a more precise inference of e_s will require new parameterizations, which is expected to increase the uncertainties and errors.

It should be emphasized that keeping T_u estimation simple, with minimum data requirement, the potential applicability of this method to remote areas where ground data are not available, increases. In this regard, remote sensors are always a feasible source of data everywhere.

2.3 Bouchet or Granger's Complementary Models?

In Chapter 1, a review of the two complementary models most widely used for ET calculations was presented. Both methods are not only conceptually different, but also differ in their derivations. Mathematically speaking, Bouchet's complementary relationship (equation 18) is presented as a simplification of Granger's complementary equation (equation 19) for the case $\Delta=\gamma$.

$$ET + E_{pot} = kE_w, \text{ where } k=2 \quad (18)$$

$$ET + E_{pot} \frac{\gamma}{\Delta} = E_w \left(\frac{\Delta + \gamma}{\Delta} \right) \quad (19)$$

These equations can also be written as follows,

$$\frac{1}{2}ET + \frac{1}{2}E_{pot} = E_w \quad (20)$$

$$\left(\frac{\Delta}{\Delta + \gamma} \right) ET + \left(\frac{\gamma}{\Delta + \gamma} \right) E_{pot} = E_w \quad (21)$$

Equation (20) clearly expresses E_w as the middle point between ET and E_{pot} . In contrast, equation (21), the re-written Granger's complementary relationship, shows how ET and E_{pot} contribute to E_w with dissimilar coefficients and those coefficients, vary

with the slope of the saturation vapor pressure curve at T_a , since γ is commonly assumed constant.

Recently, *Ramirez et al. (2005)* discussed Bouchet's coefficient $k=2$ with monthly averaged ground measurements. In their application, E_{pot} was calculated with the Penman-Monteith equation and E_w with the P-T model. They concluded that the appropriate coefficient should be slightly lower than 2. Their results may imply that Bouchet's complementary model can be used to find another expression similar to equation (11) to estimate ET. The new equation may also lead to good estimates of instantaneous ET values with remote sensing data, as shown in Chapter 3.

Introducing the relative evaporation $F = ET/E_{pot} = (T_u - T_d)/(T_s - T_d)$ in equation (18),

$$ET + \frac{ET}{F} = k E_w \quad (22)$$

Then E_w was replaced by the P-T equation.

$$ET \left(1 + \frac{1}{F} \right) = k \alpha (R_n - G) \frac{\Delta}{\Delta + \gamma} \quad (23)$$

Thus, ET can be expressed as,

$$ET = k \alpha \left(\frac{F}{F+1} \right) \left(\frac{\Delta}{\Delta + \gamma} \right) (R_n - G) \quad (24)$$

where k is Bouchet's coefficient, typically assumed equal to 2 (*Sugita et al., 2001*).

The underlying assumptions of equation (24) are the same as those behind equation (11), plus the condition that Δ is approximately equal to γ .

An analysis and contrast of equations (11) and (24) is presented in Chapter 3.

Chapter 3 : Model Application.

In absence of needed data in Argentina, the proposed methodology was applied to a region in the United States of America well known for its field data availability for model validation. The model was implemented within a code written in Interactive Data Language (IDL) (*ITT Industries-Solution* ,2005). The complete program is listed in Appendix II.

3.1 Study Area

The Southern Great Plains (SGP) region of the United State of America extends over the State of Oklahoma and southern parts of Kansas, extending in longitude from 95.3° W to 99.5° W and in latitude from 34.5° N to 38.5° N (Figure 3.1 and Figure 3.3). This region was the first field measurement site established by the Atmospheric Radiation Measurement (ARM) Program, at present the ARM program has three experimental sites. Scientists over the World are using the information obtained from this site to improve the performance of atmospheric general circulation models used for climate change research. The SGP was chosen as the first ARM field measurement site for several reasons, among them, its relatively homogeneous geography and easy accessibility, wide variability of climate and surface flux properties, and large seasonal variations in temperature and specific humidity (<http://www.arm.gov/sites/sgp.stm>).

Most of this region is characterized by irregular plains, with a relief of less than 90 m. Elevations range from 490 m to 900 m, increasing gradually from East to West. On these dissected plains, the slopes are short and steep in the valleys. In southwestern

Oklahoma, the Wichita Mountains rise as much as 300 m above the surrounding plains. The climate is semiarid-subtropical. Although the maximum rainfall occurs in summer, high temperatures make summer relatively dry. Average annual temperatures range from 14°C to 18°C. Winters are cold and dry, and summers are warm to hot. The frost-free season stretches from 185 to 230 days. Precipitation ranges from 490 to 740 mm, with most of it falling as rain.

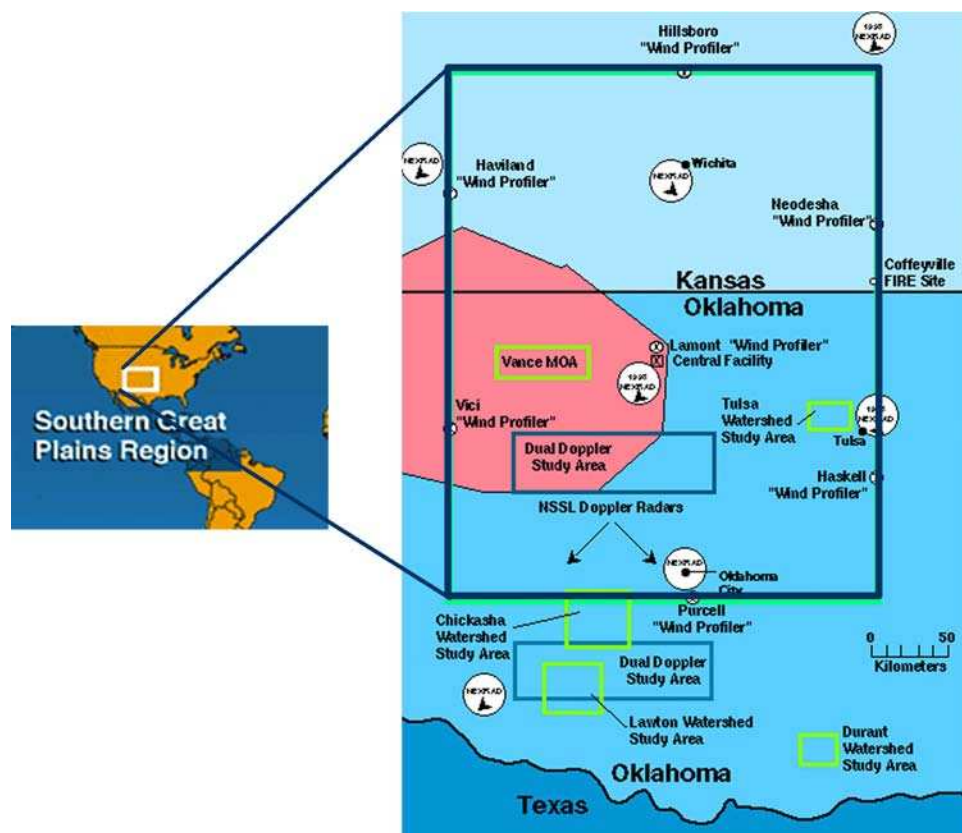


Figure 3.1: The southern Great Plains location and extension.

Grass is the dominant prairie vegetation. Most of it is moderately high and usually grows in bunches. The most prevalent type of grassland is the bluestem prairie, along with many species of wildflowers and legumes. In many places where grazing and fire

are controlled, deciduous forest is encroaching on the prairies. Due to generally favorable conditions of climate and soil, most of the area is cultivated, and little of the original vegetation remains. Oak savanna occurs along the east border of the region and along some of the major river valleys.

3.2 Ground Data Availability

The first instrumentation to the SGP site took place in 1992 and data processing capabilities have been incrementally added in succeeding years. This region has relatively extensive and well-distributed coverage of surface flux and meteorological observation stations. In this study, Energy Balance Bowen Ratio stations (EBBR), maintained by the Atmospheric Radiation Measurement (ARM) program are used for the validation of surface fluxes.

The EBBR system produces 30 min estimates of the vertical fluxes of sensible and latent heat at the local surface. Flux estimates are calculated from observations of net radiation, soil surface heat flux, and vertical gradients of temperature and relative humidity. Meteorological data collected by these stations are used to calculate bulk aerodynamic fluxes. A picture of the station setting is presented in Figure 3.2. The instruments listed below conform the EBBR system

- Vaisala Temperature/Relative Humidity probes at two heights (1 m separation), in aspirators
- PRTD temperature probes at two heights (1 m separation), in aspirators
- REBS Q*7.1 Net Radiometer (at 2 m typical)
- REBS SMP-2 (5 sets) Soil Moisture Probes at 2.5 cm depth

- REBS HFT-3 (5 sets) Soil Heat Flow Plates at 5 cm depth
- REBS STP-1 (5 sets) Soil Temperature Probes, integrated 0 to 5 cm
- Met One Instruments 090C or 090D Barometric Pressure sensor (in enclosure)
- Met One 020C Wind Direction sensor at 2.5 m
- Met One 010C Wind Speed sensor at 2.5 m
- PRTD Reference temperature of control box
- Pipe network structure for instrumentation mounting
- Automatic Exchange Mechanism (AEM). The AEM helps to reduce errors from the net radiometer offset drift
- Solar panel, battery, AC charger power source
- Enclosure holding Campbell CR10, multiplexers, J-panels, communication equipment.

The accuracies cited below are generally those specified by the manufacturer. The detection limit is normally restricted to the range (sometimes called Calibrated Operating Range) over which the accuracy applies. Some manufacturers also specify an Operating Temperature Range, in which the sensor will function both, physically and electronically, even though the calibration may not be appropriate for use throughout that range.

Air temperatures: Chromel-constant thermocouple, Omega Engineering Inc., REBS Model # ATP-1, Detection Limits -30 to 40°C, Accuracy +/- 0.5°C.

Temperature/Relative Humidity (RH) Probe: Operating Temperature Range -20 to 60°C. Temperature: Platinum Resistance Temperature Detector (PRTD); Detection Limits -30 to 40°C, Accuracy +/- 0.2°C RH: Capacitive element, Vaisala Inc., Model #s HMP 35A and HMP 35D; Detection Limits 0% to 100% RH, Accuracy +/- 2% (0-90% RH), +/- 3% (90-100%), uncertainty of RH calibration +/- 1.2%.

Soil Temperature: Platinum Resistance Temperature Detector, MINCO Products, Inc., REBS Model # STP-1, MINCO Model # XS11PA40T260X36(D), Detection Limits -30 to 40°C, Accuracy +/- 0.5°C.

Soil Moisture: Soil Moisture Probe (fiberglass and stainless steel screen mesh sandwich), Soiltest, Inc., REBS Model # SMP-2, Soiltest Model # MC-300, Accuracy not specified by manufacturer (varies significantly depending on soil moisture and soil type). Detection limits for this sensor are limited by the ability to fit a polynomial to the calibration data; for the SGP site, the detection limits are approximately 1% to 50% by volume.

Soil Heat Flow: Soil Heat Flow Probes, Radiation & Energy Balance Systems, Inc., Model #s HFT-3, HFT3.1, Accuracy not specified by manufacturer.

Barometric Pressure: Barometric Pressure Sensor, Met One Instruments, Model #s 090C-24/30-1, Detection Limits 24 to 30 kPa; 090C-26/32-1, Detection Limits 26 to 32 kPa; 090D-26/32-1, Detection Limits 26 to 32 kPa; Accuracy for all +/- 0.14 kPa.

Net Radiation: Net Radiometer, Radiation & Energy Balance Systems, Inc., Model Q*6.1 or Q*7.1, Accuracy +/- 5% of full-scale reading.

Wind Direction: Wind Direction Sensor, Met One Instruments, Model #s 5470, 020C, Detection Limits 0 to 360° physical (for greater than 0.3 ms⁻¹ wind speed), 0 to 356° electrical, Accuracy +/- 3°.

Wind Speed: Wind Speed Sensor, Met One Instruments, model #s 010B and 010C, Operating Temperature Range -50 to 85°C, Detection Limits 0.27 to 50 ms⁻¹, Accuracy +/- 1% of reading. Operational Limit on speed 60 ms⁻¹.

Datalogger: Campbell Scientific, Inc., Model CR10, Detection Limits vary by voltage range selected, Accuracy +/- 0.1% of full scale reading.

The Bowen ratio stations use a standard Bowen ratio approach that is described in *Brutsaert (2005)*. A brief description of this approach is presented here:

The surface energy balance equation is:

$$R_n + G + H + \lambda E = 0 \quad (25)$$

where each variable and its corresponding units can be found in Table 2.1, in Chapter 2.

G is estimated with five sets of soil heat flow, soil temperature, and soil moisture probes. Soil heat flow at 5 cm (shf1, shf2, shf3, shf4 and shf5) measured with soil heat flow plates and soil energy storage (ces1, ces2, ces3, ces4 and ces5) in the 0-5 cm layer (measured as the change in temperature with time) are added to obtain surface soil heat flow, i.e. $g_1 = \text{shf1} + \text{ces1}$. The expressions for g_2 , g_3 , g_4 , and g_5 are similar, where shf1 and ces1 are, respectively, the soil heat flow from the soil heat flow plate and the change in energy storage measured from the soil temperature probe of soil set #1. Soil moisture is used to adjust the measurements for soil thermal conductivity, which affects the calibration of the sensors. The surface soil heat flow is $G = [(g_1 + g_2 + g_3 + g_4 + g_5)/5]$.

When data from one or more soil set(s) is incorrect, that soil set(s) can be eliminated and the average soil heat flow determined from the remaining sets.

The Bowen ratio, B, is measured as the ratio of the temperature gradients and vapor pressure (the latter calculated from the relative humidity RH and temperature) across two fixed heights within three meters of the surface. Then, $B = H/\lambda E$ is computed on the basis of the gradients and the following computations are performed:

$$\lambda E = -(R_n + G)/(1 + B) \quad \text{and} \quad H = B * \lambda E \quad (26)$$

The latent heat data was obtained through the ARM program Web site (<http://www.arm.gov>). The ARM instruments and measurement applications are well established and have been used for validation purposes in many studies (*Fritschen and Simps, 1989; Heilman and Britti, 1989; Shuttleworth, 1991; Halldin and Lindrot, 1992; Lewis 1995*). The stations are widely distributed over the whole domain as shown in Figure 3.3. The site and name, elevation, geographic coordinates (latitude and longitude) and surface type of the stations used in this thesis are shown in Table 3.1.



Figure 3.2: Picture of an Energy Balance Bowen Ratio system installed in the study area.

3.3 MODIS Products

The method proposed here has been physically derived from universal relationships. Moreover, data sources do not represent a limitation for the applicability of equation (12), nonetheless remotely sensed data such as that provided by MODIS scientific team would

empower the potential applications of the method. Hence, the method applicability with MODIS products is explored.

Table 3.1: Site name and station name, elevation, latitude, longitude and surface type. Source: <http://www.arm.gov/sites/sgp/geoinfo.stm>

Site	Elevation (m)	Lat./Long.	Vegetation Type
Ashton, Kansas E-9	386	37.133 N/97.266 W	Pasture
Coldwater, Kansas E-8	664	37.333 N/99.309 W	Rangeland (grazed)
Cordell, Oklahoma: E-22	465	35.354 N/98.977 W	Rangeland (grazed)
Cyril, Oklahoma: E-24	409	34.883 N/98.205 W	Wheat (gypsum hill)
Earlsboro, Oklahoma: E-27	300	35.269 N/96.740 W	Pasture
Elk Falls, Kansas E-7	283	37.383 N/96.180 W	Pasture
El Reno, Oklahoma: E-19	421	35.557 N/98.017 W	Pasture (ungrazed)
Hillsboro, Kansas E-2	447	38.305 N/97.301 W	Grass
Lamont, Oklahoma: E-13	318	36.605 N/97.485 W	Pasture and wheat
Meeker, Oklahoma: E-20	309	35.564 N/96.988 W	Pasture
Morris, Oklahoma: E-18	217	35.687 N/95.856 W	Pasture (ungrazed)
Pawhuska, Oklahoma: E-12	331	36.841 N/96.427 W	Native prairie
Plevna, Kansas E-4	513	37.953 N/98.329 W	Rangeland (ungrazed)
Ringwood, Oklahoma: E-15	418	36.431 N/98.284 W	Pasture

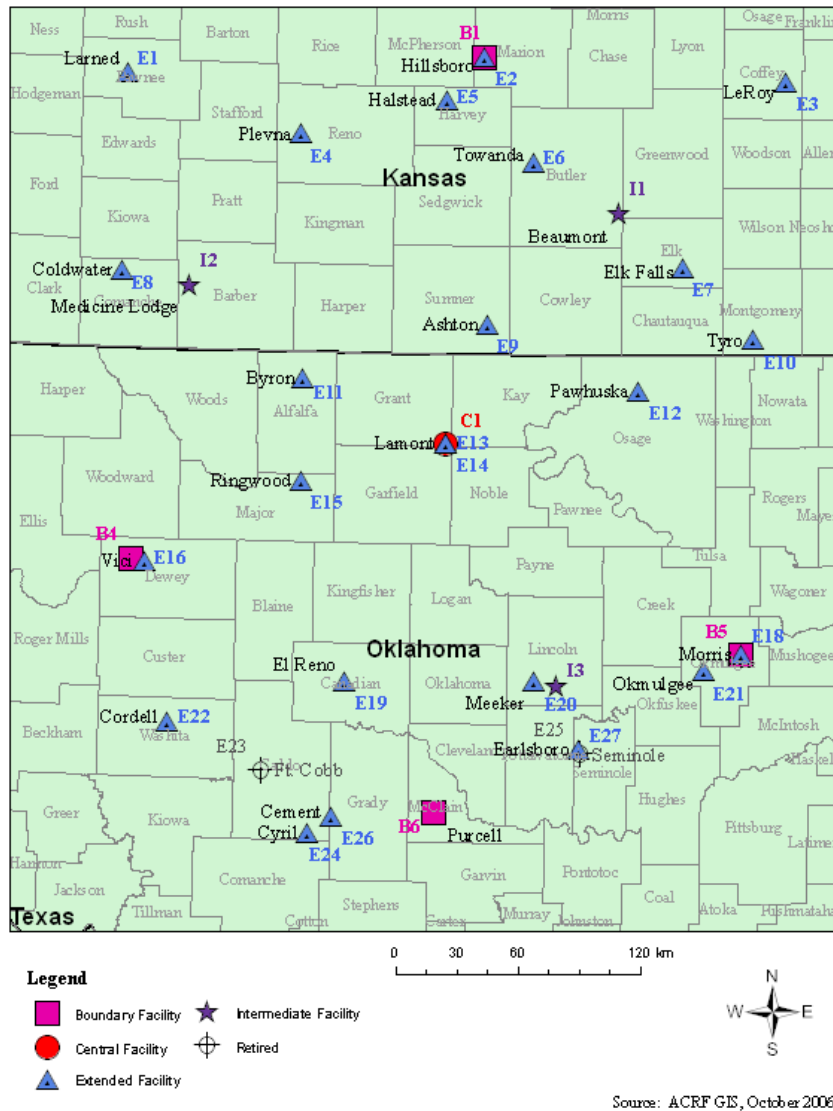


Figure 3.3: Overview of the Southern Great Plain area and EBBR stations, where the Central facility is at the center of the SGP-rectangle. The Boundary facilities are at the four boundaries of the SGP-rectangle. The extended facilities are distributed evenly over the area and the three intermediate facilities complete the Central facility.

Daytime images for seven days in year 2003 with at least 80% of the study area free of clouds were selected. Table 3.2 summarizes the images information including date, day of the year, satellite overpass time and image quality.

Geolocation is the process by which scientists specify where on the Earth's surface or in the atmosphere a specific radiance signal was detected. The MODIS geolocation dataset, called MOD03, includes eight Earth location data fields, e.g. geodetic latitude and longitude, height above the Earth ellipsoid, satellite zenith angle, satellite azimuth, range to the satellite, solar zenith angle, and solar azimuth.

Table 3.2: Date, Day of the Year, overpass time and image quality of the seven study days.

Date in 2003	Day of the Year (DOY)	Overpass time (UTC)	Image Quality (% clouds)
23rd March	82	17:05	18
31st March	90	17:55	15
1st April	91	17:00	18
6th September	249	17:10	6
19th September	262	16:40	23
12th October	285	16:45	9
19th October	292	16:50	6

The Earth location latitude and longitude reference is needed to relate the MODIS science data to other spatially referenced data sets, including other MODIS data, and to provide a uniform, worldwide spatial reference system for all data products. Earth locations are provided at each spatial element in order to capture the terrain relief parallax, the high spatial frequency variations in the locations of off-nadir spatial elements caused by the Earth's terrain. The ground point height and zenith angles are measured with respect to the local ellipsoid normal. The azimuth angles are relative to the local geodetic north.

Similar Earth location algorithms are widely used in modeling and geometrically correcting satellite image data from the Land Remote Sensing Satellite (Landsat)

Multispectral Scanner (MSS), Landsat Thematic Mapper (TM), System pour l'Observation de la Terre (SPOT), and Advanced Very High Resolution Radiometer (AVHRR) missions.

MOD11, the Land Surface Temperature and Emissivity (LST/E) products, provide per-pixel temperature and emissivity values. Average temperatures are extracted in Kelvin with a day/night LST algorithm applied to a pair of MODIS daytime and nighttime observations. This method yields 1 K accuracy for materials with known emissivities (the view angle information is included in each LST/E product). Emissivities in bands 20, 22, 23, 29, and 31-32 are estimates derived from applying algorithm outputs to database information. The LST/E algorithms use MODIS data as input, including geolocation, radiance, cloud masking, atmospheric temperature, water vapor, snow, and land cover. These products are validated, meaning that product uncertainties are well defined over a range of representative conditions. The theories behind this product can be found in http://modis.gsfc.nasa.gov/data/atbd/atbd_mod11.pdf, (Wan, 1999). Here, the basis of two MOD11 products, using MODIS team nomenclature is described.

MOD11_L2 land surface temperature (LST) Product:

This product is generated using the MODIS sensor radiance data product (MOD021KM), the geolocation product (MOD03), the cloud mask product (MOD35_L2), the quarterly landcover (MOD12Q1), and the snow product (MOD10_L2). The output file contains data of LST, quality assurance (QA), error in LST, emissivities in bands 31 and 32, viewing zenith angle and time, latitude and longitude (each set of latitude and longitude for every 5 scan lines and 5 pixels), local attributes, and global attributes. This LST product is generated by the generalized split-window LST algorithm (*Wan and Dozier, 1996*). A complete global coverage a

MOD11_L2 LST product would be generated for all swaths acquired in daytime and nighttime on the Earth including the polar regions.

A brief summary of the LST algorithm for MOD11_L2 is described here for the purpose of aiding the reader in understanding and interpreting the data product.

The LST retrieval in a MODIS swath is constrained to pixels that:

- (1) have nominal Level 1B radiance data,
- (2) are in clear-sky conditions at a 99% confidence defined in the cloud mask product, MOD35,
- (3) are on land or inland water.

In the LST processing, LST retrieval is made for lake and river pixels at clear-sky conditions with a 66% and higher confidence defined in cloud-mask MOD35 and for other land pixels in clear-sky at a 99% confidence, in order to improve the consistency between the spatial LST distributions over lakes and their surrounding lands. Clouds are masked with the MODIS Cloud Mask data product (MOD35_L2). Masking of oceans is done with the 1 km resolution land/water mask, contained in the MODIS geolocation product (MOD03).

Emissivities in bands 31 and 32 are estimated by the classification-based emissivity method (*Snyder and Wan, 1998*) according to land cover types in the pixel determined by the input data in quarterly Land Cover (MOD12Q1) and daily Snow Cover (MOD10_L2). A large uncertainty may exist in such estimated emissivities in semi-arid and arid areas. So the quality of the MOD11_L2 product may be poor in these areas.

Because band 22 is used in the 4-11 micron test to determine the cloudiness of a pixel in the MODIS cloudmask algorithm, the noisy fourth channel in band 22 produced quite a lot of (cloud) strips in the cloudmask product based on the old A-side MODIS

data (prior to October 30, 2000). To avoid the strips caused by the noisy channels, the cloudmask in all fourth channels of the scan cubes (one scan cube contains ten channels in each band) is refined with the adjacent pixels in the third and fifth channels. If both, the adjacent pixels in the third and fifth channels are clear-sky pixels at a 99% confidence (66% or higher for inland water pixels), the pixel in the fourth channel will be treated as clear-sky pixel for the LST retrieval.

MOD11B1 Daily LST:

The daily LST product at 5 km spatial resolution is a tile of daily LST product gridded in the Integerized Sinusoidal projection. A tile contains 240 by 240 grids in 240 rows and 240 columns. The exact grid size at 5km spatial resolution is 4.64km by 4.64km.

The daily MOD11B1 LST product is constructed with the results produced by the day/night LST algorithm (*Wan and Li, 1997*). The day/night LST algorithm only uses those day and night MODIS observations: the day observations with solar zenith angle not larger than 65 degrees and the night observations with solar zenith angle larger than 90 degrees (i.e., no solar radiation in the night observations).

In this thesis only MOD11_L2 product was used, however any of the described LST product can be use in ET model.

MODIS Atmospheric Profile product consists on several parameters: total-ozone burden, atmospheric stability, temperature and moisture profiles, and atmospheric water vapor. All of these parameters are produced day and night at 5×5 Km pixel. There are two MODIS Atmosphere Profile data product files: MOD07_L2, containing data collected from the Terra platform; and MYD07_L2, containing data collected from the Aqua platform. The MODIS temperature and moisture profiles are produced at 20

vertical levels. A simultaneous direct physical solution to the infrared radiative-transfer equation in a cloudless sky is used. The profiles are also used to correct for atmospheric effects for some of the MODIS products (e.g., sea-surface and land-surface temperatures, ocean aerosol properties, etc) as well as to characterize the atmosphere for global greenhouse studies.

A description of the methodologies behind MOD07 products is presented.

Statistical Regression Profile Retrieval

A computationally efficient method for determining temperature and moisture profiles from satellite sounding measurements uses previously determined statistical relationships between observed (or modeled) radiances and the corresponding atmospheric profiles. This method is often used to generate a first-guess for a physical retrieval algorithm, as is done in the International TIROS Operational Vertical Sounder (TOVS) Processing Package (ITPP, *Smith et al., 1993*). The problem is to determine the temperature (and moisture) at N levels in the atmosphere from M radiance observations. However, because the weighting functions are broad and represent an average radiance contribution from a layer, the M radiance observations are interdependent, and hence there is no unique solution. Furthermore, the solution is unstable in that small errors in the radiance observations produce large errors in the temperature profile. For this reason, the solution is approximated in a linearized form.

In order to solve the equations, for the temperature profile it is necessary to linearize the Planck function dependence on frequency. This can be achieved since in the infrared region the Planck function is much more dependent on temperature than frequency. The statistical regression algorithm seeks a “best-fit” operator matrix A that is computed using least squares methods by utilizing a large sample of atmospheric

temperature and moisture soundings, and collocated radiance observations. That is, we seek to minimize the error.

Ideally, the radiance observations would be taken from actual MODIS measurements and used with time and space co-located radiosonde profiles to directly derive the regression coefficients A . In such an approach, the regression relationship would not involve any radiative transfer calculations. However, radiosondes are routinely launched only two times each day at 0000 UTC and 1200 UTC simultaneously around the earth; Terra passes occur at roughly 1100-1200 AM and 1000-1100 PM local standard time each day. It is therefore not possible to obtain many time and space co-located MODIS radiances. Alternatively, the regression coefficients can also be generated from MODIS radiances calculated using a transmittance model with profile input from a global temperature and moisture radiosonde database. In this approach, the accuracy of the atmospheric transmittance functions for the various spectral bands is crucial for accurate parameter retrieval.

In the regression procedure, the primary predictors are MODIS infrared spectral band brightness temperatures. The regression coefficients are generated using the calculated synthetic radiances and the matching atmospheric profile. The advantage of this approach is that it does not need MODIS radiances co-located in time and space with atmospheric profile data, it requires only historical profile observations. However, it involves the radiative transfer calculations and requires an accurate forward model in order to obtain a reliable regression relationship. Any uncertainties (e.g., a bias of the forward model) in the radiative calculations will influence the retrieval.

Physical Profile Retrieval

The statistical regression algorithm has the advantage of computational efficiency, numerical stability, and simplicity. However, it does not account for the physical properties of the radiative transfer equation (RTE). After computing atmospheric profiles from the regression technique, a 11 non-linear iterative physical algorithm (*Li et al., 1998*) applied to the RTE often improves the solution. The physical retrieval approach is not currently employed in the operational algorithm due to constraints on computation time.

Operational Retrieval Implementation

The operational MODIS retrieval algorithm consists of several procedures that include cloud detection, averaging clear radiances from 5 by 5 field-of-view (FOV) areas, bias adjustment of MODIS brightness temperatures for forward model and instrument, regression retrieval, and an option to perform a physical retrieval. Because of computer limitations, the MODIS MOD07_L2 retrieval algorithm that is operational includes only the regression retrieval. The radiative transfer calculation of the MODIS spectral band radiances is performed using a transmittance model called Pressure Layer Prototype-Community Radiative Transfer Model; this model uses an input number of pressure layer vertical coordinates from 0.05 to 1100 hPa. The calculations take into account the satellite zenith angle, absorption by well-mixed gases (including nitrogen, oxygen, and carbon dioxide), water vapor (including the water vapor continuum), and ozone.

More details about MOD07 theory can be found in *Menzel et al. (2002)*. In the present study, air temperature and dew point temperatures at the vertical pressure level of 1000hPa are used to calculate the vapor pressure deficits. Also the temperatures are

assumed to be homogenous over the 5x5km grid. Table 3.3 presents a summary of the MODIS products used in the methodology application and validation.

Table 3.3: Summary of the MODIS products used and ground observations data

Variable	Origin	Method
T31	MOD02	Plank's equation
NDVI	MOD02	(Red- <i>INR</i>)/(Red+ <i>INR</i>)
Ts	MOD11	Split-window
Td	MOD07	ITPP
Ta	MOD07	ITPP
ET	Ground Bowen Ratio stations	Bowen Ratio

The study area is pulled out of each image and projected in a Plate-Carree grid of 467 columns by 444 rows, in pixels of approximately 1 km resolution.

3.3 Validation with Ground Measurements

Each component of equation (12) is obtained with instantaneous data at 1 km resolution. MODIS data provides 5 minutes snapshots of the study region, thus MODIS products used here are *instantaneous observations* and so are the ET results obtained. It should be said that instantaneous ET estimates have limited practical use, in contrast, mean daily ET estimates are required for agricultural and water management practices. The conversion of instantaneous ET values to mean daily ET values is not within the scope of the thesis, however any of the available methodologies to extend instantaneous values to daily estimates could be used (*Jackson et al., 1983; Zhang and Lemeur, 1995; Batra et al., 2006*).

In order to apply equation (12) to obtain instantaneous ET estimates, the net radiation (R_n) must be calculated. In this work, R_n was estimated with the methodology of *Bisht et al. (2005)*, which provides a spatially consistent and distributed R_n map over a large domain for clear sky days. With this method, R_n can be evaluated in terms of its components of downward and upward short wave radiation fluxes, and downward and upward long wave radiation fluxes. Several MODIS data products are utilized to estimate every component. Details of this calculations and further description of the MODIS products and its validation for the case days presented in this work can be found in *Bisht et al. (2005)*. The R_n data used in this work are those published by these authors for the same days and study area.

Soil heat fluxes G have been calculated using *Moran et al. (1989)* methodology with the daily normalized difference vegetation index (NDVI) maps, calculated with MOD021KM products. The equations used are

$$G = 0.583 R_n e^{(-2.13 \cdot \text{NDVI})} \quad \text{for NDVI} > 0 \quad (27)$$

$$G = 0.583 R_n \quad \text{for NDVI} \leq 0 \quad (28)$$

The slope of the SVP curve, Δ , was calculated at T_a using Buck's equation (*Buck, 1981*) and the MODIS T_a product. The coefficient T_u was calculated with the method proposed in Chapter 2.

Bisht et al. (2005) validated MODIS- T_a product in the SGP with Bowen Ratio observations. Not only T_a was validated, but also the instantaneous net radiation estimations. Those validations are presented in Figures 3.4. The overall T_a bias, RMSE and R^2 were -2.07°C , 5.01°C and 0.62, respectively. The modeled air temperature is underestimated which probably due to the fact that the air temperature in MOD07 at 1000hPa level does not truly represent the air temperature at screen level height.

Validation of modeled instantaneous net radiation yielded a bias, RMSE and R^2 of 59 Wm^{-2} , 74 Wm^{-2} and 0.89, respectively.

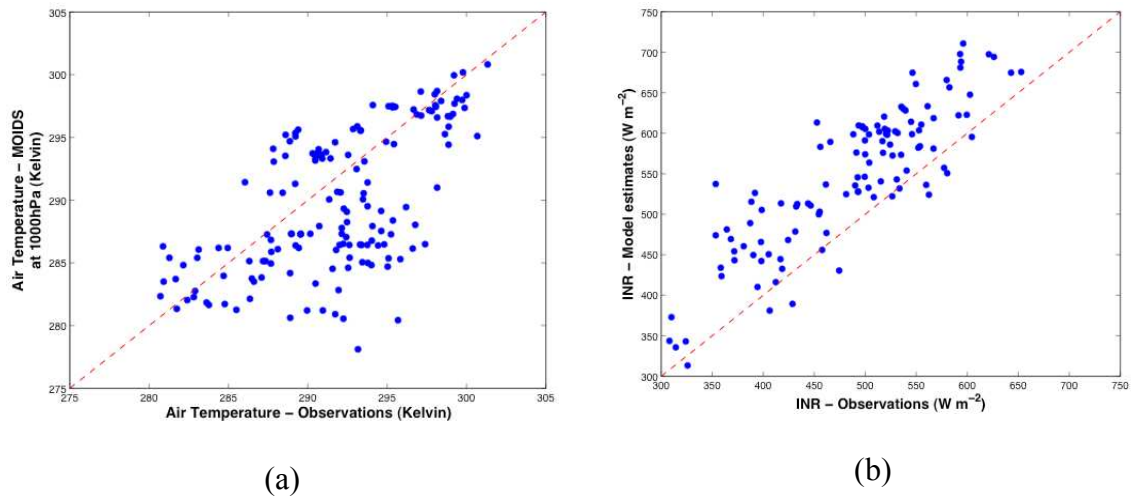


Figure 3.4: (a) Comparison between observed and retrieved air temperature from MODIS data product (MOD07) at 1000 hPa level. (b) Comparison between observed and modeled Instantaneous Net Radiation (INR) estimates for all study days.

It is known that there are no generally accepted methodologies to validate distributed ET values to point flux station observations. Hence, it is difficult to evaluate the reliability of model outputs for the remaining pixels in an image. Nonetheless unfiltered point measurements seem to be an appropriate mean to validate remote sensing applications (Jiang and Islam, 2001; Kustas et al., 2003; Nishida et al., 2003; Bisht et al., 2005; Batra et al., 2006).

Descriptive statistics for observed and model ET for every day analyzed are shown in Table 3.4 and visualized in Figure 3.4. In this case the mean and standard deviation (S) were calculated. The mean and S of the observed ET would represent the study area from ground measurements (at most 10 values per study day), while statistics for the modeled ET represent results from about 200,000 pixels of 1 km^2 . This contrast should raise a word of caution about what can be said from the comparison between these two sets of data. However, some conclusions can be outlined.

There is a good agreement between both mean ET values for each day, with differences ranging from ± 1 to $\pm 44 \text{ Wm}^{-2}$. A similar contrast was performed in studies with different ET models where reported results are comparable with those presented here (*Jiang and Islam, 1999 and 2001; Kustas et al., 2003; Batra et al., 2006*). The standard deviation seems to be systematically lower for ET estimated with the proposed method. This may be attributed to the averaging effect derived from the size of the study area. S indicates that distributed ET estimates over the study area are very close to the region mean ET. A final conclusion should be avoided because of the few available observations and the lack of an accepted method to validate distributed ET maps from limited observations.

Table 3.4: Observed, modeled regional and modeled ET (Wm^{-2}) means and standard deviations (S).

	Observed ET		Modeled Regional ET All pixels		Modeled ET Point-Pixel	
	Mean	S	Mean	S	Mean	S
DOY82	191.79	± 34.22	181.34	± 14.84	179.32	± 10.02
DOY90	148.56	± 38.33	164.45	± 14.25	206.95	± 5.26
DOY91	232.55	± 41.58	234.20	± 17.59	227.57	± 21.92
DOY249	284.35	± 40.81	308.86	± 27.54	304.98	± 26.92
DOY262	190.02	± 40.74	197.1	± 13.06	196.37	± 19.46
DOY285	203.97	± 33.38	214.57	± 16.27	219.01	± 11.37
DOY292	212.20	± 46.10	231.24	± 17.78	224.06	± 22.22

The pixel scale mismatches the point-station scale. Therefore, the validation of the present results at the pixel scale presumes that ET observations are representative of the surrounding 1 km^2 area. Generally, Instruments are located out of strong edges. In some cases the station is close to the center of the pixel and others is close to the pixel border.

The geographic coordinates of each station are used to locate the corresponding pixel for local comparison purposes.

The comparison between ground measurements and the ET estimates at the corresponding pixel is shown in Table 3.5 and Figure 3.5. In Table 3.5, the number of available observations, root mean square errors (RMSE), bias (Observed – Calculated) and correlation coefficients (R^2) are presented for every analyzed day. In general, RMSE's are less than 18% of the mean values for each day presented in Table 3.4. The biases also tend to be low (lower than 15% of the observed mean ET). R^2 values indicate that ET estimates correlate relatively well with measurements except for the last two analyzed days. Similar results were presented by *Batra et al. (2006)*; *Grago and Crowley (2005)*; *Gomez et al. (2005)*; *Rivas and Caselles (2004)*; *Jacobs et al. (2000)*; *Shuurmans et al. (2003)*; *Nishida et al. (2003)*; *Norman et al. (2003)*; *Jiang and Islam (2001)*; *Kustas and Norman (2000)*; *Anderson et al. (1997)*.

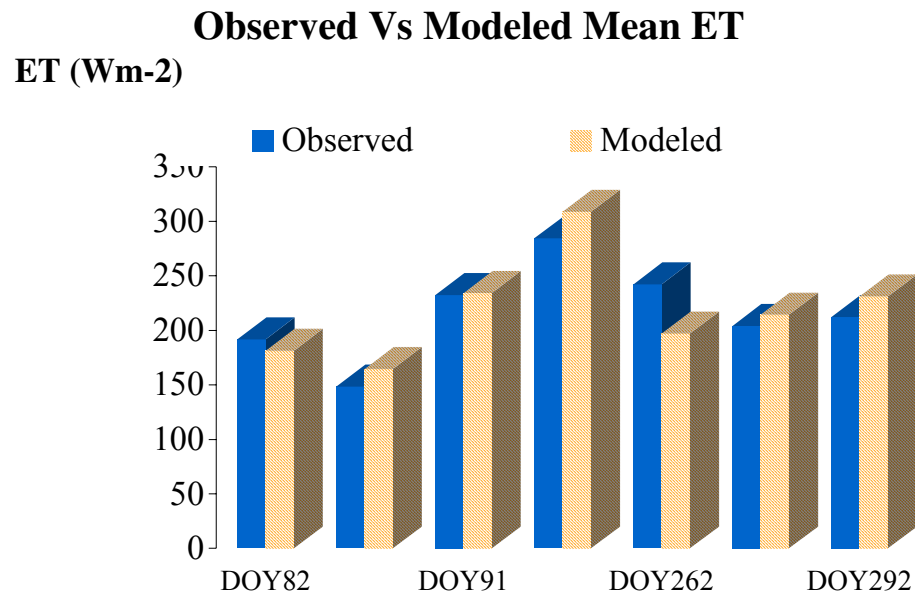


Figure 3.5: Observed and modeled mean ET (Wm-2).

Table 3.5: ET (Wm^{-2}) Comparison between observations and proposed method estimates at the pixel scale. Calculated refers to estimated value at the pixel where the ground station is located.

	# of observations	RMSE	BIAS (Obs.- Mod.)	R²
DOY82	6	31.65	12.48	0.62
DOY90	3	35.34	-31.70	0.98
DOY91	4	18.83	4.98	0.97
DOY249	8	34.95	-20.63	0.67
DOY262	6	30.77	-6.24	0.60
DOY285	8	30.47	-14.68	0.56
DOY292	5	41.38	13.98	0.36

The overall statistics are obtained with all the observations together, regardless the day they were registered. Thus, the overall RMSE and bias are 33.89 (15% of the mean ET) and -10.96 Wm^{-2} respectively, with an R^2 of about 0.79. *Batra et al. (2006)* reported a RMSE of about 50 Wm^{-2} for the same region and days. They applied Jiang-Islam methodology, which is simpler, and does not include atmospheric variables (*Jiang and Islam, 2001*). *Crago and Crowley (2005)* published similar RMSE using a more complex application of Granger's complementary relationship where resistance factors and wind function are included in the estimates.

In general, modeled ET overestimates observed ET, as shown in Figure 3.5. Even though the biases and the RMSE presented here are lower than or equal to those reported in the literature, it is acknowledged that Tu estimates may not completely represent the surface characteristics, as explained in Chapter 2.

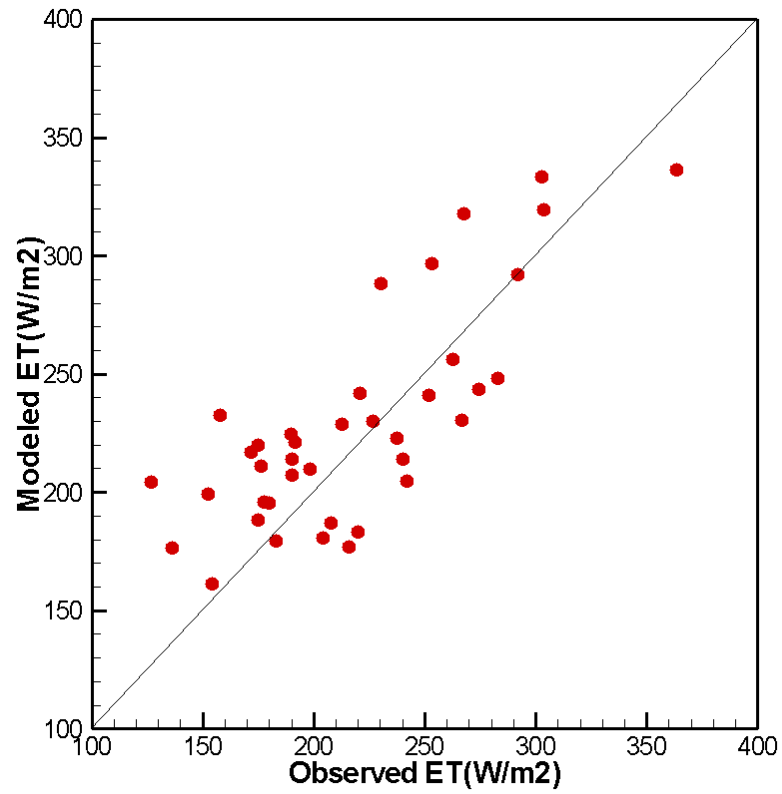
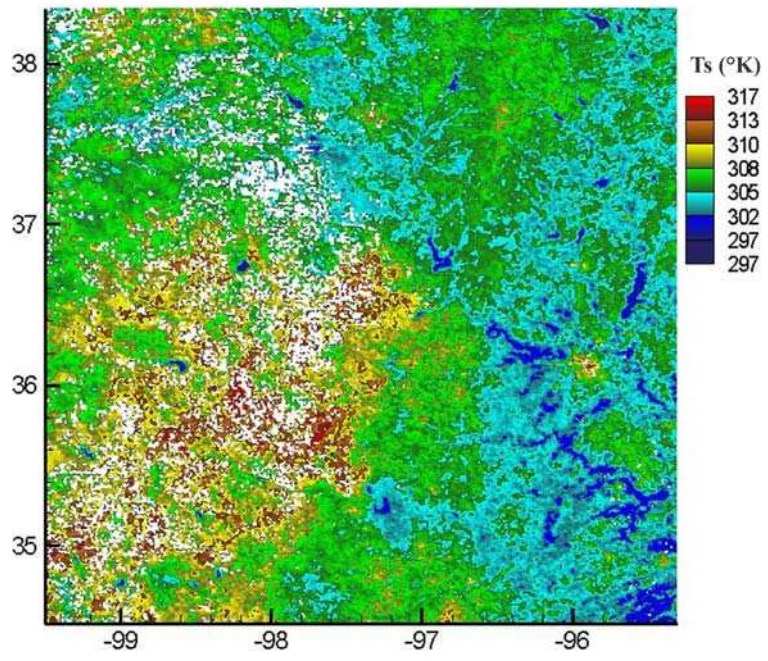
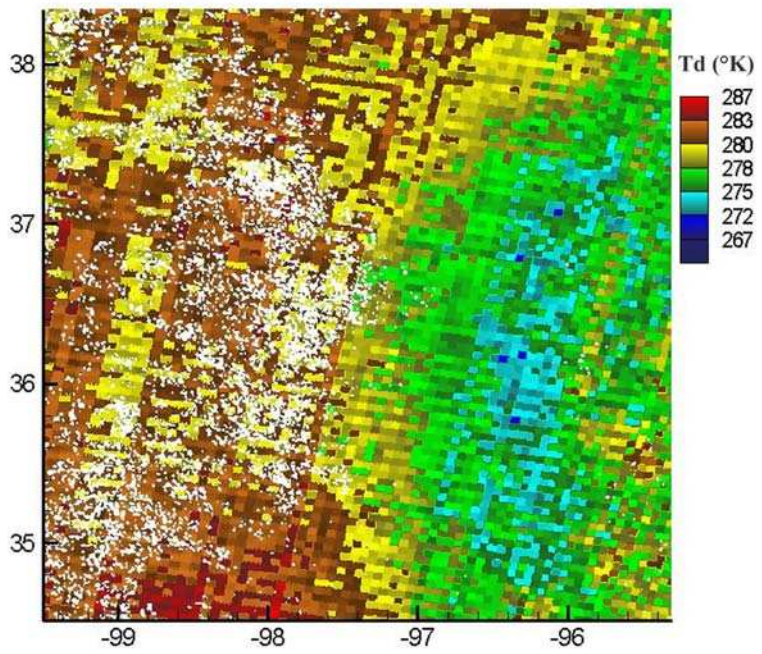


Figure 3.6: Point-to-pixel contrast between calculated and observed ET (Wm^{-2}) for seven clear sky days.

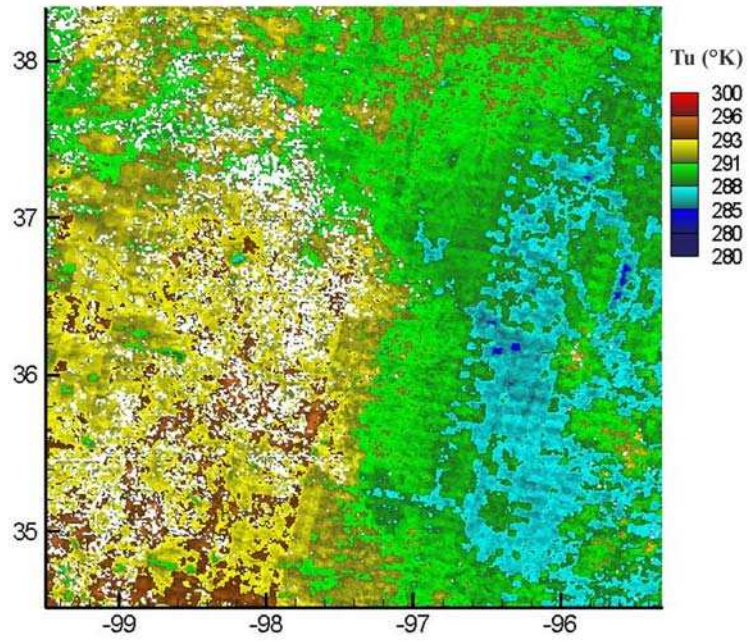
Figure 3.6 shows spatially distributed T_s , T_d , T_u and ET maps generated from the proposed model for September 6th, 2003.



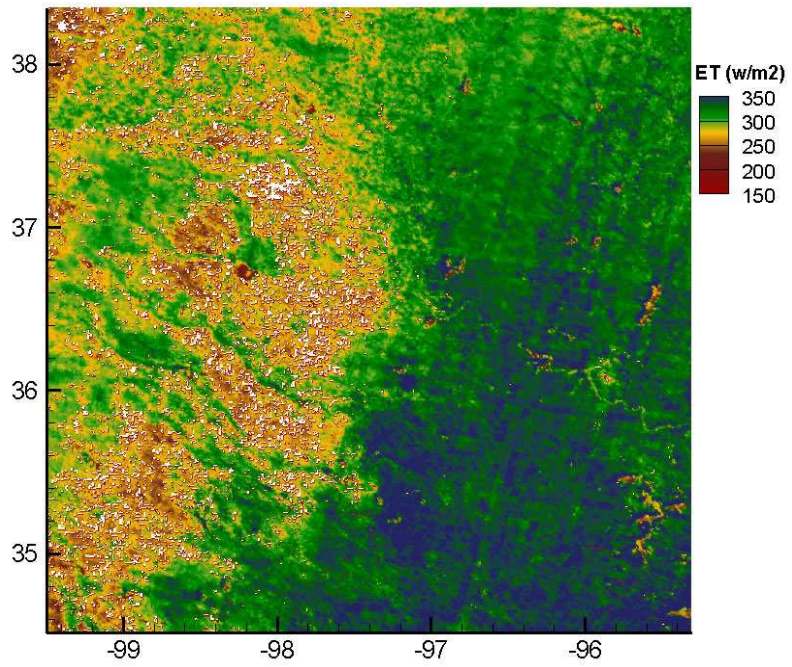
(a)



(b)



(c)



(d)

Figure 3.7: Maps of (a) T_s , (b) T_d , (c) T_u and (d) ET for September 6th, 2003

3.4 Contrast Between Equation 12 and 24

In Chapter 2 an alternative ET equation, equation (24), was derived with Bouchet complementary model. In this Chapter results obtained from equation (12) and (24) are compared to demonstrate the strength of the proposed model. The contrasted results were obtained with equation (12) and (24) assuming $k=2$. These results are shown in Table 3.6, where RMSE's and biases are about 25 Wm^{-2} , indicating that equation (24), obtained with Bouchet complementary model, would lead to larger ET estimates. Then, ground measurements were compared with results obtained using equation (24), (see Figure 3.7). The overall RMSE is about 52,29 and the bias (Bouchet-Granger) is -37.90 Wm^{-2} , suggesting that the equation derived with Bouchet's complementary relationship, estimates ET with larger errors than equation (12).

Table 3.6: ET (Wm^{-2}) comparison between Bouchet and Granger complementary relationships.

	RMSE	BIAS (Bouchet-Granger)	R ²
DOY82	5.42	0.91	0.990
DOY90	7.38	0.86	0.993
DOY91	13.70	13.01	0.983
DOY 249	31.74	31.56	0.995
DOY 262	25.51	25.33	0.991
DOY 285	26.79	26.40	0.990
DOY 292	28.24	28.11	0.999

Clearly, Bouchet's simplification, i.e. assuming that ET and E_{pot} contribute with the same coefficient to E_w, results in larger ET estimates than those obtained with

Granger's complementary relationship, overestimating ground observations. These results reinforce the role of atmospheric variables in ET estimation.

Equating equations (12) and (24), the constant k can be calculated for instantaneous ET values. Thus,

$$\frac{F\Delta}{F\Delta + \gamma} = \frac{kF\Delta}{(F+1)(\Delta + \gamma)} \quad (29)$$

$$k = \frac{(F+1)(\Delta + \gamma)}{F\Delta + \gamma} \quad (30)$$

Bouchet's coefficient k is calculated for every pixel in every case day and the overall mean k was 2.341, with an overall minimum of 1.784, maximum of 2.710 and standards deviations varying from 0.025 to 0.078. These results are close to those reported by *Ramirez et al. (2005)*. These authors reported a mean k of about 2.21 and a variance equal to 0.07 using uncorrected pan evaporation data as a surrogate of E_{pot} .

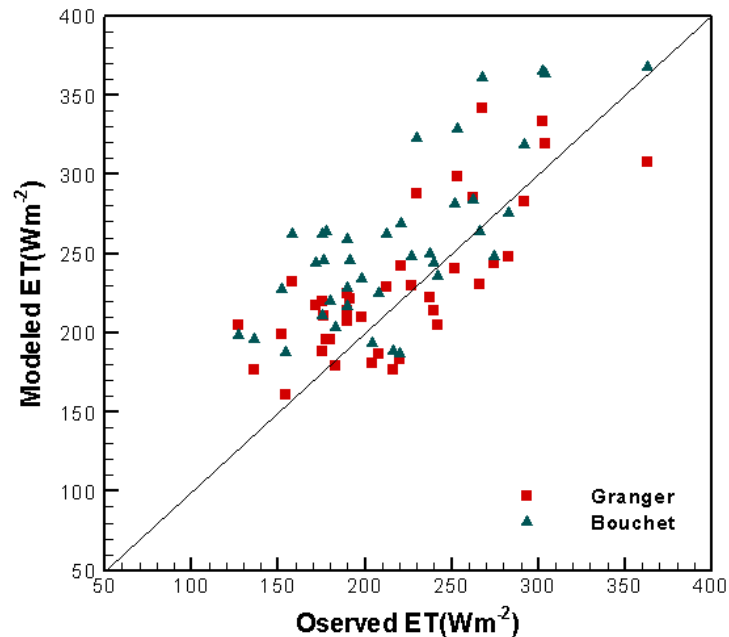


Figure 3.8: Comparison between Bouchet and Granger's complementary models against ground measurements

Both complementary models yield similar ET estimates, however Granger's model lead to more accurate results than Bouchet's method. The slope of the SVP curve at the air temperature sets a k value slightly different from 2.

Chapter 4 : Uncertainty Analysis.

4.1 First Order Analysis of Uncertainty

Hydrologic uncertainties can be natural or inherent. The first one arises from the random variability of natural phenomena. Model uncertainties result from the approximation and parameterization introduced in the mathematical formulation of the hydrological phenomena, which in turn give rise to parameters uncertainties stemmed from the unknown nature of the coefficients in the equations (*Chow et al., 1988*).

A first order analysis is appropriate to quantify the uncertainties introduced in a dependent variable by independent variables and parameters due to the inherent uncertainties in measurements and estimates. This type of analysis assumes that the model is unbiased or in others word, that the model is exact (*Coleman and Steele, 1999*). Therefore, a first order analysis was performed to evaluate the error introduced in ET results by errors in temperature estimates, i.e. Ts, Tu and Td.

To introduce the first order analysis, suppose a variable w is expressed as a function of x , such that $w=f(x)$. If the model f is correct, the uncertainties of w are associated to x measurement errors. A mean value of x , denoted by \bar{x} , is selected and the corresponding value of w is calculated as $\bar{w} = f(\bar{x})$. If the true value of x differs from \bar{x} by a certain amount, the effect of this disagreement on w can be examined by expanding $f(x)$ as a Taylor series around $x = \bar{x}$:

$$w = f(\bar{x}) + \left. \frac{d f}{d x} \right|_{x=\bar{x}} (x - \bar{x}) + \frac{1}{2!} \left. \frac{d^2 f}{d x^2} \right|_{x=\bar{x}} (x - \bar{x})^2 + \dots \quad (31)$$

where the derivatives $\left. \frac{df}{dx} \right|_{x=\bar{x}}$, $\left. \frac{d^2f}{dx^2} \right|_{x=\bar{x}}$, are evaluated at $x = \bar{x}$.

If the second and higher order terms are neglected, the resulting first order expression of the error is,

$$w - \bar{w} = \left. \frac{df}{dx} \right|_{x=\bar{x}} (x - \bar{x}) \quad (32)$$

The variance of the error is $S_w^2 = E[(w - \bar{w})^2]$, where E is the expectation operator, therefore,

$$S_w^2 = E\left\{ \left[\left. \frac{df}{dx} \right|_{x=\bar{x}} (x - \bar{x}) \right]^2 \right\} = \left(\left. \frac{df}{dx} \right|_{x=\bar{x}} \right)^2 S_x^2 \quad (33)$$

where S_x^2 is the variance of x .

Equation (33) represents the variance of the dependent variable w as a function of the variance of the independent variable x , assuming the model f is unbiased. This methodology can be extended to several mutually independent variables, i.e. x_1, x_2, x_3 , ect, (Chow *et al.*, 1988).

In first place, the uncertainties in the F (see equation (5)) parameter were analyzed. Tu is not independent of Ts and Td, however Td and Ts are estimated independently. Consequently, the first order analysis provides a good idea of the errors introduced in F by uncertainties in surface and dew point temperature observations and Tu estimates, although Tu is not a truly independent variable.

Following the first order analysis and equation (33), the variance of F, S_F^2 , is obtained using equation (5):

$$S^2_F = \frac{(\overline{T_u} - \overline{T_d})^2}{(\overline{T_s} - \overline{T_d})^4} S^2_{T_s} + \frac{1}{(\overline{T_s} - \overline{T_d})^2} S^2_{T_u} + \left[\frac{(\overline{T_u} - \overline{T_d})^2}{(\overline{T_s} - \overline{T_d})^4} + \frac{1}{(\overline{T_s} - \overline{T_d})^2} \right] S^2_{T_d} \quad (34)$$

where $S^2_{T_s}$, $S^2_{T_u}$ and $S^2_{T_d}$ are the variance of T_s , T_u and T_d , respectively, and $\overline{T_u}$, $\overline{T_d}$ and $\overline{T_s}$ are the mean T_u , T_s and T_d , respectively.

To quantify equation (34), two sets of arbitrary temperatures values have been designed. The mean and standard deviation (S) of each set are shown in Table 4.1. The temperature standard deviations used in set 1 are slightly higher than the normal errors found in the observed and remotely sensed temperatures and those applied in set 2 are higher than in set 1, representing an extreme situation.

Table 4.1: Mean and standard deviation (S) values for F first order analysis

	Mean (K)			S (K)		
	Ts	Tu	Td	Ts	Tu	Td
Set 1	297	285	275	±2	±2	±2
Set 2	302	290	280	±3	±5	±3

The quantification of equation (34) with set 1 produces a maximum S^2_F of 0.0183 (13% of F). A minimum S^2_F of 0.00004 is estimated for $\overline{T_s} \pm 2K$. T_u and T_d variances of ± 2 K result in S^2_F of about 0.01. For set 2, the maximum S^2_F is 0.074, which represents 27% of F. A minimum S^2_F of 0.0052 is found for $\overline{T_s} \pm 3K$. T_u variances of ± 5 K increase S^2_F in about 0.05 (22%) and T_d variances of ± 3 K cause an increase of S^2_F of 0.022.

These outcomes indicate that F is more sensitive to T_u and T_d than to T_s estimates. Errors of 5°K in the calculation of T_u may cause an approximate $\pm 30\%$ error in the relative evaporation, thus the implication of these errors in ET equation is analyzed in more detail.

In order to examine the errors introduced in ET by F, the derivative of equation (11) with respect to F was derived, thus the variance of ET, S_{ET}^2 , is

$$S_{ET}^2 = \left[\alpha (\overline{R_n} - \overline{G}) \right]^2 (\gamma \Delta)^2 \frac{1}{(\overline{F} \Delta + \gamma)^4} S_F^2 \quad (35)$$

where $\overline{R_n}$, \overline{G} and \overline{F} are the mean Rn, G and F, respectively.

The factor $\left[\alpha (\overline{R_n} - \overline{G}) \right]^2 (\gamma \Delta)^2 \frac{1}{(\overline{F} \Delta + \gamma)^4}$ is constant, thus S_{ET}^2 due to errors in F can

be obtained from S_F^2 . Results from set 1 and set 2 were used to study two potential common situations, one with $\overline{R_n} - \overline{G} = 350 \text{ Wm}^{-2}$ and the other with $\overline{R_n} - \overline{G} = 500 \text{ Wm}^{-2}$, while α , Δ and γ were kept constant with values of $\alpha=1.26$, $\Delta = 1.4 \text{ hPa}/^\circ\text{C}$ and $\gamma=0.67 \text{ hPa}/^\circ\text{C}$. The mean value of F was 0.5. Quantifying equation (35) with results from set 1 yields a maximum and a minimum S_{ET} of 6 and 2 Wm^{-2} , respectively. The extremes S_{ET} were 23 and 4 Wm^{-2} , respectively, for set 2. It should be noted that the standard deviation (S) was chosen to explain the first order analysis of ET because of its unit, which is directly comparable with mean ET estimates.

Uncertainties in the calculation of R_n and G will increase these errors. Although this analysis is not exhaustive, it may be concluded that uncertainties in the estimation of F and T_u are not likely to introduce errors larger than the corresponding measurement errors for ET over large areas.

4.2 One-channel Brightness Temperature Vs. MODIS Ts Product.

The Temperature T_s is one of the key variables for estimating F. There are different methods to approximate the actual T_s from thermal infrared sensors, for instance, one-

channel and multi-channel methods. *Dash et al. (2002)* revised common methodologies and described their advantages and disadvantages.

The MOD11 product used in this work is obtained with two multi-channel methods, i.e. Split windows and Day-Night method (*Wan and Dozier, 1996; Wan, 1999*). This MODIS product was validated and the published error is about 1K. However, the one-channel approach is an easy-to-use method to approximate T_s , and is commonly utilized with other thermal infrared satellite sensors (*Venturini et al., 2004*).

One of the main criticisms of using the one-channel brightness temperature to estimate T_s , is that it is largely affected by atmospheric variables and viewing angle (*Price, 1983; Wan and Dozier, 1996*). Although the bands allocated in the 10-12 μm window are transparent to radiation, water vapor absorption is likely to produce errors which, in turn, may cause the brightness temperature to differ from the actual surface temperature by 5 to 10 K (*Price, 1983*).

In order to investigate the effect of atmospheric conditions in T_s and hence, in ET estimates, the MODIS band 31 brightness temperature (T31) without atmospheric corrections was contrasted against MOD11 product. Then ET was derived with T31 and T_s . Information about MODIS band characteristics can be found in <http://modis.gsfc.nasa.gov/about/specifications.php>.

T31 was calculated with Planck's equation (*Rees, 2001*) from MOD021KM images, which provide the calibrated digital counts of the 36 bands of the MODIS sensor, at 1 km spatial resolution. Applying the scale and offset coefficients of the band 31 to the digital counts, the radiance values of Planck's equation are attained. A simple cloud mask based on NDVI and T31 thresholds was applied to the T31 image.

Figure 4.1 compares T31 and Ts from MOD11 for 3 clear days in March-April. Every processed day presents different patterns, however differences of larger 10 K can be observed in all of them. It should be remarked that low T31 values may come from cloud-contaminated pixels, given that a very simple cloud mask was applied to those images.

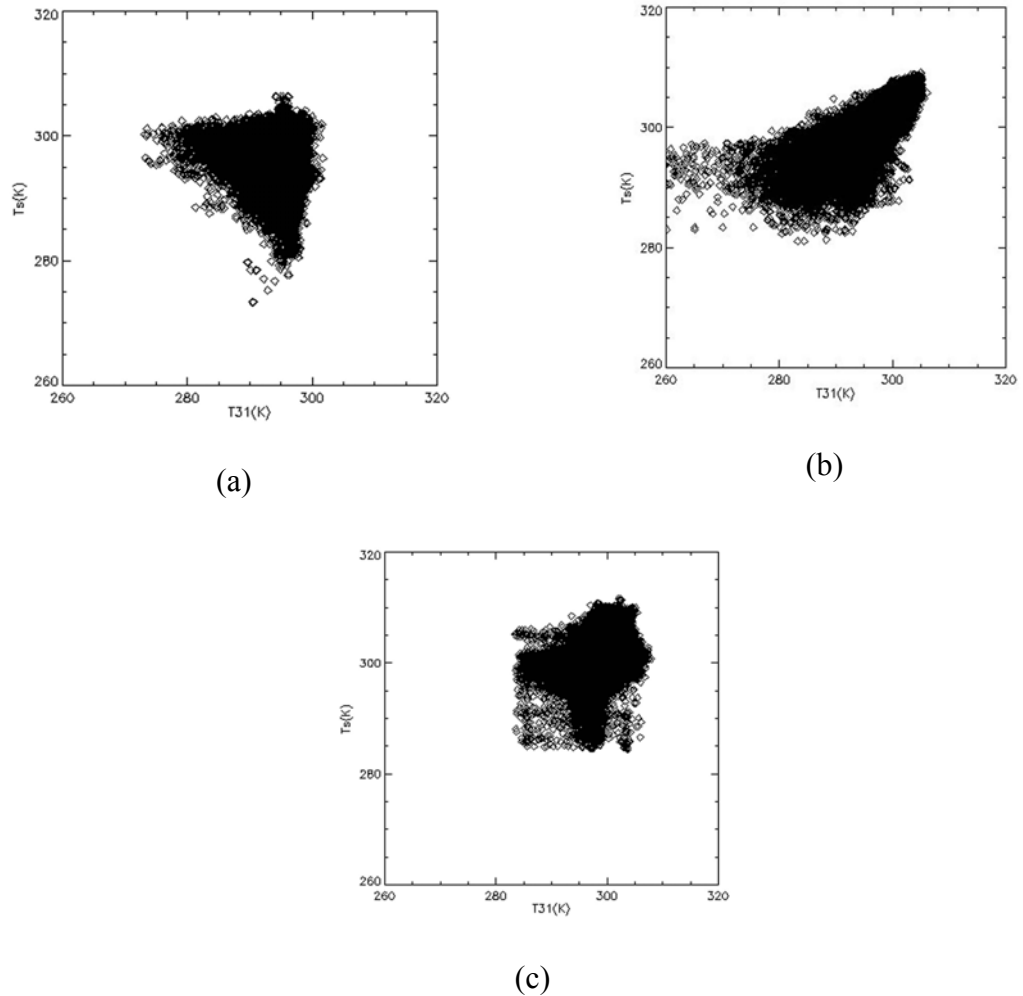


Figure 4.1: Comparison between Ts y T31 for (a) March 23rd, (b) March 31st and (c) April 1st of 2003

Table 4.2 presents T31 and Ts means, maximum, minimum and standard deviations (S) for the three processed days. Mean values differ in no more than 4K, however larger differences, up to 23°K, are observed in maximum and minimum values, indicating

important effects of the atmospheric conditions in some parts of the region. The values of the standard deviation of Ts and T31 are relatively low and comparable in every case. Similar results and conclusions were published for South Florida – USA (Venturini *et al.*, 2004).

Table 4.2: Ts y T31 mean, Maximum, Minimum and Standard deviations.

	Media		Max.		Min.		S	
	Ts	T31	Ts	T31	Ts	T31	Ts	T31
DOY82	298.3	295.3	306.3	329.6	295.0	273.2	1.8	1.8
DOY90	300.2	296.5	309.1	306.1	296.1	273.1	2.5	3.3
DOY91	300.3	297.4	311.6	307.9	296.7	283.4	2.4	2.5

The temperature Ts is one of the three variables involved in the definition of the coefficient F [see Chapter 2, equation (5)]. The theoretical analysis of errors in Ts, Td and Tu and their influence in F were presented previously in this Chapter. The T31 and Ts results presented here render differences larger than 5 k, therefore the convenience of using T31 maps to compute F must be further explored.

Two sets of F coefficients, one with T31 (F-31) and one with Ts (F-s) were calculated and compared (Figure 4.2). Results for March 23rd (a) and April 1st (c) show moderate dispersions around the 1:1 line. For March 31st, large differences between F-31 and F-s are observed [Figure 4.2 (b)]. A small amount of pixels with very different F-31 and F-s are detected in all three plots, probably due to cloud-contaminated F-31 pixels. The correlation coefficients (R^2), between both F calculations are 0.727, 0.834 and 0.913, respectively for DOY82, DOY90 and DOY91. The analysis of these plots and the good R^2 suggest from a moderate to a good agreement between F-31 and F-s.

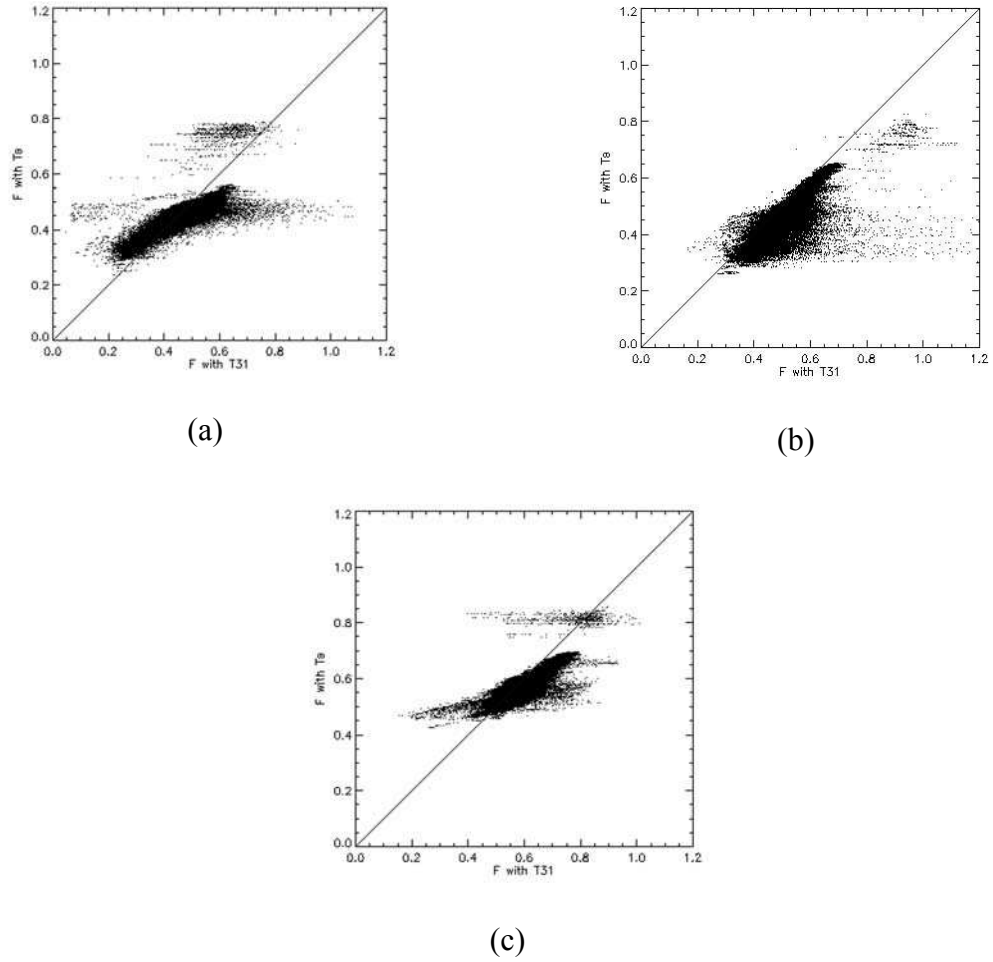
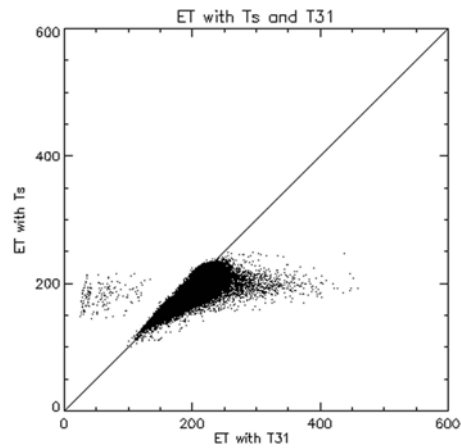


Figure 4.2: Comparison between F-31 and F-s for (a) March 23rd , (b) March 31st and (c) April 1st of 2003.

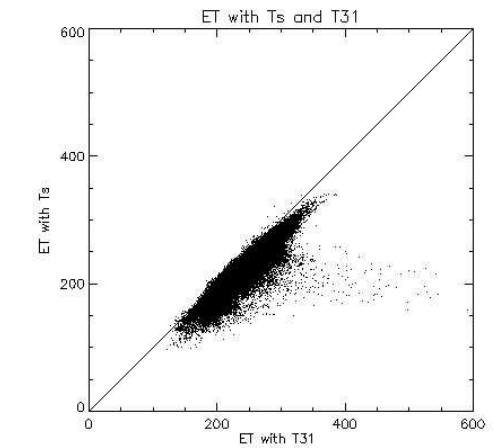
ET was calculated, with both F-31 and F-s in equation (12), keeping the other variables as calculated in Chapter 3. Figure 4.3 displays the contrast between both ET sets. In general, F-31 yields lower ET values than F-s, however the cloud of pixels lays close to the 1:1 line.

The RMSE, bias and R^2 are summarized in Table 4.3. The RMSE is about 20 Wm^{-2} the bias lower than 19 Wm^{-2} and the relation between both ET sets is very good, with R^2 larger than 0.8. The differences observed are about 5-10 % of the mean ET and in the order of the common errors found in ground observations. Thus, the one-channel

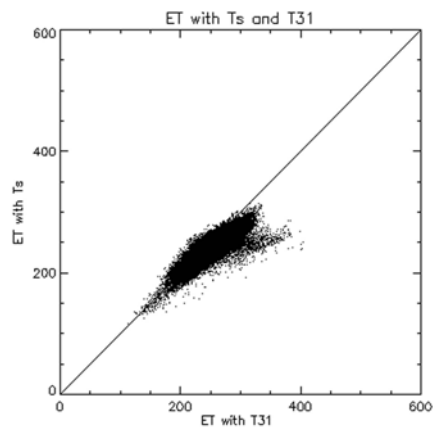
brightness temperature seems to yield acceptable ET estimates, keeping the calculation very simple.



(a)



(b)



(c)

Figure 4.3: Comparison between ET with F-31 and ET with F-s for (a) March 23rd, (b) March 31st and (c) April 1st of 2003

Table 4.3: Contrast of ET calculated with F-s and F-31 (Wm^{-2}) measured in terms of RMSE, bias and correlation coefficient (R^2)

	# of pixel for validation	RMSE	bias (ETFs- ETF31)	R^2
DOY82	5	19.69	13.4	0.8
DOY90	3	22.90	18.9	0.9
DOY91	4	18.50	13.5	0.8

Finally, both ET sets were validated with the ground observations presented in Chapter 3. For these three images, the amount of pixels with ground data is presented in Table 4.3. Figure 4.4 shows the validation of both ET sets with ground observations. The overall RMSE for ET with Ts is 17 Wm^{-2} and the bias $15,5 \text{ Wm}^{-2}$ while RMSE and bias for ET with T31 is about 22 Wm^{-2} and 23 Wm^{-2} , respectively. Clearly, both surface temperatures overestimate ET however MOD11 product yields better ET estimates.

The atmospheric corrections introduced in MODIS land surface product differs from T31 estimates in up to 20 K, however these MOD11 corrections would not have the same impact over F and ET estimates. It should be noted that *Batra et al. (2006)*; *Grago and Crowley (2005)*; *Gomez et al. (2005)*; *Rivas and Caselles (2004)*; *Nishida et al. (2003)*; *Norman et al. (2003)*; *Jiang and Islam (2001)* reported results similar to the ET estimates with T31 reported in this thesis.

The results presented in this Chapter suggest that the modified P-T equations are not very sensitive to Ts estimates and that the sensitive factor in this type of equations is the available energy, which is the driving force for ET. In this regard, ET is not linearly related to F as it is to Rn, and Ts is only one of the three variables involved in F coefficient. Similar results were published by *Venturini et al. (2004)* applying Jiang and Islam's modified P-T equation (*Jiang and Islam, 2001*).

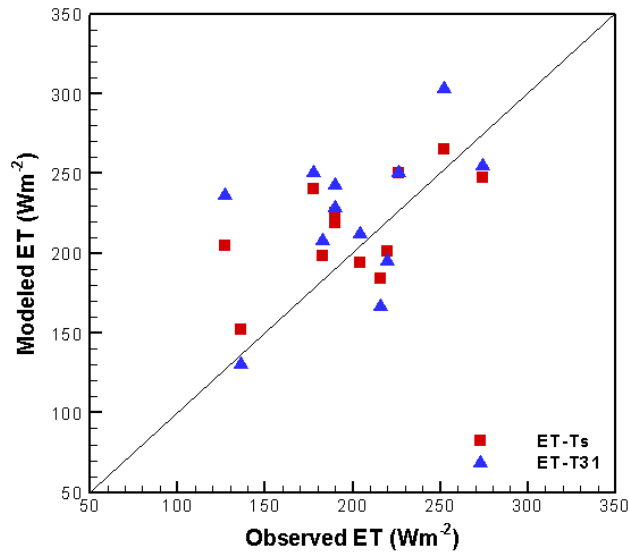


Figure 4.4: Contrast between ground observations and ET estimates with Ts and T31.

4.3 The Wind Speed effect.

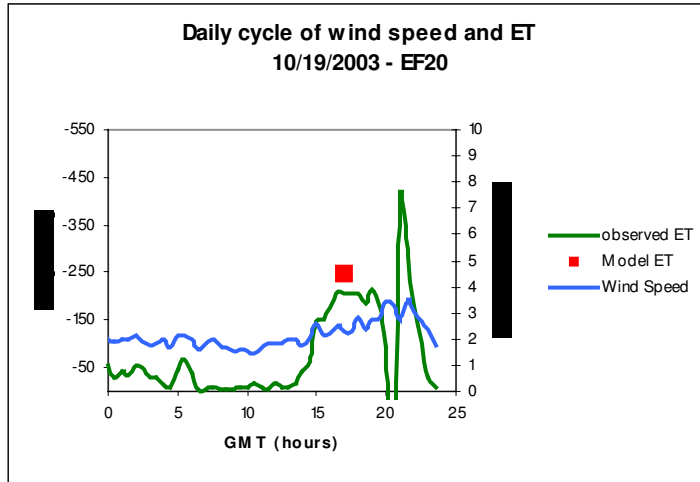
In Chapter 2, the rationale behind the wind speed function (f_u) was discussed. In this Chapter ground observations of ET and wind speed are analyzed in order to verify the hypothesis that f_u does not affect ET results.

Examples of daily cycles of ET and wind speed for three study days are shown in Figure 4.5. The data displayed in Figure 4.5 correspond to Bowen Ratio stations located in pastures, ungrazed pastures, grassland and rangeland, as described in Chapter 3, Table 3.1. By convention, the ARM Program provides negative latent heat flux because it is an outgoing flux.

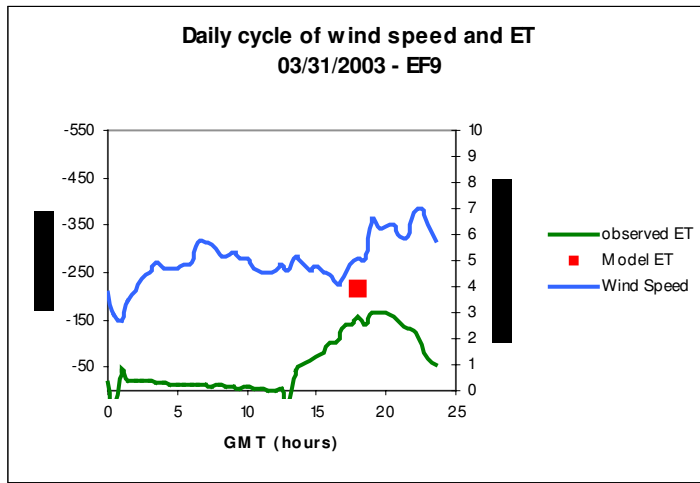
In Figure 4.5 it can be seen that the ET daily cycle is not closely related to the wind speed cycle. In Figure 4.5 (a), (c), (d) and (g) the mean wind speed (MWS) is 2.5 ms^{-1} approximately. In Figures 4.5 (b), (e), (f) and (h) the MWS is about $5.5\text{-}6 \text{ ms}^{-1}$. However ET records appear to follow the R_n pattern and cloud movements and do not seem to be affected by the wind speed variation in all the cases. For instance, the wind speed seems

to increase while ET decreases as R_n decreases in the afternoon. At night, when the solar energy is down, ET is also low regardless the MSW value. Although in some cases [Figure 4.5 (d), (e), (f) and (h)] the wind speed increases in the morning creating the sense that ET follows those wind speed increments, in fact it may be thought that both variables are affected by the solar heating.

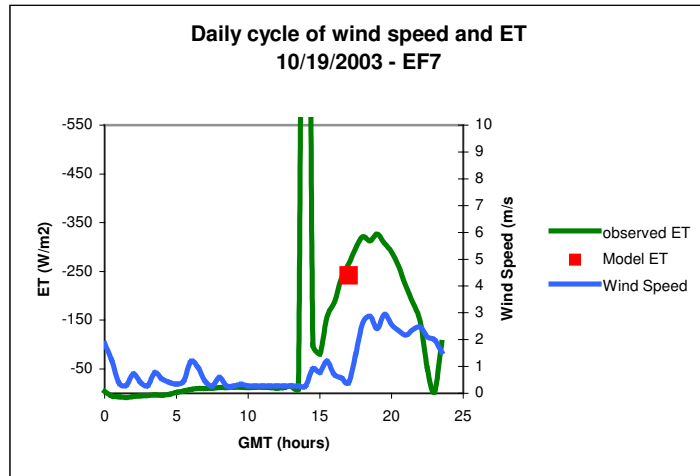
The instantaneous ET obtained with the proposed model are shown in red squares in Figure 4.5.



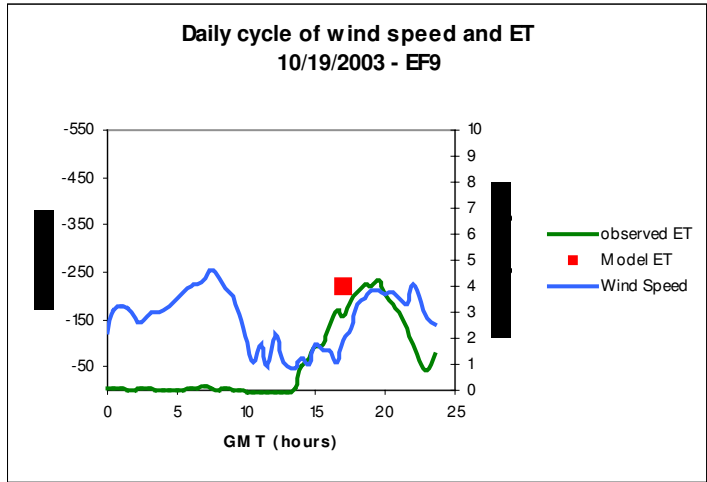
(a)



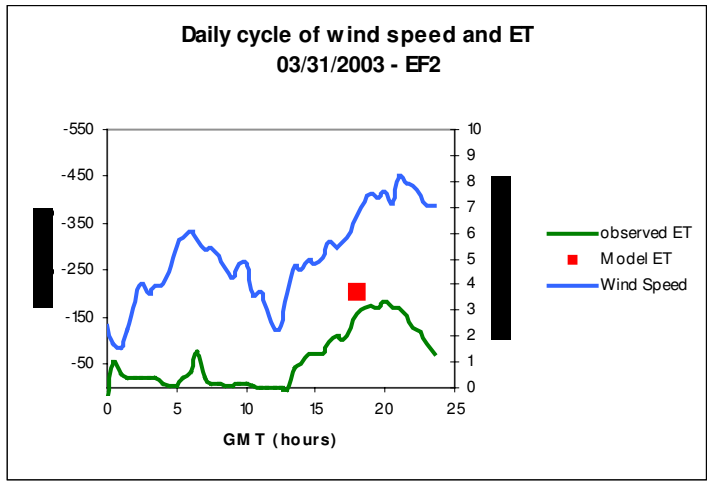
(b)



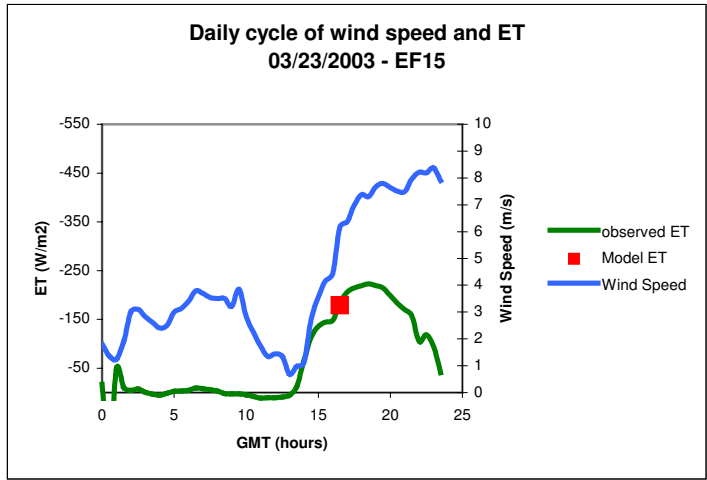
(c)



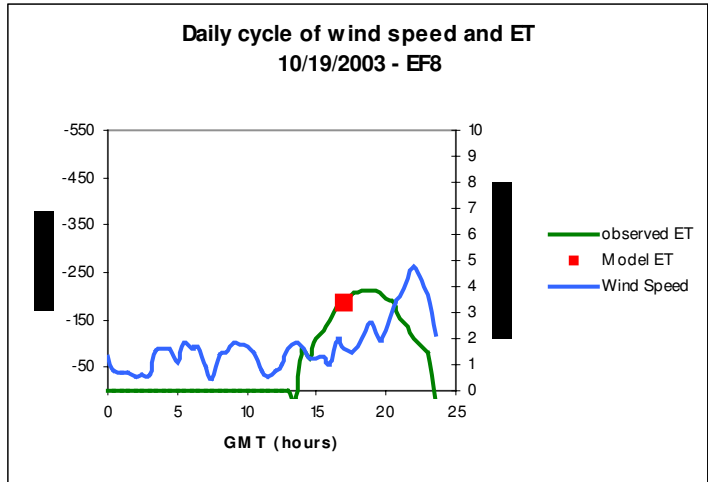
(d)



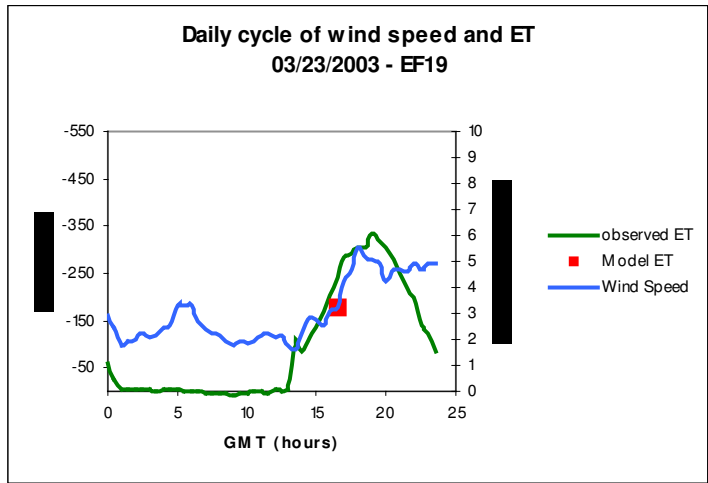
(e)



(f)



(g)



(h)

Figure 4.5: Examples of observed daily cycle of ET (Wm^{-2}), wind speed (ms^{-1}) variation and modeled instantaneous ET(Wm^{-2}).

Chapter 5 : Comparison with Different Modified Priestley and Taylor's Equation for Unsaturated Surfaces.

5.1 Introduction

Evapotranspiration (ET) comprises and links atmospheric and surface processes, hence its estimation and modeling involves complex interactions between the atmosphere and the Earth's surface. The scientific community has developed a variety of models to estimate ET. The range of models available goes from elaborated models that simulate the radioactive transfer process (*Deardorff, 1970; Parlange and Katul, 1995; Brutsaert and Sugita, 1990; Sugita et. al., 2001*) to simple methods that entail very few variables and parameters (*Priestley and Taylor, 1972; Barton, 1979; Jiang and Islam, 1999*).

Nowadays, remote sensing sensors are crucial sources of data for any of these models, not only for their efficiency in monitoring different terrestrial ecosystems but also for the type and quality of the information delivered. Thus, one of the main concerns is the accuracy of spatially distributed ET maps, obtained with this source of data (*French et al., 2005; Batra et al., 2006*).

Despite the overwhelming advances in remote sensing technology, several models and methods stem from equations such as those proposed by *Penman (1948)* and *Priestley and Taylor (1972)*, previously referred to as P-T. These authors provided two remarkable methodologies that support many of the models available today, whether they strive on energy fluxes estimation or water vapor mass transport.

The P-T physically based model stands for its simplicity and data requirements. Although the original equation was developed for saturated surfaces, it has been extended to unsaturated surfaces by *Stricker and Brutsaert (1978)*; *Barton (1979)*; *Jiang and Islam (1999)* among others. Most of the simplest extended methods are based on parameters that relate the saturated and unsaturated states of a surface, while others involve complex atmospheric and resistance parameters. In this thesis, a modified P-T equation based on a complementary relationship was derived. The proposed method makes use of the relative evaporation concept, defined as the ratio between ET and potential evapotranspiration (Epot), and accounts for the surface and air actual water vapor pressure. Table 5.1 presents the different assumptions used by *Venturini et al. (2007)*, *Barton (1979)*, *Jiang and Islam (1999)* and *Granger and Gray (1989)*.

Table 5.1: Summary of different methods to modify Priestley and Taylor’s equation.

Assumption	Author	Equation	Main Parameter
ET depends on atmospheric and surface conditions	<i>Venturini et al. (2007)</i>	$ET = \alpha \left(\frac{F\Delta}{F\Delta + \gamma} \right) (R_n - G)$	F
Surface conditions	<i>Barton (1979)</i>	$ET = \alpha \left(\frac{\sigma\Delta}{\sigma\Delta + \gamma} \right) (R_n - G)$	σ
rule ET process	<i>Jiang and Islam (1999)</i>	$ET = \phi \left(\frac{\Delta}{\Delta + \gamma} \right) (R_n - G)$	ϕ
Air vapor pressures index ET from unsaturated surfaces	<i>Granger and Gray (1989)</i>	$ET = GG \text{ Epot}$	GG

In order to evaluate the significance of atmospheric and surface parameters on ET estimates, different approaches to modify P-T's equation for unsaturated surfaces with remotely sensed data were compared.

First, an overview of the methodologies listed in Table 5.1 is provided. Then, a detailed discussion on the results obtained from the comparisons is presented, followed by conclusions.

5.2 Overview of Different Approaches to Estimate ET

5.2.1 Surface and Atmospheric Parameterization

A new parameter F that calculates the relative evaporation, defined as the ratio between potential evaporation (E_{pot}) and ET was presented in Chapter 2. The derivation of F is based on the expression proposed by *Granger and Gray (1989)*, i.e. $ET/E_{pot} = f_u (e_s - e_a) / f_u(e_s^* - e_a)$, which relates the surface actual vapor pressure (e_s), the surface saturation vapor pressure (e_s^*), the air actual vapor pressure (e_a) and the wind speed function (f_u). The assumption made to obtain F is that the wind speed function (f_u) similarly affects ET and E_{pot} since it does not depend on the surface moisture condition. Under these assumptions, an expression for F was derived in Chapter 2, [see equation (5)].

The key variable introduced in F is T_u , defined as the temperature of the surface if it is brought to saturation without changing the actual surface vapor pressure. Equation (5) was used to abridge equation (2) by expressing E_{pot} in terms of ET and F . E_w was computed with P-T equation. Consequently, combining the P-T equation with equations (2) and (5) yielded the expression,

$$ET = \alpha \left(\frac{F\Delta}{F\Delta + \gamma} \right) (R_n - G) \quad (36)$$

Expression (36) was already presented in Chapter 2 as equation (11), it is repeated here for completeness of this chapter. Equation (36) retains the simplicity of P-T while incorporating the atmospheric and surface variables in the F parameter.

5.2.2 Surface Parameterization

Barton (1979) extended P-T's hypotheses to unsaturated surfaces, asserting that ET would be explained by the surface actual vapor pressure (e_s). The author defined a coefficient, $\sigma = e_s / e_s^*$, to characterize the surface departure from the saturation condition (represented by e_s^*). Thus, the following equation was derived,

$$ET = \alpha \left(\frac{\sigma\Delta}{\sigma\Delta + \gamma} \right) (R_n - G) \quad (37)$$

Barton empirically related σ to bare soil moisture content calculated with data from microwave sensors. The author proposed the following relationship,

$$\begin{aligned} \sigma &= \frac{1.8M}{M + 30} & M < 37.5 \\ \sigma &= 1 & M \geq 37.5 \end{aligned} \quad (38)$$

where M is the soil moisture content (in percentage).

The coefficient σ represents the variability of the soil moisture content. Equation (37) was attained for bare soil surfaces and it is not evident how σ was obtained for mixed soil-vegetation surfaces. No further applications of Barton's method with remotely sensed data were found in the literature review.

Although Barton's methodology differs from the method presented here in its derivation and foundations, equation (36) is similar to equation (37), which seems to be

the form of P-T equation for unsaturated surfaces. These two equations significantly diverge regarding the definition and meaning of σ and F . F is an expression for ET/E_{pot} and accounts for the air and surface actual vapor pressure or water content, while σ only accounts for the soil moisture content.

Jiang and Islam (2001) (henceforth referred to as J-I) also modified P-T equation for heterogeneous unsaturated surfaces. Their approach was based on an interpretation of the Triangle Method (*Gillies and Carlson, 1995*), so-called because of the triangular distribution of pixels customarily observed when the data is plotted in the surface radiant temperature (T_o)-vegetation index (i.e. NDVI) space. Most of the discussions related to the triangle bounds have been focused on the warm edge of the pixel distribution, where the highest surface temperatures tend to exhibit a well-defined boundary over a range of vegetation amounts. *Jiang and Islam (2001)* interpreted that the pixels along the warm edge represent the minimum ET for each vegetation class, while the cold edge bounds the maximum ET, thus the actual magnitude of ET can vary within these bounds. Further, a coefficient ϕ was estimated by a simple two-step linear interpolation between the sides of the triangle. This coefficient links physical characteristics of the pixels to ET.

It has been proposed by *Moran et al. (1994)* that the interior of the triangle scales linearly with respect to the surface turbulent energy fluxes. Such an interpretation of the $T_o - NDVI$ relationship provides a basis to obtain ϕ parameter and ET for each pixel in an image, as

$$ET = \phi \left[\frac{\Delta}{\Delta + \gamma} \right] (R_n - G) \quad (39)$$

J-I's parameter ϕ replaces P-T parameter α . ϕ varies from zero, for a dry bare soil surface, to 1.26, for a saturated surface.

This methodology represents ET for a given pixel based on a NDVI-T_o contextual interpretation. Therefore, ϕ only involves physical characteristics of the surface such as surface wetness, surface conductance and temperature (*Jiang and Islam, 2001*).

5.2.3 Atmospheric Parameterization

As already mentioned in Chapter 1, *Granger and Gray (1989)*, hereafter refer to as G-G, derived a model to calculate ET following a development analogous to that of *Penman (1948)* and the relative evaporation concept. These authors stated that as ET increases, the vapor pressure of the air also increases, assuming that the drying power of air, E_a , reflects the drying process of the surface. Hence, for a nonsaturated surface, ET is a function of E_a . A coefficient $GG \approx ET/E_{pot}$ was empirically related to $D = E_a/(E_a+Q)$, and the following expression of GG was obtained,

$$GG = \frac{ET}{E_{pot}} \approx \frac{1}{1 + 0.028 * \exp(8.045 * D)} \quad (40)$$

where $Q = R_n - G$ is the available radiant energy.

The expression of GG is obtained under the assumption that the air water vapor deficit explains ET, thus the surface condition is not represented in equation (40). The expression of GG is complex and may require site-specific calibration (*Granger and Gray, 1989*). *Eichinger et al. (1996)* derived an analytical expression of P-T parameter α for well-watered surfaces, and revealed that E_a is a prevailing factor in that particular case, however more surface variables are involved in P-T parameter α when the surface is not saturated.

The first regression between GG and D obtained by G-G was linear, suggesting that ET was proportional to E_a . In a second test, re-arranging ground data, the authors

obtained a non-linear expression between GG and D [equation (40)]. Assuming that E_a reflects the drying-surface process and that E_a is linearly related to ET, the relative evaporation could be written as,

$$\frac{ET}{E_{pot}} \approx \frac{E_a}{E_{pot}} \approx \frac{f_u (e_a^* - e_a)}{f_u (e_s^* - e_a)} \quad (41)$$

The advantage of the approximation made in equation (41) is that it can be easily calculated from T_s , T_a and T_d and does not need site-specific calibration as equation (40) does, while G-G's hypothesis stays the same. As a result, ET/ E_{pot} could be estimated from the following expression,

$$\frac{ET}{E_{pot}} \approx \frac{(T_a - T_d)}{(T_s - T_d)} \quad (42)$$

It is not the intent of this comparison to apply Granger and Gray's ET model. Only the relative evaporation parameterization represented by equation (41) is analyzed here. This new expression of ET/ E_{pot} does not account for the surface actual moisture, since T_s represents the saturation condition and the actual surface wetness is not characterized in equation (42).

5.3 Compare and Contrast Different ET Estimation Approaches

In order to estimate ET with all these methods, R_n , soil heat fluxes, Δ and T_u were calculated as described in Chapter 3. Indeed, the MODIS products and ground observations used for this comparison are those presented in Chapter 3.

Firstly, the atmospheric-surface parameterization, represented by the proposed method, was compared with Barton and J-I methods that only use information about the

surface. Finally, the proposed method was contrasted with the atmospheric parameterization, similar to that presented by *Granger and Gray (1989)*.

5.3.1 Surface Vs Atmospheric-Surface Parameterizations

Barton method Vs this thesis' method

As presented in Section 5.2.2, *Barton (1979)* extended P-T equation for nonsaturated surfaces by defining a coefficient $\sigma = e_s/e_s^*$. His approach assumes that soil moisture is the only variable limiting ET.

The F equivalent expression of Barton's coefficient σ is obtained by assuming that the air is dry and does not limit the ET process. It also assumes that T_a and air relative humidity are homogeneous over the entire study area. Under these assumptions F would be equal to e_s/e_s^* , similar to σ . Accordingly, e_s was estimated from T_u and e_s^* from T_s .

Table 5.2 presents the regional mean and standard deviation of observed and derived ET. Barton's method gives mean ET estimates close to the observed means. The differences among the observed and derived mean ET values are lower than 76 Wm^{-2} . The proposed method matches the observed means with an error less than 45 Wm^{-2} . The observed standard deviations are higher than those obtained with this thesis' method and Barton's approach. Figure 5.1 illustrates the mean ET values presented in Table 5.2

Table 5.2: Observed and modeled ET (Wm^{-2}) means and standard deviations (S).

Julian Day	Observed		Thesis model		Barton		J-I		G-G	
	Mean	S	Mean	S	Mean	S	Mean	S	Mean	S
DOY82	191.79	34.22	181.34	14.84	174.82	29.64	196.77	38.60	286.51	32.14
DOY 90	148.56	38.33	164.45	14.25	185.85	37.15	194.92	50.54	235.20	51.68
DOY 91	232.55	41.58	234.20	17.59	213.97	27.71	211.76	44.49	296.47	27.71
DOY 249	284.35	40.82	308.86	27.53	300.09	27.39	356.99	57.99	373.13	40.68
DOY 262	242.07	40.74	197.10	13.06	255.47	26.43	285.92	32.97	304.86	23.52
DOY 285	203.97	33.38	214.57	16.27	279.97	29.41	320.51	29.45	337.49	28.02
DOY 292	212.20	46.10	231.24	17.78	250.71	25.38	236.69	37.09	311.54	25.81

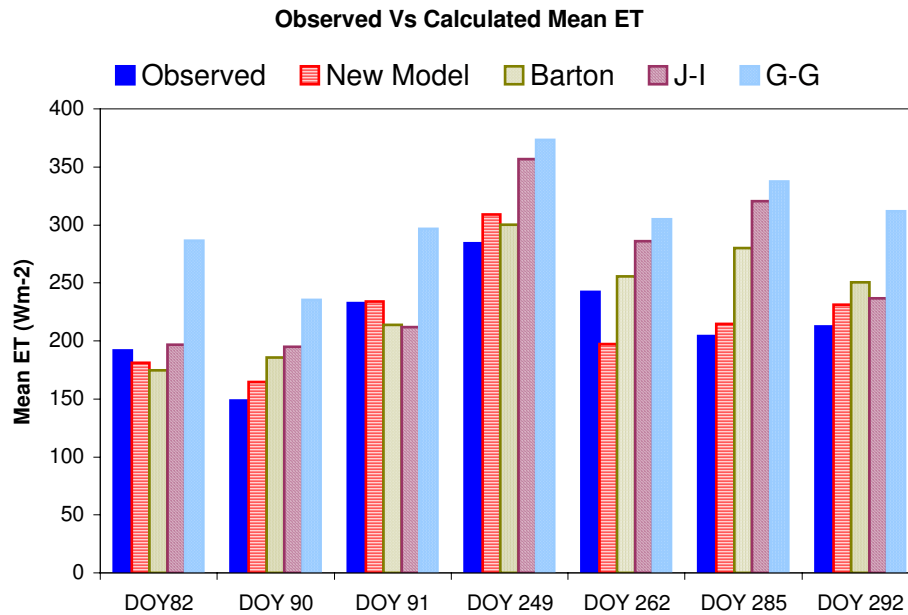


Figure 5.1: Mean ET (Wm^{-2}) observed and calculated with the proposed equation, Barton's equation, Jiang and Islam methodology and Granger and Gray approach.

In Table 5.3 ET results with Barton's approach and with the new proposed method are compared. The root mean square errors (RMSE) and the bias (Barton- New approach) range from 20 to 60 Wm^{-2} and from -10 to 60 Wm^{-2} , respectively, while the

correlation coefficient (R^2) varies from 0.59 to 0.90. In general, Barton’s model results in larger ET estimates than the new method. These results are consistent with the postulates made to derive each method. Barton’s model implies that the only limiting factor is the surface moisture and that atmospheric conditions do not restrict ET. On the other hand the proposed method considers that the atmosphere as well as the surface vapor pressure are limiting factors for ET. The proposed assumptions would grant more realistic and less overestimated ET estimates.

To further explore the implications of these assumptions, estimates with Barton model and ground measurements were contrasted (Figure 5.2).

Table 5.3: ET (Wm^{-2}) comparison between Barton’s and proposed method estimates.

Julian Day	RMSE	BIAS (Barton - New)	R^2
DOY 82	20.74	-9.52	0.78
DOY 90	34.14	-23.88	0.76
DOY 91	30.94	-21.88	0.59
DOY 249	17.37	-8.77	0.85
DOY 262	58.29	55.14	0.72
DOY 285	62.23	60.36	0.90
DOY 292	23.23	18.04	0.84

The overall RMSE and bias (Obs-Cal) obtained with Barton’s parameterization are 58.93 and -31.17 Wm^{-2} , respectively and the R^2 is 0.69. The proposed method, with atmospheric and surface variables, yields RMSE and bias of about 33.9 and -11 Wm^{-2} , respectively and an R^2 equal to 0.78. These statistics support the hypothesis that atmospheric and surface variables would play a significant role in estimating ET from

unsaturated surfaces. In fact, this contrast can be recapitulated in terms of e_a , which is the main difference between F and σ estimates.

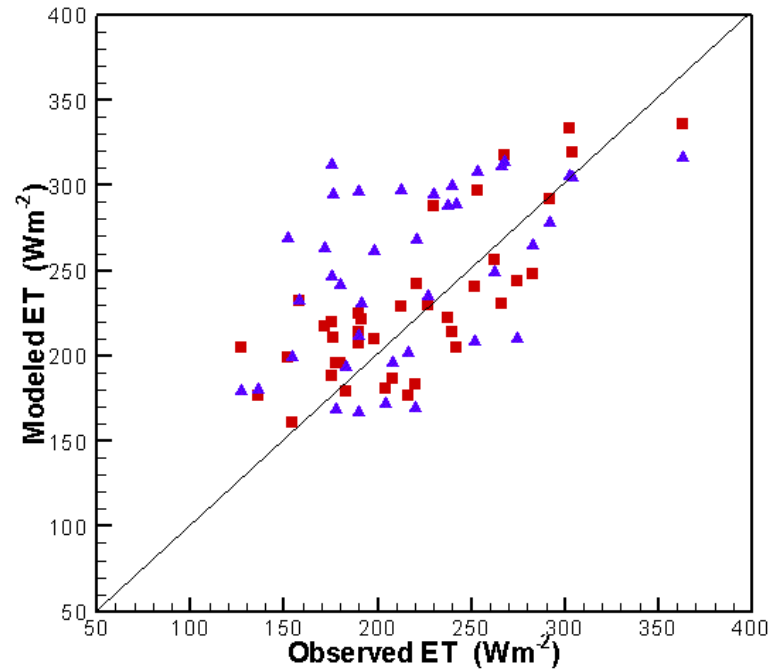


Figure 5.2: Comparison between Barton and proposed method against ground measurements.

It should be noted that Barton's empirically related σ with soil moisture content, variable that would explain only part of the water source in a mixed pixel, while the surface temperature (T_s) reflects the surface type, cover and moisture. Even though the calculation of σ presented here is different from Barton's application (*Barton, 1979*), it seems more representative of the unsaturated surface, given it is calculated from T_s and T_u , without site-specific calibration. Therefore, it may be concluded that the inclusion of atmospheric variables significantly improves ET estimates.

Jiang and Islam methodology Vs this thesis' method

Jiang and Islam (2001) support their methodology on empirical evidences of a unique relationship between the range of ϕ and physical characteristics of the surface.

Table 5.2 includes the mean and standard deviation of observed and derived ET with the J-I method. The difference between the observed and J-I derived regional mean ET values range from 5 to 116 Wm^{-2} (Figure 5.1), while the derived and the observed standard deviations are very close.

The results obtained with J-I method are compared with the new proposed method and presented in Table 5.4 in terms of RMSE, biases and R^2 . In general, J-I model results in larger ET estimates than the new method, with an average RMSE of about 55 Wm^{-2} .

Table 5.4: ET (Wm^{-2}) comparison between Jiang and Islam's method (J-I) and new proposed method estimates.

Julian Day	RMSE	BIAS (J-I - New)	R^2
DOY 82	72.14	66.549	0.73
DOY 90	56.15	-14.80	0.19
DOY 91	47.81	-24.09	0.38
DOY 249	77.94	58.13	0.84
DOY 262	60.58	50.41	0.81
DOY 285	61.79	20.45	0.65
DOY 292	32.47	4.011	0.49

The results presented in Table 5.4 are comparable to those obtained with Barton's parameterization and exhibited in Table 5.3. Although both methods were derived from diverse approaches, they both involve only surface characteristics.

The contrast between ground measurements and J-I estimates are shown in Figure 5.3. The overall RMSE and bias are 59.26 and -32.67 Wm^{-2} , respectively, and R^2 is about 0.70 .

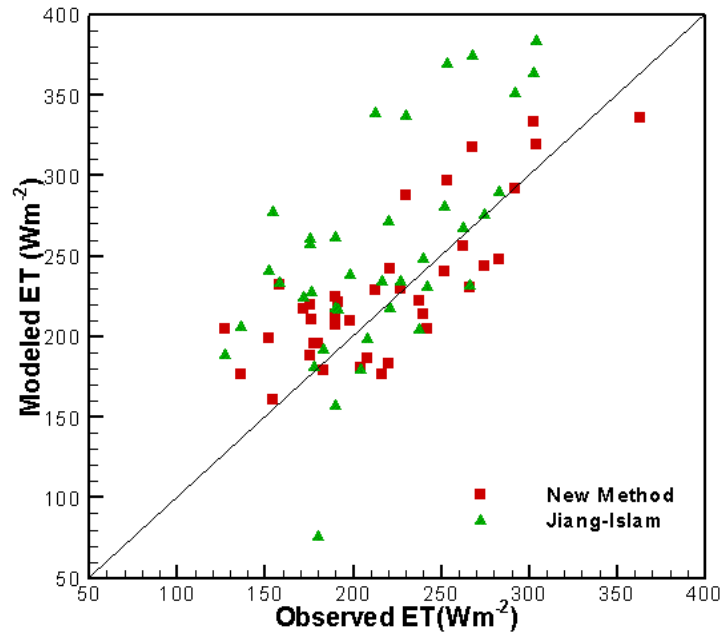
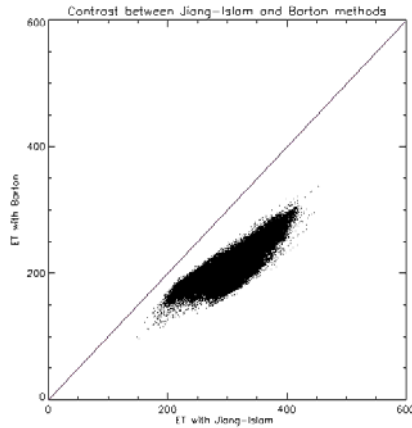
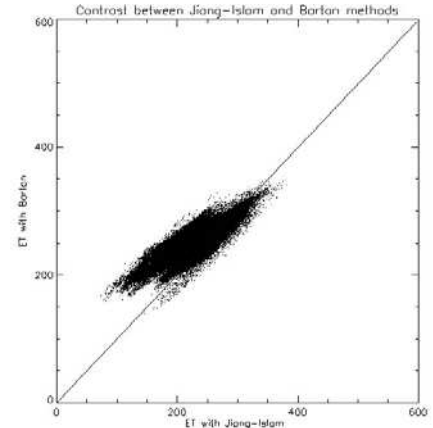


Figure 5.3: Comparison between Jiang and Islam (J-I) and proposed method against ground measurements.

Barton’s methodology and J-I models result in similar errors suggesting that ET estimates would be closely related to the assumptions made, i.e. the surface condition controls the ET process. However, the differences in equations (37) and (39) are observed in Figure 5.4, where a pixel-to-pixel contrast is presented. These two methods not only differ in the form of their equations but also in the parameterization of the surface condition. J-I’s is based on the surface fluxes partition manifested in the NDVI-To triangle space while Barton’s equation parameterize the soil water content. Figure 5.4 shows that these two methodologies do not always yield similar ET estimates.



April 1st 2003



October 19th, 2003

Figure 5.4: Comparison between ET estimates from Jiang and Islam (J-I) and Barton methods for two days.

5.3.2 Atmospheric Vs Atmospheric-Surface Parameterizations

The relative evaporation expression obtained with G-G assumptions [equation (42)] is used to estimate the F coefficient in equation (36) and the results contrasted with those obtained using equation (5) and equation (36). Table 5.2 displays the mean and standard deviation of observed and derived ET with G-G method. The differences between the observed and G-G derived regional mean ET values range from 60 to 130 Wm^{-2} , while derived standard deviations match those observed.

Table 5.5 displays the RMSE, biases and R^2 resulting from the contrast between G-G and the new method. The RMSE and the bias (G-G – New approach) range from 34 to 156 Wm^{-2} and from 25 to 156 Wm^{-2} , respectively, while R^2 values are around 0.95. Assuming ET is a function of E_a leads to larger ET estimates than those obtained with the proposed methodology. Although E_a may reflect ET in some cases, it basically assumes that the surface is wet and water is always available. Equation (42) is also comparable

with the analytical expression of P-T parameter α for saturated surfaces, proposed by

$$Eichinger \text{ et al. (1996), i.e. } C = \frac{e_a^* - e_a}{e_s^* - e_a}.$$

Table 5.5: ET (Wm⁻²) comparison between Granger and Gray’s assumption (G-G) and the proposed method estimates.

Julian Day	RMSE	BIAS (G-G - New)	R²
DOY82	156.93	156.29	0.97
DOY 90	33.90	25.47	0.97
DOY 91	62.19	60.62	0.92
DOY 249	66.15	64.27	0.97
DOY 262	128.23	127.92	0.99
DOY 285	145.02	144.59	0.96
DOY 292	79.97	78.87	0.89

The aforementioned assumption may be the cause of the large range of RMSE and biases observed in Table 5.5 for some days. In order to illustrate this point, Figure 5.5 shows the relationship between all the variables involved in F coefficient, i.e. e_s , e_a , T_d , T_u and T_a , for two studied days. In fact, during DOY262 (b), T_a is around 290 °K in the entire study area, which seems to be drier than during DOY90 (a), i.e. clearly separated from the SVP curve (see the purple diamonds in Figure 5.5). A Similar situation is observed for surface variables (black dots in Figure 5.5). The large errors detected in DOY262 may be explained by the dry air and surface observed in the study area, while during DOY90 a mixture of dry and wet (air and surface) pixels is observed.

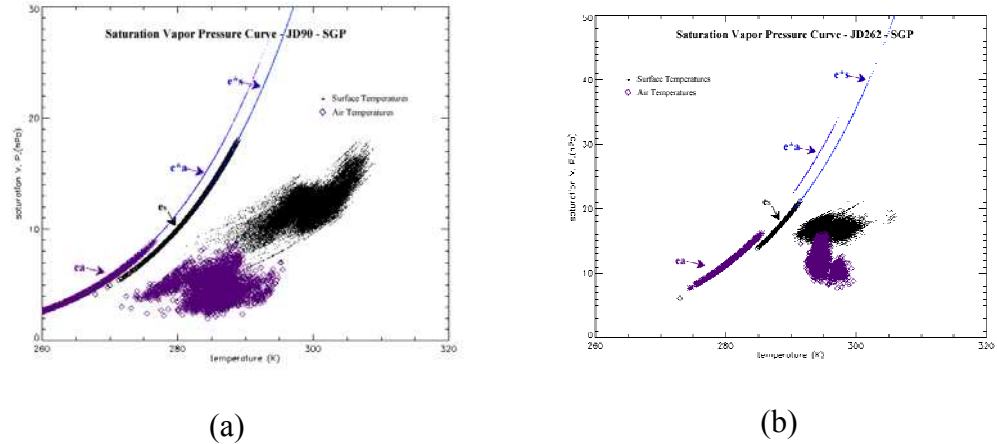


Figure 5.5: Buck's saturation vapor pressure curve. e_a was obtained with T_d , e_s with T_w , e_a^* with T_a and e_s^* with T_s . T_a vs. e_a are shown with violet diamonds and T_s vs. e_s with black dots. (a) corresponds to March 31st, 2003 and (b) corresponds to September 19th, 2006.

Figure 5.6 displays the validation with ground observations, where a large dispersion of ET values, similar to that obtained with P-T equation is observed. The overall RMSE and bias obtained with G-G's assumptions are 110.41 and -102.35 Wm^{-2} , respectively.

The results obtained in this Chapter would indicate that a combination of atmospheric and surface parameters is needed to attain accurate results. Atmospheric variables alone would not fully explain the drying process of the surface for every atmospheric-surface condition. However, considering surface variables alone (as proposed by Barton and Jiang-Islam) would lead to more realistic estimates than considering only atmospheric parameters. Figure 5.1 clearly summarizes the main conclusion of this chapter.

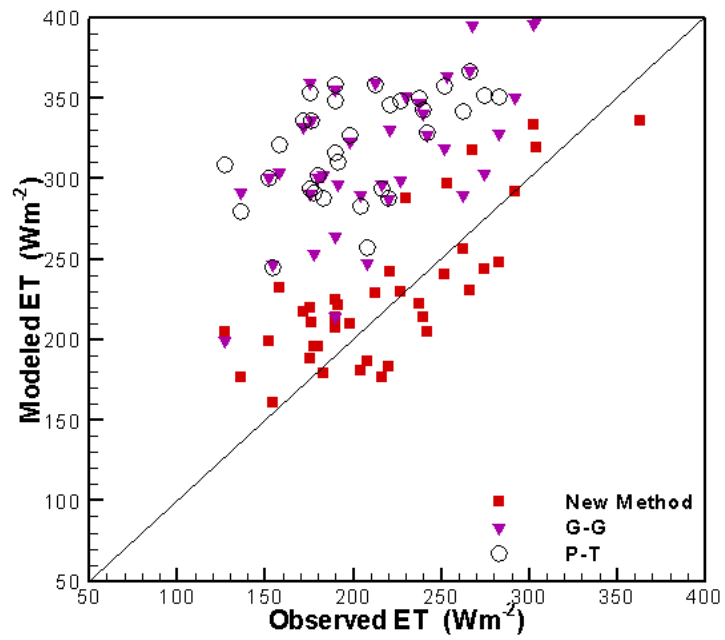


Figure 5.6: Comparison between Granger and Gray (G-G) and proposed method against ground measurements. Results with Priestley-Taylor's equation (P-T) are also over plotted as a reference.

Chapter 6 : Conclusions and Future Work

6.1 Conclusions

Many hydrologic modeling and agricultural management applications require accurate estimates of the evapotranspiration (ET) and the evaporative fraction (EF). Over the last two decades, several models have been developed to estimate ET for the wide range of spatial and temporal scales provided by remote sensing data.

The recent introduction of the Atmospheric Profiles Product derived from MODIS sensors onboard of EOS-Terra and EOS-Aqua satellites is a significant advance for the scientific community. The MODIS Atmospheric profile product (MOD07 and MYD07) provides atmospheric and dew point temperature profiles on a daily basis at 20 vertical atmospheric pressure levels and at 5x5km spatial resolution (*Menzel et al., 2002*). When combined with readily available land surface temperature (Ts) maps obtained from different sensors, this new remote source of atmospheric data offers a new opportunity to revise the complementary relationship concepts that relate ET and E_{pot}. In addition, *Crago and Crowley (2005)* validated the complementary relationships at very short time scales (10-30 min). They published promising results that encourage the exploration of nearly instantaneous remotely sensed data and complementary models.

This work makes use of these newly available products, revisiting complementary formulations that were not utilized by researchers in recent years. The proposed approach to estimate ET is based on Granger's complementary formulation and the P-T equation.

The P-T equation is used to compute E_w, which has been widely used for wet environments where the main driving force is the available radiant energy (*Preistley and*

Taylor, 1972; Brutsaert and Stricker, 1979; Morton, 1983; Crago and Crowley, 2005; Ramirez et al., 2005). The complementary model is here enhanced by the relative evaporation concept, F , that it introduces a new dimensionless coefficient to relate E_{pot} and ET with readily available data. Thus, the model avoids the calculation of friction factor and wind speed functions to estimate spatially distributed ET maps over vast areas.

The physically based ET derivation presented here, uses a modified version of P-T equation and corrects the ET estimate for saturated surfaces based on surface and atmospheric local conditions. This new approach is perhaps one of the simplest modified P-T formulations that incorporates atmospheric conditions in a relative evaporation coefficient, F , without the need for site-specific relationships. In the application of equation (11), empirical relationships are involved in R_n and G calculations. The estimation of G and R_n uses auxiliary relationships that do not require any site specific calibration and can be estimated directly from remote sensors.

A key variable introduced in the proposed formulation is T_u . A similar concept has been defined to estimate the regional equilibrium evaporation temperature used in the Ts-NDVI contextual space (*Moran and Jackson, 1991; Moran et al., 1994; Jackson et al., 1988; Price, 1990; Carlson et al., 1995; Jiang and Islam, 1999*). In the proposed method, T_u is associated to the surface actual vapor pressure that may vary at local scales with land cover and soil moisture. Thus, T_u was estimated from the saturation vapor pressure curve, assuming that water in unsaturated surfaces behaves similarly to that in saturated surfaces. Although this assumption involves a simplification of the physics behind T_u , it was adopted in order to avoid complex parameterizations that would introduce uncertainties in F coefficient and ET estimates.

The complementary theory assumes a surface without advection influences. The same assumption was made by *Priestley and Taylor (1972)* to solve the one dimensional diffusion equations of temperature and specific humidity. So there is a regional component in the proposed model that is inherited from the aforementioned theories. The relative evaporation concept defined by *Granger (1989)* involves the bulk water vapor mass transfer theory, which implies a local scale. In a more practical way, it can be said that the new method corrects the ET from a saturated surface (where $R_n - G$ is the main driving force for ET) with the local surface-atmosphere conditions at the pixel scale. The absence of regional assumptions makes the method applicable to a wide range of scales. equation (11), i.e. the ET model, can be solved in every pixel of homogenous or heterogeneous areas with spatially distributed atmospheric and surface data. *Barton (1979)* derived an equation similar to equation (11), however both models differ not only on the theory behind them but also on the concept of relative evaporation F , the concept of σ and parameterization.

It should be noted that the proposed approach makes no distinction between soil and vegetation temperature profiles within the 1 km pixel used in the analysis. However, it is worthwhile to remark that this methodology was derived independently of the data source. The proposed methodology was applied to a region in the United States known for its data availability for model validation: the Southern Great Plains.

Daytime images for seven days in year 2003 with at least 80% of the study area free of clouds were selected. The relative evaporation is estimated from remotely sensed T_s and T_d acquired from MODIS sensors. The T_d product was used to estimate the air vapor pressure at 1000 hPa. Traditionally, atmospheric variables are observed at screen level; however the vapor pressure theory was applied to data observed at different heights

(*Priestley and Taylor, 1972; Monteith and Unsworth, 1990; Eichinger, et al, 1996*). The bulk mass transfer establishes a balance between the surface and the air above it (*Granger, 1989; Priestley and Taylor, 1972*) without specifying the elevation of the air above the surface. *Bisht et al., (2005)* used MODIS atmospheric profile to derive spatially distributed R_n maps. Their results showed that MODIS products render better results than those obtained with sparse ground stations. In this work, results suggest that the vapor pressure mass transfer can be calculated with MODIS products to estimate fluxes at the surface level. Besides, MODIS products in combination with a topographic model may be used to obtain maps of T_a and T_d at the screen level.

There are no generally accepted methodologies to validate distributed ET values to point flux station observations, and hence it is difficult to evaluate the reliability of model outputs over the entire domain. Nonetheless unfiltered point measurements seem to be an appropriate mean to validate remote sensing applications (*Jiang and Islam, 2001; Kustas et al., 2003; Nishida et al., 2003; Bisht et al., 2005; Batra et al., 2006*). Several descriptive statistics for observed and model ET for days analyzed were compared, as shown in Table 3. In this case the mean and standard deviation (S) were calculated. The mean and S of observed ET would represent the study area from ground measurements (at most 10 values per study day), while statistics for the modeled ET represent results from about 200,000 pixels over the domain. This contrast should raise a word of caution about what can be inferred from the comparison between these two sets of data.

There is a good agreement between observed and modeled mean ET values for each day, with differences ranging from ± 1 to $\pm 44 \text{ Wm}^{-2}$. Similar contrast was found in other studies with different ET models where the reported results are compared with those presented here (*Jiang and Islam, 1999 and 2001; Kustas et al., 2003; Batra et al., 2006*).

The overall comparison between ground measurements and the matching ET estimates at the corresponding pixel yield a RMSE and bias are 33.89 (15% of the mean ET) and -10.96 Wm^{-2} respectively, with an R^2 of about 0.79.

A first order analysis was performed to evaluate the error introduced in the modeled ET from estimation errors in T_s , T_u and T_d . First, the errors introduced in the relative evaporation F caused by uncertainties in temperature estimates were analyzed. Then, the uncertainties on ET due to errors in F coefficient were calculated. Results show that errors of about 5 K in T_u and 3 K in T_s and T_d would result in an error of about 10% in ET. From this preliminary analysis, it appears that uncertainties in the estimation of F and T_u are not likely to introduce errors larger than the corresponding measurement errors for ET over large areas.

The sensitivity of the new method to T_s errors was further studied applying the one channel brightness temperature. MODIS T_s product was replaced by MODIS's band 31 brightness temperature without atmospheric corrections. The errors in T_{31} can be as large as 20°K, however ET estimates with equation (11) would have errors lower than 10% of the mean ET. Equation (11) not only provides distributed maps of ET but also seems to compensate the common errors of T_s estimates. This new methodology seems to provide acceptable ET results with simple estimates of T_s .

Many works focus on analyzing the accuracy of spatially distributed ET maps by contrasting different methods. In this work ET parameterizations for unsaturated surfaces were contrasted. Thus, different hypotheses and methods that modified Priestley and Taylor's equation for unsaturated surfaces were compared and validated.

The results suggest that atmospheric and surface variables would play an important role in ET estimation and that they both should be incorporated in P-T extended ET

models. Considering only atmospheric variables would produce ET estimates closer to E_w , given that the underlying assumption is a saturated surface. Conversely, the surface parameterization alone yields significantly better results.

The proposed method to estimate ET incorporates a relative evaporation coefficient computed with air and surface actual vapor pressures. When compared with ground observations, model results yield errors of around 18%. The contrast with Barton's approach and Jiang and Islam's method, which parameterize only the surface conditions, indicates that this thesis' method matches ET ground measurements with smaller errors than the other two. Indeed, Barton's ET estimates are about $\pm 31\%$ of the mean ET while Jiang and Islam's results are $\pm 30\%$ of the mean ET. These preliminary results suggest that relating ET with surface variables alone is sufficient to compute ET with errors similar to those obtained with complex parameterizations (*Kustas et al., 2003; Rivas and Caselles, 2004; Nishida et al., 2003; Norman et al., 2003, French et al. 2005*). However, intricate ET models would introduce larger uncertainties than Barton's and Jiang-Islam's simple methodologies. Granger and Gray's hypothesis that the drying power of air reflects the ET process was applied to parameterize the relative evaporation ratio. Results from validating this assumption yield errors of $\pm 55\%$ of the mean ET, similar to those obtained the original equation proposed by Priestley and Taylor, i.e. $\pm 60\%$.

Although the results presented along this thesis are not exhaustive, our proposed method seems to consider a set of variables that lead to errors in ET estimates of less than 20% of the mean ET, without forfeiting the simple form of Priestley and Taylor's equation and the benefits of remotely sensed data.

6.2 Future Work

At present, ongoing research is addressing an extension of this methodology for partially cloudy and cloudy days using data from passive microwave sensors, such as the Advanced Microwave Scanning Radiometer - Earth Observing System (AMSR-E) instrument on the NASA EOS Aqua satellite. Preliminary results show that the common spatial resolutions of passive microwave sensors may introduce errors in T_s estimates, however further research must be carried on.

The estimation of T_u could be improved by introducing the surface water content condition to the night-day methodology presented in Appendix III. Up to now, the alternative method to calculate T_u has not yielded better results than those obtained with the SVP method, therefore and more research must be done to explore the night-day methodology even further.

References

- Anderson, M. C., Norman, J. M., Diak, G. R., Kustas, W. P., & Mecikalski, J. R. (1997). A two-source time-integrated model for estimating surface fluxes using thermal infrared remote sensing. *Remote Sensing of Environment*, 60, 195–216.
- Atmospheric Radiation Measurements (ARM) Program, (1989). <http://www.arm.gov>.
- Barton, I. J. (1979). A parameterization of the evaporation from nonsaturated surfaces. *Journal of Applied Meteorology*, 18, 43-47.
- Batra, N., Islam, S., Venturini, V., Bisht, G. & Jiang, L. (2006). Estimation and Comparison of Evapotranspiration from MODIS and AVHRR sensors for Clear Sky Days over the southern Great Plains. *Remote Sensing of Environment*, 103, 1-15.
- Bastiaanssen, W.G.M., Pelgrum, H., Menenti, M. A & Feddes, R.A. (1996). Estimation of surface resistance and Priestley-Taylor α -parameter at different scales. In Stewart J., et al., (Editors.). NewYork: John Wiley and Sons. *Scaling up in Hydrology using Remote Sensing*, 93-111.
- Bastiaanssen, W.G.M., Menenti, M. A, Feddes, R.A. & Hollslag, A. A. M. (1998). A remote sensing surface energy balance algorithm for land (SEBAL) 1. Formulation. *Journal of Hydrology* 212 (13), 198-212.
- Bisht, G., Venturini, V., Jiang, L. & Islam, S. (2005). Estimation of Net Radiation using MODIS (Moderate Resolution Imaging Spectroradiometer) Terra Data for clear sky days. *Remote Sensing of Environment*, 97, 52-67.
- Bolton, D. (1980). The computation of equivalent potential temperature. *Monthly Weather Review*, 108, 1046-1053.

- Bouchet, R.J. (1963). Evapotranspiration réelle et potentielle, signification climatique. International Association of Scientific Hydrology. *General Assembly of Berkeley, Transactions*, 2, Evaporation, Berkeley, Calif.
- Brutsaert, W. & Stricker, H. (1979). An advection-aridity approach to estimate actual regional evapotranspiration. *Water Resources Research*, 15(2), 443–450.
- Brutsaert, W. & Sugita, M. (1990). The extent of the unstable Monin-Obukhov layer for temperature and humidity above complex hilly grassland. *Boundary Layer Meteorology*, 51, 383-400.
- Brutsaert, W. & Parlange, M. B. (1998). Hydrologic cycle of explanations the evaporation paradox. *Nature*, 396 (5), 30.
- Brutsaert, W. (2005). Hydrogy. An Introduction. Cambridge University Press, New York, USA, 605 pages. ISBN 0521824796.
- Buck, A. L. (1981). New equations for computing vapor pressure and enhancement factor. *Journal of Applied Meteorology*, 20, 1527-1532.
- Calvet, J.C., Noilhan, J. & Besseoulin, P. (1998). Retrieving the root zone soil moisture from surface soil moisture or temperature estimates: A feasibility study on field measurements. *Journal of Applied Meteorology*, 37, 371-386.
- Campbell J. B. (2002) Introduction to Remote Sensing. The Guilford Press, 3rd edition. New York, USA, 621 pages. ISBN 1572306408.
- Carlson, T. N., Gillies, R. R., & Schmugge, T. J. (1995). An interpretation of methodologies for indirect measurement of soil water content. *Agricultural and Forest Meteorology*, 77, 191-205.

- Castelli, F., Entekhabi, D. & Caporali E. (1999). Estimation of surface heat flux and an index of soil moisture using adjoint-state surface energy balance. *Water Resources Research*, 35(10), 3115–3125.
- Chauhan, N. S., Miller, S. & Ardanuy, P. (2003) - Spaceborne soil moisture estimation at high resolution: a microwave-optical/IR synergistic approach. *International Journal of Remote Sensing*, 24(22), 4599-4622.
- Chow, V. T., Maidment, D. R. & Mays, L. W. (1988). Applied Hydrology. McGraw-Hill, Inc. New York, 572 pages. ISBN 0070108102.
- Coleman, H. W. & Steele, W. G. (1999). Experimentation and Uncertainty Analysis for Engineers. John Wiley & Sons. 2nd edition. New York, 296 pages.
- Courault, D., Seguin, B. & Olioso, A. (2005). Review to estimate Evapotranspiration from remote sensing data: Some examples from the simplified relationship to the use of mesoscale atmospheric models. *Irrigation and Drainage Systems*, 19, 223-249.
- Crago, R. & Crowley, R. (2005). Complementary relationship for near-instantaneous evaporation. *Journal of Hydrology*, 300, 199-211.
- Crago, R., Hervol, N. & Crowley, R. (2005). A complementary evaporation approach to the scalar roughness length. *Water Resources Research*, 41, W06017, doi:10.1029/2004WR003521.
- Dash, P., Göttsche, F. M., Olesen, F. S. & Fischer, H. (2002). Land surface temperature and emissivity estimation from passive sensor data: theory and practice-current trends. *International Journal of Remote Sensing*, 23(13), 2563-2594.
- Deardorff, J. W. (1970). Preliminary results from numerical integrations of the unstable planetary boundary layer. *Journal of Atmospheric Sciences*, 27, 1209-1211.

- Eichinger, W. E., Parlange, M. B. and Stricker, H. (1996). On the concept of equilibrium evaporation and the value of the Priestley-Taylor coefficient. *Water Resources Research*, 32 (1), 161-164.
- French, A.N., Jacob, J., Anderson, M.C., Kustas, W. P., Timmermans, W., Gieske, A., Su, Z., Su, H., McCabe, M. F., Li F., Prueger, J. & Brunsell N. (2005). Surface energy fluxes with the Advanced Spaceborne Thermal Emission and Reflection radiometer (ASTER) at the Iowa 2002 SMACEX site (USA). *Remote Sensing of Environment*, 99, 55-65.
- Fritschen, L., & Simpson, J. R. (1989). Surface energy and radiation balance systems: General description and improvements. *Journal of Applied Meteorology* 28, 680-689.
- Granger, R.J. (1989). A complementary relationship approach for evaporation from nonsaturated surfaces. *Journal of Hydrology*, 111, 31-38.
- Granger, R.J. & Gray, D.M. (1989). Evaporation from natural nonsaturated surfaces. *Journal of Hydrology*, 111, 21-29.
- Granger, R.J. & Gray, D.M. (1990). Examination of Morton's CRAE model for estimating daily evaporation from field-sized areas. *Journal of Hydrology*, 120, 309-325.
- Granger, R. J. (2000). Satellite-derived estimates of evapotranspiration in the Gediz basin. *Journal of Hydrology*, 229, 70-76.
- Gillies, R.R., Carlson, T.N., Cui, J., Kustas, W.P. & Humes, K.S. (1997). A verification of the 'triangle' method for obtaining surface fluxes from remote measurements of the Normalized Difference Vegetation Index (NDVI) and surface radiant temperature. *International Journal of Remote Sensing*, 18(15), 3145-3166.

- Gillies, R. R. & Carlson, T. N. (1995). Thermal remote sensing of surface soil water content with partial vegetation cover for incorporation into climate models. *Journal of Applied Meteorology*, 34, 745-756.
- Gómez, M., Oliso, A., Sobrino, J. A. & Jacob, F. (2005). Retrieval of evapotranspiration over the Alpillles/ReSeDA experimental site using airborne POLDER sensor and a thermal camera. *Remote Sensing of Environment*, 96, 399-408.
- Halldin, S & Lindroth, A. (1992). Errors in net radiometry: Comparison and evaluation of six radiometer designs. *Journal of Atmospheric Oceanic Technology*, 9, 762-783.
- Heilman, J.L. & Brittin, C. L. (1989). Fetch requirements for Bowen ratio measurements of latent and sensible heat fluxes. *Agricultural and Forest Meteorology*, 44, 261-273.
- Hobbins, M. T., Ramírez, J. A. & Brown, T. C. (2001). The complementary relationship in estimation of regional evapotranspiration: An enhanced advection-aridity model. *Water Resources Research*, 37(5), 1389– 1403.
- Holwill, C. J., & Stewart, J. B. (1992). Spatial variability of evaporation derived from Aircraft and ground-based data. *Journal of Geophysical Research*, 97(D17), 19061-19089.
- ITT Industries-Solution for data visualization and images analysis. ENVI version 4.2. August 2005. Boulder, Colorado-USA.
- Jackson, R.D., Reginato, R.J., & Idso, S.B. (1977). Wheat canopy temperature: A practical tool for evaluating water requirements. *Water Resources Research*, 13, 651-656.

- Jackson, R. D., Hatfield, J. L., Reginato, R. J., Idso, S. B., & Pinter, J. P. J. (1983). Estimates of daily evapotranspiration from one time of day measurements. *Agricultural Water Management*, 7, 351–362.
- Jackson, R. D., Kustas, W. P. & Choudhury, B. J. (1988). A reexamination of the crop water stress index. *Irrigation Science*, 9(4), 309-317.
- Jacobs, J. M., Myers, D. A., Anderson, M. C., & Diak, G. R. (2000). GOES surface insolation to estimate wetlands evapotranspiration. *Journal of Hydrology*, 266, 53-65.
- Jiang, L., & Islam, S. (1999). A methodology for estimation of surface evapotranspiration over large areas using remote sensing observations. *Geophysical Research Letters*, 26(17), 2773-2776.
- Jiang, L. & Islam, S. (2001). Estimation of surface evaporation map over southern Great Plains using remote sensing data. *Water Resources Research*, 37(2), 329-340.
- Kahler, D. M. & Brutsaert, W. (2006). Complementary relationship between daily evaporation in the environment and pan evaporation. *Water Resources Research*, 42, W05413, doi:10.1029/2005WR004541
- Kustas, W. P., Norman, J.M., Anderson, M.C. & French, A.N. (2003). Estimating sub-pixel surface temperature and energy fluxes from the vegetation index-radiometric temperature relationship. *Remote Sensing of Environment*, 85, 429-440.
- Kustas, W. P., & Norman, J. M. (2000). A two-source energy balance approach using directional radiometric temperature observations for sparse canopy covered surface. *Agronomy Journal*, 92, 847– 854.

- LeDrew, E. F. (1978). A Diagnostic Examination of a Complementary Relationship between Actual and Potential Evapotranspiration. *Journal of Applied Meteorology*, 18(4), 495–501.
- Lewis, J.M. (1995). The story behind the Bowen ratio. *Bulletin of the American Meteorological Society* 76, 2433-443.
- Li, J., Nelson, J. P. III, Schmit T., Menzel W. P, Schmidt C. C. & Huang H. L. (1998). Retrieval of total atmospheric ozone from GOES sounder radiance measurements with high spatial and temporal resolution. *Proceedings of SPIE*, Vol. 3501, 291-300.
- Menzel, W. P., Seemann, S. W., Li, J., & Gumley, L. E. (2002). MODIS Atmospheric Profile Retrieval Algorithm Theoretical Basis Document, Version 6, *Reference Number: ATBD-MOD-07*. http://modis.gsfc.nasa.gov/data/atbd/atbd_mod07.pdf (accessed on 12/04/2003).
- Monteith, J.L. & Unsworth, M. (1990). Principles of Environmental Physics. Butterworth-Heinemann, 2nd edition. Burlington-MA, 304 pages. ISBN: 071312931X .
- Moran, M. S., Jackson, R.D., Raymond, L.H, Gay, L. W. & Slater, P.N. (1989). Mapping surface energy balance components by combining Landsat thematic mapper and ground-based meteorological data, *Remote Sensing of Environment*, 30, 77-87.
- Moran, M.S. and Jackson, R.D. (1991). Assessing the spatial distribution of evapotranspiration using remotely sensed inputs. *Journal of Environmental Quality*, 20, 725-737.

- Moran, M. S., Clarke, T.R.; Inoue, Y., Vidal, A. (1994). Estimating crop water deficit using the relation between surface-air temperature and spectral vegetation index . *Remote Sensing of Environment*, 49 (3) 246-263.
- Morton, F. I. (1969). Potential evaporation as a manifestation of regional evaporation. *Water Resources Research*, 5(6), 1244-1255.
- Morton, F. I. (1983). Operational estimates of areal evapotranspiration and their significance to the science and practice of hydrology. *Journal of Hydrology*, 66, 1-76.
- Murray, F. W. (1967). On the computation of saturation vapor pressure. *Journal of Applied Meteorology*, 6, 203-204.
- Nishida, K., Nemani, R. R., Running, S. W. & Glassy, J.M. (2003). An operational remote sensing algorithm of land evaporation. *Journal of Geophysical Research*, 108(D9), 4270.
- Noilhan, J. & Planton, S. (1989). GCM gridscale evaporation from mesoscale modelling. *Journal of Climate*, 8, 206-223
- Norman, J. M., Kustas, W. P. & Humes, K.S. (1995). Sources approach for Estimating soil and vegetation energy fluxes in observations of directional radiometric surface temperature. *Agricultural Forest and Meteorology*, 77, 263-293.
- Norman, J. M., Anderson, M. C., Kustas, W. P., French, A. N., Mecikalski, J., Torn, R., Diak, G. R., Schmugge, T. J., & Tanner, B. C. W. (2003). Remote sensing of surface energy fluxes at 10^1 -m pixel resolutions. *Water Resources Research*, 39(8), 1221-1232.
- Penman, H. L. (1948). Natural evaporation from open water, bare soil and grass. *Proceedings of the Royal Society of London, Series A*, (193), 120-145.

- Parlange, M. B. & Katul, G. G. (1995). Watershed scale shear stress from tethered sonde wind profile measurements under near neutral and unstable atmospheric stability. *Water Resources Research*, 31(4), 961–968.
- Price, J. C. (1983). Estimation of surface temperature from satellite thermal infrared data – a simple formulation for the atmospheric effect. *Remote Sensing of Environment*, 13, 353-361.
- Price, J.C. (1990). Using spatial context in satellite data to infer regional scale evapotranspiration. *IEEE Transactions on Geoscience and Remote Sensing*, 28(5), 940-948.
- Priestley, C. H. B. & Taylor, R. J. (1972). On the Assessment of Surface Heat Flux and Evaporation Using Large-Scale Parameters. *Monthly Weather Review*. 100, 81–92.
- Ramírez, J. A., Hobbins, M.T. & Brown, T.C. (2005). Observational evidence of the complementary relationship in regional evaporation lends strong support for Bouchet’s hypothesis. *Geophysical Research Letters*, 32, L15401, doi:10.1029/2005GL023549.
- Rees, W. G. (2001). *Physical Principles of Remote Sensing*. Cambridge University Press, 2nd edition. Cambridge, UK, 343 pages. ISBN 0521669480.
- Rivas, R. & Caselles, V. (2004). A simplified equation to estimate spatial reference evaporation from remote sensing-based surface temperature and local meteorological data. *Remote Sensing of Environment*, 83, 68-76.
- Sandholt, I., Rasmussen, K. & Andersen, J. (2002). A simple interpretation of the surface temperature/vegetation index space for assessment of surface moisture status. *Remote Sensing of Environment*, 49 (3) 246-263.

- Seguin, B., Assad, E., Fretaud, J. P., Imbernom, J. P., Kerr, Y., & Lagouarde, J. P. (1989). Use of meteorological satellite for rainfall and evaporation monitoring. *International Journal of Remote Sensing*, 10, 1001-1017.
- Shuttleworth, W. J. (1991). Insight from large-scale observational studies of land/atmosphere interactions. *Surveys in Geophysics* 12, 3-30.
- Shuurmans, J. M., Troch, P.A., Veldhuizen, A.A, Bastiaanssen, W.G.M. & Bierkens, M.F.P. (2003). Assimilation of remotely sensed latent heat flux in a distributed hydrological model. *Advances in Water Resources*, 26, 151-159.
- Smith, W. L., Woolf, H. M., Nieman, S. J. & Achtor T. H. (1993). ITPP-5 - The use of AVHRR and TIGR in TOVS Data Processing. *Technical Proceedings of the Seventh International TOVS Study Conference*, Austria 10 to 16 February 1993, J. R. Eyre Ed., 443-453.
- Snyder, W. & Wan, Z. (1998). BRDF models to predict spectral reflectance and emissivity in the infrared. *IEEE Transactions on Geoscience and Remote Sensing*, 36, 214-225.
- Stricker, H. & Brutsaert, W., (1978). Actual evaporation over a summer period in the Hupsel Catchment. *Journal of Hydrology*, 39, 139-157.
- Su, B. (2002). The surface energy balance system (SEBS) for estimation of turbulent heat fluxes. *Hydrology and Earth system Sciences*, 6, 85-99.
- Sugita, M. & Brutsaert, W. (1991). Daily evaporation over a region from lower boundary-layer profiles measured with radiosondes. *Water Resources Research*, 27(5), 747-752.

- Sugita, M., Usui, J., Tamagawa, I. & Kaihotsu, I. (2001). Complementary relationship with a convective boundary layer to estimate regional evaporation. *Water Resources Research*, 37(2), 353-365.
- Sun, D. & Pinker, R. T. (2004). Case study of soil moisture effect on the land surface temperature retrieval. *IEEE Geoscience and Remote Sensing Letters*, 1 (2), 127-130.
- Venturini, V., Bisht, G., Islam, S. & Jiang, L. (2004). Comparison of evaporative fractions estimated from AVHRR and MODIS sensors over South Florida. *Remote Sensing of Environment*, 93, 77-86.
- Venturini, V., Islam, S. & Rodríguez, L., (2007). Estimation of evaporative fraction and evapotranspiration from MODIS products using a complementary based model. *Remote Sensing of Environment*. *In print*.
- Wan, Z., & Dozier, J. A. (1996). A generalized split-window algorithm for retrieving land-surface temperature from space, *IEEE Transactions on Geoscience and Remote Sensing*, 34(4), 892-905.
- Wan, Z., & Li, Z. L. (1997). A Physics-Based Algorithm for Retrieving Land-Surface Emissivity and Temperature from EOS/MODIS data. *IEEE Transactions of Geoscience and Remote Sensing*, 35(4), 980-996.
- Wan, Z. (1999). MODIS Land-Surface Temperature Algorithm Basis Document (LST ATBD): version 3.3. www.ices.ucsb.edu/modis/atbd-mod-11.pdf.
- Xu, Y. & Cracknell, A. P. (1995). Advanced thermal inertia modelling. *International Journal of Remote Sensing*, 16(3), 431-446
- Xu, C. Y. & Singh, V.P. (2004). Evaluation of three complementary relationship evapotranspiration models by water balance approach to estimate actual regional

evapotranspiration in different climatic regions. *Journal of Hydrology*, 308, 105-121.

Zhang, L. & Lemeur, R. (1995). Evaluation of daily evapotranspiration estimates from instantaneous measurements. *Agricultural and Forest Meteorology*, 74, 139-154.

Appendix I: Abstract of Published Paper.

We present a new formulation to derive evaporative fraction (EF) and evapotranspiration (ET) maps from remotely sensed data without auxiliary relationships or site-specific relationships. This formulation is based on Granger's complementary relationship and Priestley-Taylor's equation. The proposed model eliminates the wind function and resistance parameters commonly applied to ET calculation by including a relative evaporation parameter (ET/E_{pot}). By combining this relative evaporation parameter, Granger's complementary relationship and Priestley-Taylor equation, we obtain a simple equation to estimate ET. We tested and validated the proposed formulation over the Southern Great Plains (SGP) region of the United States for seven clear sky days during March-October 2003. MODIS Atmospheric and Land products were the only source of data used in this study. Estimates of ET show an overall root mean square error and bias of 33.89 and -10.96 Wm^{-2} , respectively. Our results suggest that the proposed approach is robust and valid for a wide range of atmospheric and surface conditions.

Appendix II: IDL Code to Calculate ET

```
;Function to Resample the image after the geo-registration
function re_sample_int, data, bw
ss=size(data)
ncol=ss[1]
nrow=ss[2]
data_fill=fltarr(ncol,nrow)
data_fill[0:ncol-1,0:nrow-1]=-1
ln=fix(bw/2)
for i=ln, ncol-ln-1 do begin
;print, i
for j=ln, nrow-ln-1 do begin
nearbox=data[i-ln:i+ln,j-ln:j+ln]
nb=[nearbox,nearbox]
idx=where(nb NE -1)
if (idx[0] NE -1) then begin
data_fill[i,j]=(data[i,j] EQ -1)?mean(nb[idx]):data[i,j]
endif
endfor
endfor
return, data_fill
end
;
;
function re_sample_dbl, data, bw
ss=size(data)
ncol=ss[1]
nrow=ss[2]
data_fill=dblarr(ncol,nrow)
data_fill[0:ncol-1,0:nrow-1]=-1
ln=fix(bw/2)
for i=ln, ncol-ln-1 do begin
;print, i
for j=ln, nrow-ln-1 do begin
nearbox=data[i-ln:i+ln,j-ln:j+ln]
nb=[nearbox,nearbox]
idx=where(nb NE -1)
if (idx[0] NE -1) then begin
data_fill[i,j]=(data[i,j] EQ -1)?mean(nb[idx]):data[i,j]
endif
endfor
endfor
return, data_fill
end
;
;Function to matrix vector input data
function matrix,b
ncol=467
nrow=444
bcol=dblarr(ncol,nrow)
k=0
for ro=0,443 do begin
for co=0,466 do begin
bcol(co,ro)=b(k)
k=k+1
```

```

k=ulong(k)
endfor
endfor
return,bcol
end

function mat,b
ncol=467
nrow=444
bcol=fltarr(ncol,nrow)
k=0
for co=0,466 do begin
for ro=0,443 do begin
bcol(co,ro)=b(k)
k=k+1
k=ulong(k)
endfor
endfor
return,bcol
end
;***** Program begins *****
pro Tgcom_GSP_TW_Buck_night
;*****

ndl=dblarr(207348)
tsl=fltarr(207348)
map_net1=fltarr(207348)
air_net1=fltarr(207348)
Tdew=fltarr(207348)
lati=fltarr(207348)
lonn=fltarr(207348)
vp=fltarr(207348)
Tsnight=fltarr(207348)
filename=DIALOG_PICKFILE()
openr, 4, filename
readu, 4, ndl
close, 4

;Read TS day image
filename=DIALOG_PICKFILE()
openr, 5, filename
readu, 5, tsl
close, 5

;Read Net Radiation output file from Bisht's program
filename=DIALOG_PICKFILE()
openr, 6, filename
readu, 6, map_net1
close, 6

;Read Ta MODIS product as output file from Bisht's program
filename=DIALOG_PICKFILE()
openr, 7, filename
readu, 7, air_net1
close, 7
;Read Tw MODIS product as output file from Bisht's program
filename=DIALOG_PICKFILE()
openr, 5, filename

```

```

readu, 5, tdew
close, 5
; Read Latitud
filename=DIALOG_PICKFILE()
openr, 7, filename
readu, 7, lati
close, 7
;Read Longitud
filename=DIALOG_PICKFILE()
openr, 5, filename
readu, 5, lonn
close, 5
; Read VP MODIS product as output file from Bisht's program. This file
is used ;only for checking purposes.
;filename=DIALOG_PICKFILE()
;openr, 5, filename
;readu, 5, vp
;close, 5
;Read Ts night
filename=DIALOG_PICKFILE()
openr, 5, filename
readu, 5, Tsnight
close, 5

ndvi=dblarr(467,444)
ts=fltarr(467,444)
rn=fltarr(467,444)
ta=fltarr(467,444)
Tw=fltarr(467,444)
lat=fltarr(467,444)
lon=fltarr(467,444)
vpa=fltarr(467,444)
Tsn=fltarr(467,444)
Tsn=Tsnight*0.02 ; applying MODIS coefficients
Tsn[where(tsn lt 0)]=200 ;masking clouds

;Converting Vector to Matrix
nd=matrix(nd1)
ts=mat(tsl)
net=mat(map_net1)
ta=mat(air_net1)
td=mat(Tdew)
lat=mat(lati)
lon=mat(lonn)
vpa=mat(vp)
;Tsn=mat(tsn)
k=0
for ro=0,443 do begin
for co=0,466 do begin
Tsn(co,ro)=Tsn(k)
k=k+1
k=ulong(k)
endfor
endfor
;Tsn=tsn+273
indices_cld=where((Ts LT 0 or Tsn LT 0), countclo)
if (indices_cld[0] NE -1) then nu=100*countclo/207348
print, '((((((((((((((((((((((((((((((((((((((((((((((((((((((((((((((((

```

```

print, 'clouds %', nu

live_image, Ts, title='LST day'
live_image, Tsn, title='LST night'
T31=Ts ;re-defining the Ts matrix
window,0
Plot, ts, tsn, psym=3,BACKGROUND = 255, COLOR =
0,xrange=[260,320],yrange=[260,320],$
ytitle='Ts at night (K)', xtitle='Ts (K) ', title='Day Surface
Temperatures Vs. Night Surface temp.',/isotropic
;*****
;start the TSS vs NDVI triangle estimation and Jiang-Islam phi parameter
;*****
t31=ts
device, DECOMPOSED=0
LOADCT,39
;*****
;*****

;device, /close

NDmax=max(nd)
NDmin=min(nd)
NDmin=0.0

jjj=[where(T31 gT 273.15)] ;first screening of cloud pixels

;Define Tmax, Tmin for the triangle or tripozoid bound
Tmin=mean(T31[where((nd lt 0) and (nd gt -1) and (t31 gt 273.15 ))]);
;Tmin=mean(T31[where((nd lt 0) and (t31 gt 273.15 ))]);
indices_cloud=where(T31 LT Tmin)

ND_max=max(nd)
Te=max(T31[where(nd GT (ND_max-0.02))]) ;maximum temperature at ND_max
ND_i=ND_max-0.2 ;an arbitrary ND value

jj=where((nd GT ND_i-0.01) AND (nd LT ND_i+0.01))
if (jj[0] NE -1) then begin
Ti_max=max(T31[jj]) ;maximum T corresponding to ND_i
Tmax=(ND_max*Ti_max-ND_i*Te)/(ND_max-ND_i)

phi_max=1.26
phind=phi_max*(Tmax-T31)/(Tmax-Tmin)

;phind[indices_cloud_2]=-1
phind[where(nd lt 0)]=phi_max
if (indices_cloud[0] ne -1) then phind[indices_cloud]=-1
endif
;End of Jiang Islam Method to estimate Phi

;*****
;NEW COEFFICIENTE F=(Tu-TDEW)/(TSURFACE-TDEW)
;*****

knet=where(net gt 0)
net[where(net lt 0)]=mean(net[knet])

```



```

print, ' '
print, 'New Method statistics'
print, 'Mean ET      ', mean(ETF[jj]), ' Min. ET      ', min(ETF[jj]), ' Max.
ET      ', max(ETF[jj]), ' ET S. Deviat      ', STDDEV(ETF[jj])
print, ' '
print, 'Priestley and Taylor statistics'
print, 'Mean      ', mean(ETP_T[jj]), ' Min.      ', min(ETP_T[jj]), ' Max.
      ', max(ETP_T[jj]), ' S. Deviat      ', STDDEV(ETP_T[jj])
print, ' '
print, 'Bolton statistics'
print, 'Mean      ', mean(ETB[jj]), ' Min.      ', min(ETB[jj]), ' Max.
      ', max(ETB[jj]), ' S. Deviat      ', STDDEV(ETB[jj])
print, ' '
print, 'Grager and Gray statistics'
print, 'Mean      ', mean(ETGG[jj]), ' Min.      ', min(ETGG[jj]), ' Max.
      ', max(ETGG[jj]), ' S. Deviat      ', STDDEV(ETGG[jj])
print, ' '
print, 'Net Radiation statistics'
print, 'Mean Rn', mean(net[jj]), ' Min. Rn      ', min(net[jj]), ' Max.
Rn      ', max(net[jj]), ' Rn S. Deviat.      ', STDDEV(net[jj])
;window,21
;plot, ETphi[jj], ETF[jj], psym=3, xrange=[0,600],
yrange=[0,600],xtitle='ET with Jiang-Islam ', $
; ytitle='ET with F',title='ET (Jiang-Islam Vs New Method)', $
;BACKGROUND = 255, COLOR = 0,/isotropic
;oplot, [0,600],[0,600], COLOR = 8,THICK=1.
; ;*-*-*-*-*-*-*-*-*-*-*-*-*-*-*-*-*-*-*-*-*-*-*-*-*-*-*-*-*-*
;TS-COMPARIZON BETWEEN ETs with Jiang_islam AND F with TS
;*-*-*-*-*-*-*-*-*-*-*-*-*-*-*-*-*-*-*-*-*-*-*-*-*-*-*-*-*
tmax=(ETphi-ETF)
d=(ETphi-ETF)
sd=(ETphi-ETF)^2
print,'ET (with Jian-Islam and New Method) regression analysis
jj=where((F gt -1) and (phind ge 0) and (phind lt 1.26), countT)
Trmse=double(sqrt(total(sd[jj])/countT))
Tbias=double(total(d[jj])/countT)
Tmaxdif=max(Tmax)
cc=correlate(ETphi[jj], ETF[jj])
print,'RMSE',TRMSE,'BIAS',Tbias
print,'correlation',cc
;*-*-*-*-*-*-*-*-*-*-*-*-*-*-*-*-*-*-*-*-*-*-*-*-*-*-*-*-*
;TS-COMPARIZON BETWEEN ETs with PT AND F with TS
print,'ET (with PT and new method ) regression analysis'
tmax=(ETP_T-ETF)
d=(ETP_T-ETF)
sd=(ETP_T-ETF)^2
Trmse=double(sqrt(total(sd[jj])/countT))
Tbias=double(total(d[jj])/countT)
Tmaxdif=max(Tmax)
cc=correlate(ETP_T[jj], ETF[jj])
print,'RMSE',TRMSE,'BIAS',Tbias
print,'correlation',cc
;window,23
;plot, ETP_T[jj], ETF[jj], psym=3, xrange=[0,600],
yrange=[0,600],xtitle='ET with Priestley-Taylor ', $
; ytitle='ET with F',title='ET (Priestley-Taylor Vs New Method)', $
;BACKGROUND = 255, COLOR = 2,/isotropic
;oplot, [0,600],[0,600], COLOR = 0,THICK=1.

```



```

for y=0,16 do begin
for j=0,466 do begin
for i=0,443 do begin
dif(j,i)=(lat(j,i)-Lat1(y))*(lat(j,i)-Lat1(y))+(lon(j,i)-
Lon2(y))*(lon(j,i)-Lon2(y))
endfor
endfor
mdif(y)=min(dif)
;print,'mdif(y)',mdif(y)
endfor

;^^^^^^^^^^^^^^^^^^^^ Station Coordinates ^^^^^^^^^^^^^^^^^^^^^^^^^^^^^^^^^^^^^^^^^^^^^^^^^^^^^^^^^^^^^^6

for y=0,16 do begin
for j=0,466 do begin
for i=0,443 do begin
dif(j,i)=(lat(j,i)-Lat1(y))*(lat(j,i)-Lat1(y))+(lon(j,i)-
Lon2(y))*(lon(j,i)-Lon2(y))

if(dif(j,i) EQ mdif(y)) then begin

st=ETF(j,i)
st1=ETphi(j,i)
st2=ETP_T(j,i)
ndvi=nd(j,i)
ee=e(y)
Tu=Tw(j,i)
Tsss=Ts(j,i)
print,'-----'
_'

print,'lat_SGP      ',lat(j,i),'      lat_station      ',Lat1(y)

print,'lon_SGP      ',lon(j,i),'      lon_station      ',Lon2(y)

print,'ET with New method at station      ',ee,'      is      ',st
print,'ET with Jiang-Islam at station      ',ee,'      is      ',st1
print,'ET with Priestley-Taylor at station      ',ee,'      is      ',st2
print,'Tu at station      ',ee,'      is      ',Tu
print,'Ts at station      ',ee,'      is      ',Tsss
;print,'rn at station      ',ee,'      is      ',net(j,i)

print,'NDVI at station      ',ndvi

;<<<<<<<<<<<<<<<<<<<<<<<<<<<<<<<<<<<<<<<<<<<<<<<<<<<<<<<<<<<<<<<<<<<<<<<<<<<<<<<<<<<<<<<<<<<<<<<<<<<<<<<<<<<<<<<<'

endif
endfor
endfor
endfor
;-*-*-*-*-*-*-*-*-*-*-*-*-*-*-*-*-*-*-*-*-*-*-*-*-*-*-*-*-*-*-*-*-*-*-*-*-*-*-*-*-*-*-*-*-*-*-*-*-*-*-*
*_
;Tw, Ts, Ta and ET for a given es

```

```
;*****  
*
```

```
indices_cld=where(T31 LT 273.15)  
indice_clean=where(Ts gt -1)  
nd[indices_cld]=-1  
T31[indices_cld]=273.  
Ts[indices_cld]=273  
Ta[indices_cld]=min(ta[indice_clean])  
Td[indices_cld]=min(td[indice_clean])  
net_clean=where(net gt -7)  
net[indices_cld]=min(net[net_clean])
```

```
endfor  
endfor  
close,7  
end
```

Appendix III: An Introduction to an Alternative Tu Calculation

Introduction

As previously explained, Tu was estimated from the saturation vapor pressure curve (SVP). Its calculation was based upon two equations having the dew point temperature as one of the variables involved. In Chapter 2, Section 2.2, the limitations of the SVP methodology were acknowledged, for instance, estimating Tu from the SVP makes this surface temperature dependent on Td, i.e. depending in some degree on the air relative humidity (RH). However, the definition of Tu suggests that it would only depend on Ts and the surface moisture content (SM) which is not routinely assessed or measured. Although there are methodologies available that utilize remotely sensed data, it may be difficult to validate SM with soil-vegetation ground observations.

The thermal inertia (P) and SM are highly correlated (*Castelli et al., 1999; Chauhan et al., 2003; Sun and Pinler, 2004*). P measures a substance tendency to resist temperature changes. Thus, materials with low P resist changes in temperature, those substances with high P cool and heat quickly (*Campbell, 2002*). Metals have the highest P values while wood is the natural material with the lowest P. Different geological materials present different P values, however P values for water and saturated ground may not be distinguished from those of minerals. Nevertheless, a water surface is warmer at night and cooler at daytime than soil and rocks due to the ET effect. Consequently, SM could be assessed from the day-night temperature variation with an accuracy of about 15% (*Rees, 2001*). In contrast, dry vegetation may be distinguished from bare surfaces at night because of the insulating effect of vegetation. The estimation of P itself may not be

useful for calculating T_u , however the difference of day-night temperatures due to P properties can be advantageous.

The amplitude of the daily variation of T_s changes with the surface type and the water content. T_s daily amplitude is commonly calculated from the differences between T_s at night and T_s at near-noon (Xue and Cracknell, 1995). Figure III.1 shows a sketch of a characteristic T_s daily variation for three different types of surfaces.

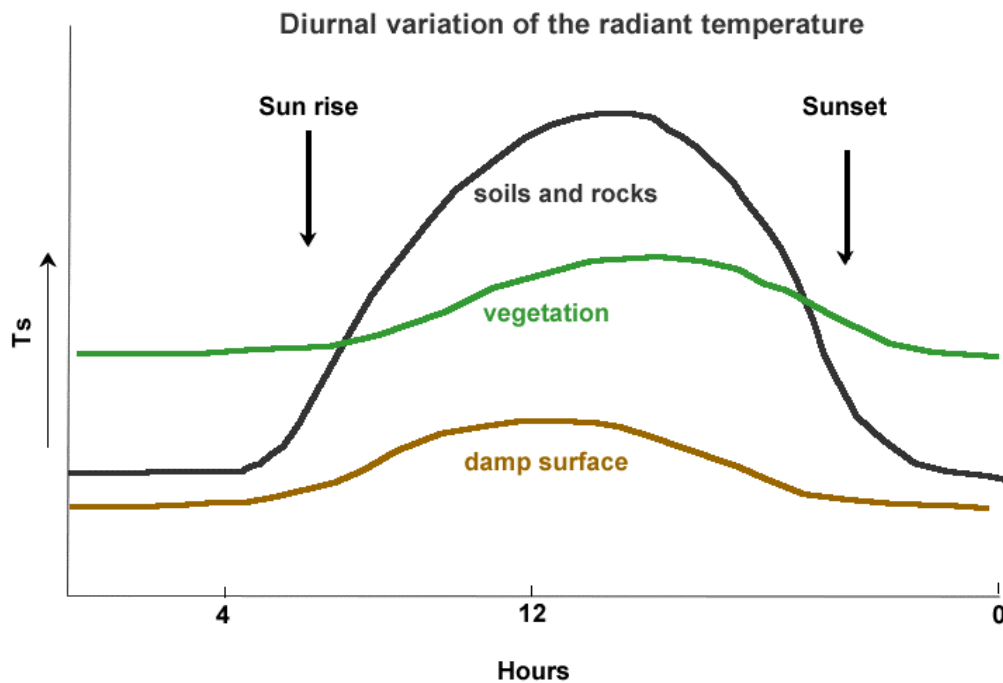


Figure III.1: Typical daily variation of surface temperature for different surfaces.

During nighttime T_s experiences little variations. Typically, the lowest value is observed after 3:00 AM local time (Rees, 2000). In contrast, after sunrise, T_s varies as the solar radiation heats the surfaces. The magnitude of the T_s change mainly depends on the surface type and water content. In general, T_s increases during the morning until 2 to 3 PM and then decreases until sunset time.

The difference between T_s at the peak ($T_{s_{peak}}$) and T_s at the sunrise time ($T_{s_{sunrise}}$) would be an indication of the surface water content condition, if no drastic changes occur during morning hours due to precipitation events. The average rate of the daily variation along the ascending branch of the T_s curve could be computed as,

$$Avg = \frac{T_{s_{peak}} - T_{s_{sunrise}}}{t_{peak} - t_{sunrise}} \quad (43)$$

In equation (43), t_{peak} is the time at which $T_{s_{peak}}$ takes place and $t_{sunrise}$ is the local sunrise time. For practical purposes, $T_{s_{peak}}$ is approximated by T_s at the near-noon satellite overpass time; therefore t_{peak} corresponds to the satellite overpass time (t_s). The temperature at sunrise time is approximated by T_s at night overpass times (T_{sn}). Thus, larger average rates would indicate drier pixels and vice versa (see Figure III.1). The approximation of equation (43) would be,

$$Avg \approx \frac{T_s - T_{sn}}{t_s - t_{sunrise}} \quad (44)$$

Method to Estimate T_u from Night-Day T_s Maps

If the air is saturated with water vapor, condensation is commonly observed during early morning hours when T_a becomes equal to T_d . By analogy, this may be extended to T_u , i.e. early morning surface temperature may be an approximation to T_u . Near sunrisetime, T_s can be interpreted as the lowest temperature that the surface can have for any given moisture condition. Thus, it can also be assumed that at sunrise, e_s^* is closer to e_s .

After sunrise time, T_s can be interpolated from equation (44) and

assumed equal to T_u , as follows,

$$T_u = T_s - \text{Avg}(t_s - t_u) \quad (45)$$

where Avg is calculated with equation (44) and t_u is any time after sunrise time.

In this methodology, T_u is assumed constant during the morning although changes during daytime could be expected. In fact, T_s increases during daytime due to solar radiation while the SM decreases by evapotranspiration in most common scenarios.

F and ET Estimation with Night-Day T_s Maps

In order to compute F and then ET, T_u was approximated with equation (45) for the same region and days described in Chapter 3.

T_{sn} and T_s were obtained from MOD11 or MYD11 products acquired with night and near-noon images, respectively. The sunrise time for the study days were taken from the US Naval Observatory, Astronomical Application Department (<http://aa.usno.navy.mil/>). Hence, the T_u equation for each day was obtained assuming t_u one hour after sunrise time and t_s was selected as the satellite near-noon overpass time. Table III.1 shows the day of the year, the nocturnal overpass time of EOS-Terra, sunrise time, t_u time, image quality, and T_u equation for five study days. It should be mentioned that the night T_s map for April 1st and September 19th, 2003 had more than 20% of cloudy pixels, so they were discarded. As an example of T_{sn} images, Figure III.2 shows MODIS T_s map obtained with nighttime image for March 23rd, 2003 (DOY 82). In this image, the Southern part of the study region was outside the satellite overpass; this is the reason why that area is simulated as cloudy pixels.

Tu was estimated with the equations displayed in Table III.1 and plugged into F equation [equation (5)]; ET was estimated with equation (12).

Table III.1: Day of the Year, nighttime EOS-Terra overpass time, sunrise time, t_u , image quality in term of cloudy pixels and Tu equation from equation (45).

Day of the Year	EOS-Terra nighttime overpass (UTC)	Sunrise time (UTC)	t_u (UTC)	Day-night cloudy pixels %	Tu equation
DOY82	11.008	6.483	7.483	28	$Tu = T_{sn} + (ts - tu) * 0.22$
DOY 90	11.829	6.283	7.283	16	$Tu = T_{sn} + (ts - tu) * 0.18$
DOY 249	11.166	6.066	7.066	9	$Tu = T_{sn} + (ts - tu) * 0.20$
DOY 285	10.751	6.550	7.550	7	$Tu = T_{sn} + (ts - tu) * 0.24$
DOY 292	10.833	6.666	7.666	13	$Tu = T_{sn} + (ts - tu) * 0.24$

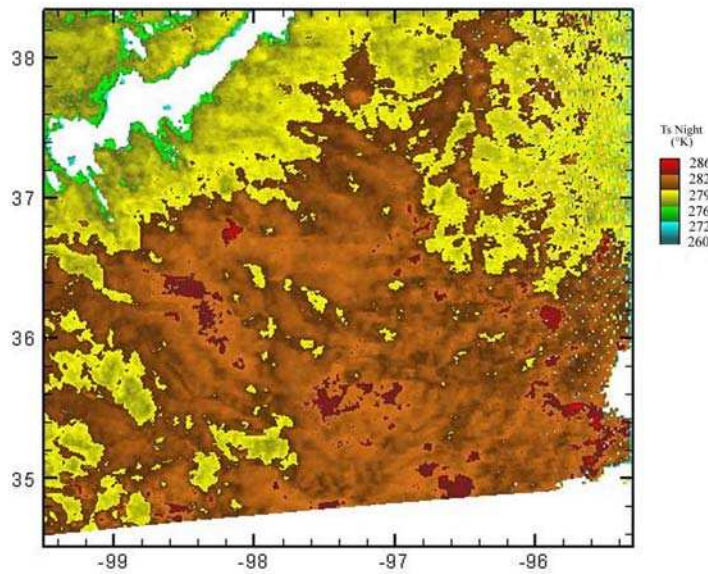


Figure III.2: Tsn map from MOD11 product. March 23rd, 2003 (DOY82)

Comparisons between regional ET calculated using the SVP method and night-day temperatures are presented in Table III.2, where the regional ground observations are

also included. In general, modeled mean ET values with both methods seem to accord with the observed. Results for DOY90 and DOY285 present significantly better regional statistics with Tu estimated from SVP method. These differences may be due to the assumptions behind the night-day method. Although there is not a significant amount of observations to draw a statistically meaningful observed S value, it seems that the night-day method to estimate Tu would render ET maps with more realistic dispersion around the mean regional ET, i.e. with modeled ET standard deviation closer to that observed.

The comparison between both sets of modeled ET estimates at the pixel scale is shown in Table III.3. The root mean square errors (RMSE), bias (SVP – Night-Day method) and correlation coefficients (R^2) are presented for every analyzed day. Differences in ET of about $\pm 27 \text{ Wm}^{-2}$ between both modeled ET sets are observed. In general, R^2 is very good. The large amount of cloudy pixels may explain the low correlation observed for DOY82.

Table III.2: Observed and modeled ET (Wm^{-2}) means and standard deviations (S)

Day of the year 2003	Observed ET		Model ET (SVP)		Model ET (night-day)	
	Mean	S	Mean	S	Mean	S
DOY82	191.79	34.22	181.34	14.84	198.66	25.59
DOY 90	148.56	38.33	164.45	14.25	210.38	32.98
DOY 245	284.35	40.82	308.86	27.53	261.72	29.37
DOY 285	203.97	33.38	214.57	16.27	143.69	30.01
DOY 292	212.20	46.10	231.24	17.78	197.69	32.47

Even though the alternative method to compute T_u would yield realistic regional ET, this methodology may cause ET results to differ in about 14% of the mean value at the pixel scale.

Table III.3: Comparison between ET results with night-day and the SVP method at the pixel scale.

Day of the year 2003	RMSE	Bias	R ²
DOY82	30,03	-29,68	0,51
DOY 90	13,74	6,36	-0,98
DOY 245	44,18	43,81	0,98
DOY 285	28,73	-27,80	0,88
DOY 292	20,95	16,03	0,87

To further explore both T_u methods, point ET observations and matching pixel ET estimates were contrasted as previously done in Chapter 3 for the SVP method. The warnings raised in pages 53 and 54 must be taken into account to interpret the RMSE and bias presented in this Chapter. Figure III.3 exhibits the contrast of ET estimates and ground observations. The night-day method to calculate T_u seems to overestimate small ET observations and underestimate large ET measurements.

The overall RMSE with the SVP method for these 5 days was 36.05, bias (observed-modeled) equaled to -14.11 Wm^{-2} and R^2 was about 0.80. On the other hand, with the night-day T_s method, $\text{RMSE}= 42.31$, bias $=-0.04$ and $R^2=0.65$, indicating a poorer correlation.

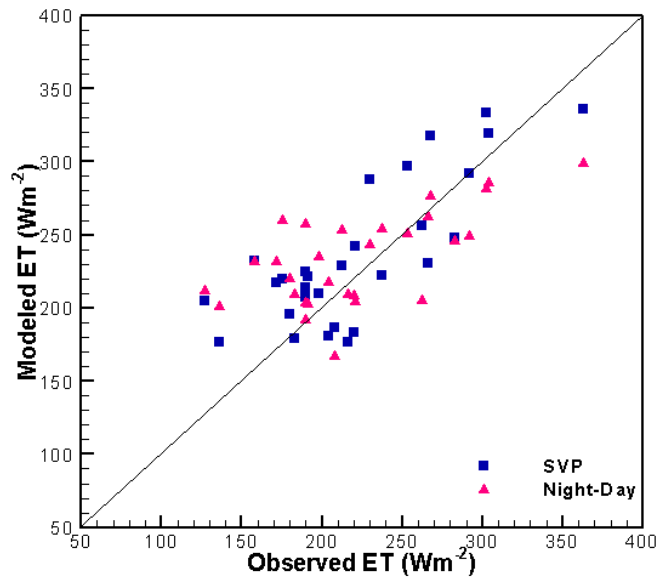


Figure III.3: Comparison between ground observations and ET obtained with Tu derived from the SVP and night-day methods

Even though the metrics obtained in this contrast are comparable to those published with other methods (*Batra et al., 2006; Grago and Crowley, 2005; Gomez et al., 2005; Rivas and Caselles, 2004; Jacobs et al., 2000; Nishida et al., 2003; Norman et al., 2003; Jiang and Islam, 2001; Kustas and Norman, 2000*), the SVP method seems to yield more realistic ET estimates than the night-day methodology.

The surface actual SM is not explicitly taken into account in the night-day method. In turn, it was assumed that Ts daily variation is due mainly to the surface SM, however there are factors such as geology, type of vegetation cover, etc., that contribute to shape the Ts daily curve. Therefore, the early morning temperature seems to be a reasonable estimate for Tu for some surface water content conditions, but Tu may be underestimated for dry surfaces. These two factors may be the main source of errors in this method.

The preliminary results presented in this thesis suggest that the SVP method to compute Tu yields better results than this alternative method. The assumptions behind the night-day method seem to be stronger than those behind the SVP method, yet further research should be done with both Tu methodologies.